Surface-related multiple estimation and removal with focus on shallow water

Zhang, D.

DOI
10.4233/uuid:b46b14e3-c0cf-4aca-a21d-b7eeda6eb2df

Publication date
2022

Document Version
Final published version

Citation (APA)
Zhang, D. (2022). *Surface-related multiple estimation and removal with focus on shallow water*. [Dissertation (TU Delft), Delft University of Technology]. https://doi.org/10.4233/uuid:b46b14e3-c0cf-4aca-a21d-b7eeda6eb2df

SURFACE-RELATED MULTIPLE ESTIMATION AND REMOVAL WITH FOCUS ON SHALLOW WATER

SURFACE-RELATED MULTIPLE ESTIMATION AND REMOVAL WITH FOCUS ON SHALLOW WATER

Proefschrift

ter verkrijging van de graad van doctor
aan de Technische Universiteit Delft,
op gezag van de Rector Magnificus Prof. dr. ir. T.H.J.J. van der Hagen,
voorzitter van het College voor Promoties,
in het openbaar te verdedigen op donderdag 27 oktober 2022 om 10:00 uur

door

Dong ZHANG

Master of Engineering in Geological Resources and Geological Engineering
China University of Petroleum (Beijing), Beijing, China
geboren te Shanxi, China.

Dit proefschrift is goedgekeurd door de

promoters: Dr. ir. D.J. Verschuur and Prof. dr. ir. N. de Jong

Samenstelling promotiecommissie:

Rector Magnificus,	voorzitter
Dr. ir. D.J. Verschuur,	promotor, Technische Universiteit Delft
Prof. dr. ir. N. de Jong,	promotor, Technische Universiteit Delft
Onafhankelijke leden:	
Prof. dr. ir. E.C. Slob	Technische Universiteit Delft
Prof. dr. ir. A.J. van der Veen	Technische Universiteit Delft
Prof. dr. Y. Wang	Imperial College London
Dr. J.C. van Gemert	Technische Universiteit Delft
Dr. C.V. Kostov	Schlumberger Cambridge Research Center (retired)

The work in this dissertation was conducted at the section Computational Imaging (CI), Faculty of Applied Sciences, Delft University of Technology and was financially supported by Delphi Consortium.

Printed by: Ridderprint B.V.

ISBN 978-94-6366-614-5

An electronic version of this dissertation is available at
http://repository.tudelft.nl/.

May there be enough clouds in our lives to make a beautiful sunset

CONTENTS

SUMMARY

For exploration and development of the earth, seismic surveys are acquired to provide information about the subsurface, within specifications of accuracy set by geologists and engineers, and within business constraints on budgets and turn-around time for processing and interpretation of the data. The case of seismic surveys that are acquired, partly or entirely, in shallow water is relevant for the industry worldwide. However, the acquisition and processing for shallow water seismic surveys requires considerable modifications of standard procedures to meet the survey goals. In this work, the focus is on modifications in processing and in particular with respect to the handling of multiply scattered energy, assuming standard acquisition practices.

Multiple scattering is a significant wave phenomenon when seismic waves propagate through the earth. Its corresponding energy, i.e., seismic multiples, are usually unwanted due to the interference with primary reflections. The traditional seismic surface-related multiple estimation and removal method is limited by both the unrecorded data reconstruction (e.g., the missing near offsets and the data gap between the crosslines) and the subsequent multiple adaptive subtraction performance. These issues become even more severe for the shallow-water environment, which is typically defined as being around 50-200 m within the exploration seismic frequency range (i.e., 2-120 Hz) in this thesis. Shallow water creates highly curved seismic reflection events with strong lateral amplitude variations, and complex overlap between primaries and surface-related multiples. Conventional data reconstruction methods fail to tackle the missing data in shallow water, and are even more problematic in 3D. In addition, the dilemma between primary damage and surface multiple leakage during the adaptive subtraction is very much present for shallow-water data.

An integrated closed-loop surface-related multiple estimation (CL-SRME) and full-wavefield migration (FWM) framework for better primary and surface-related multiple estimation, which is able to support CL-SRME with good-quality near offsets in order to avoid primary estimation failure that typically occurs in shallow-water environments, is proposed to attack the unrecorded data reconstruction issue. We suggest to use multiples to provide information on the missing near-offset data by using FWM, where primaries and surface multiples together create an image of the shallow subsurface. Taking advantage of FWM - with its closed-loop simultaneous primaries and multiples imaging approach - as the data reconstruction method and feeding the reconstructed near offsets to CL-SRME are the most important components to tackle the shallow-water issues in a physically consistent manner. This new integrated framework will have its main impact on a full 3D implementation with coarse sampling. Therefore, a similar cascaded framework for 3D surface-related multiple estimation in shallow-water scenarios, which consists of a data reconstruction step via 3D FWM and a surface multiple estimation step via a 3D SRME-type method, is also introduced in the thesis. Improvements on estimating surface multiples and primaries, due to good data reconstruction via FWM, have been

proved on both 2D and 3D synthetic data. Despite of lacking an accurate subsurface velocity model for 2D field data, the FWM reconstructed near-offset water-bottom reflection still improves the quality of the estimated surface multiples and primaries.

In order to mitigate the surface-related multiple adaptive subtraction dilemma, we have also introduced a two-step framework for surface multiple leakage extraction in this thesis, and thus extended our seismic multiple processing toolbox. The aforementioned two-step framework based on local primary-and-multiple orthogonalization (LPMO) is both versatile and efficient for leaked multiple extraction, therefore, primaries can be better preserved without leaving much multiple energy. The initial estimation step usually prefers SRME with a conservative adaptive subtraction or any conservative multiple estimation method, and LPMO is followed to compensate the initial estimated primaries and multiples. Promising multiple leakage extraction has been achieved on both synthetic and field data sets. Although effective compared to standard subtraction, LPMO is slow and computationally intensive. Therefore, a fast LPMO (FLPMO) using a scaled point-by-point division, rather than the time-consuming shaping regularization-based iterative inversion, is further introduced to accelerate the whole process. Results on two different field data sets display a very similar multiple leakage extraction performance compared to LPMO, while indicating that the scaled point-by-point division in FLPMO is approximately 40 times faster than the shaping regularization-based inversion in LPMO. Moreover, the complete FLPMO framework is approximately four times faster than the LPMO framework, and thereby is now equivalent to the industry-standard $L2$ adaptive subtraction.

With the advance of deep learning (DL) technology, the aforementioned two issues in shallow water can also be investigated via a U-Net based DL neural network (NN) framework. More specifically, a DL-based de-aliasing NN is introduced for the initial surface multiple estimation, where the strong data fitting power of DL can directly project the aliased multiples, due to coarse sampling, to its corresponding unaliased target multiples. Meanwhile, a DL-based adaptive subtraction NN is proposed with both total full wavefield and the predicted multiples as two input channels to overcome the adaptive subtraction dilemma. In this way, the robust physics, i.e., the estimated multiples, is used and the synthetic primary labels can be helpful to the framework. Note that the data distribution between training and test data plays a significant role on these U-Net based applications. Training on field data and test on nearby field data shows the best performance due to a similar data distribution.

Shallow water is very challenging for surface-related multiple estimation. Physics-based deterministic approaches, e.g., FWM-based data reconstruction and LPMO, can help geophysicists better understand and partially solve the essentials of the problem. For poorly described deterministic problems, e.g., adaptive subtraction and multiple de-aliasing, DL can find the underlying relationships that are not easily achievable by the deterministic methods. Combination of deterministic methods and DL will result in an optimal performance. This is where further research should concentrate on.

SAMENVATTING

Voor de exploratie en ontwikkeling van de aarde worden seismische onderzoeken verricht om informatie over de ondergrond te verkrijgen, met inachtneming van door geologen en ingenieurs vastgestelde nauwkeurigheidsspecificaties en met inachtneming van de zakelijke beperkingen inzake budgetten en doorlooptijd voor de verwerking en interpretatie van de meetgegevens. De situatie waarbij seismisch onderzoek geheel of gedeeltelijk in ondiep water wordt verricht, is relevant voor de industrie in de hele wereld. De acquisitie en verwerking van seismisch onderzoek in ondiep water vereist echter aanzienlijke aanpassingen van de standaardprocedures om aan de onderzoeksdoelstellingen te voldoen. In dit werk ligt de nadruk op wijzigingen in de dataverwerking, in het bijzonder met betrekking tot de behandeling van meervoudige reflecties, uitgaande van standaard acquisitiepraktijken.

Meervoudige verstrooiing is een significant golf fenomeen als seismische golven zich voortplanten door de aarde. De overeenkomstige energie, d.w.z., seismische meervoudige reflecties, zijn meestal ongewenst vanwege de interferentie met primaire reflecties. De traditionele seismische oppervlakte-gerelateerde meervoudige reflectievoorspellings- en verwi-jderings-techniek wordt gelimiteerd door zowel de reconstructie van niet-gemeten data (zoals bijvoorbeeld vanwege een minimale bron-ontvanger afstand en het grote interval tussen de kruislijnen) als de daaropvolgende prestatie van de zogenoemde meervoudige reflectie adaptive aftrekkingstechniek. Deze kwesties worden nog verergerd voor situaties met ondiep water, wat typisch wordt gedefinieerd als een waterdiepte van 50–200 m binnen de seismische exploratie frequentieband (d.w.z., 2–120 Hz) in deze thesis. Ondiep water creëert sterk gebogen seismische reflectie-aankomsten met sterke laterale amplitude variates, en complexe overlap tussen primaire en oppervlakte-gerelateerde meervoudige reflecties. Conventionele data reconstructie methoden schieten tekort voor missende data in ondiep water, en zijn nog problematischer in 3D. Daarbij is voor data in ondiep water ook nog aanwezig het compromis tussen schade aan de primaire reflecties en lekkage van oppervlakte-meervoudige reflecties tijdens het adaptive aftrekkingsproces.

Om de ongemeten data reconstructie kwestie aan te pakken is voorgesteld een geïntegreerde, gesloten-kring, voorspelling van oppervlakte-gerelateerde meervoudige reflecties (zogenaamde CL-SRME) en een zogenoemd volledig golfveld afbeelding, of full-wavefield migration (FWM) raamwerk voor betere primaire en oppervlakte-gerelateerde meervoudige reflectie voorspelling, die CL-SRME kan ondersteunen met goede kwaliteit nabije-afstand-sdata om de problemen met het voorspellen van primaire reflecties, dat typisch optreedt in situaties met ondiep water, te omzeilen. Wij stellen voor om meervoudige reflecties te gebruiken om informatie te leveren voor de missende nabije-afstandsdata door FWM te gebruiken, waar primaire en meervoudige reflecties gezamenlijk een beeld creëren van de ondiepe ondergrond. Gebruik maken van FWM met zijn gesloten-kring, gelijktijdige primaire en meervoudige reflectie beeldvormingsaanpak als data reconstructie methode, en het doorvoeren van de gereconstrueerde nabije-afstanden naar CL-SRME, zijn de belangrijkste componenten om de kwesties met ondiep water op een fysisch-consi-

stente manier aan te pakken. Dit nieuwe, geïntegreerde raamwerk heeft de grootste impact op een volledige 3D implementatie waarbij de metingen op een incompleet grid verkregen zijn. Daarom wordt ook een vergelijkbaar, trapsgewijs raamwerk voor 3D oppervlakte-gerelateerde meervoudige reflectievoorspelling in situaties met ondiep water voorgesteld in deze thesis, bestaande uit een data-reconstructie stap via 3D FWM en een oppervlakte-meervoudige voorspellingsstap via een 3D SRME methode. Verbeterde voorspellingen voor oppervlakte-meervoudinge en primaire reflecties, veroorzaakt door de goede data reconstructie van FWM, zijn bewezen voor zowel 2D als 3D synthetische data. Ongeacht het ontbreken van een nauwkeurig ondergronds-snelheidsmodel voor 2D veld-data, verbetert de FWM-gereconstrueerde nabije-afstands waterbodemreflecties nog steeds de kwaliteit van de voorspelde oppervlakte-meervoudige en primaire reflecties.

Om het dilemma van oppervlakte-gerelateerde meervoudige adaptieve aftrekkingsproces te verlichten, hebben we ook een tweetraps raamwerk voor oppervlakte-meervoudige reflectie lekkage extractie geïntroduceerd in deze thesis, en daarbij onze gereedschapskist voor het verwerken van seismische meervoudige reflecties uitgebreid. Het bovengenoemde tweetraps raamwerk, gebaseerd op lokale primairen-en-meervoudige reflectie orthogonalisatie (LPMO), is zowel veelzijdig als efficiënt voor gelekte meervoudige reflectie extractie, waardoor primaire reflecties beter worden behouden zonder veel meervoudige reflectieenergie over te laten. De voorkeur voor de initiële voorspellingsstap gaat over het algemeen uit naar SRME met een conservatieve adaptieve aftrekking, of een andere conservatieve meervoudige reflectievoorspellingsmethode, waarna LPMO volgt om de initieel voorspelde primaire en meervoudige reflecties te compenseren. Veelbelovende meervoudige reflectie-lekkage extractie is bereikt op zowel synthetische als veld-datasets. Hoewel efficiënt in vergelijking met een standaard aftrekking, is LPMO langzaam en rekenintensief. Daarom is een snelle LPMO (FLPMO) geïntroduceerd, gebaseerd op een geschaalde punt-per-punt deling, in plaats van de tijdsintensieve, shaping-regularisatie gebaseerde, iteratieve inversie, om zodoende het hele proces te versnellen. Resultaten voor twee verschillende veld-datasets laten een zeer vergelijkbare meervoudige reflectie-lekkage extractie zien vergeleken met LPMO, terwijl de geschaalde punt-per-punt divisie in FLPMO ongeveer 40 keer sneller is dan de shaping-regularisatie gebaseerde inversie in LPMO. Daarmee is het complete FLPMO raamwerk ongeveer vier keer sneller dan het LPMO raamwerk, waarmee het nu equivalent is aan de industriestandaard L2 adaptieve aftrekking.

Met de vooruitgang van deep-learning (DL) technologieën kunnen de bovengenoemde twee kwesties in ondiep water ook onderzocht worden via een U-Net-gebaseerd, DL neuraal netwerk (NN) raamwerk. Specifiek wordt een DL-gebaseerd de-alias NN geïntroduceerd voor de initiële oppervlakte-meervoudige reflectievoorspelling, waar de sterke data-fitting van DL direct de ge-aliasde meervoudige reflecties kan projecteren. Daarnaast is een DL-gebaseerd NN voor adaptieve aftrekking voorgesteld met zowel het totale golfveld en de voorspelde meervoudigen als twee ingangskanalen om het eerdergenoemde adaptieve aftrekkingsdilemma te overkomen. Op deze manier wordt de robuuste fysica, d.w.z., de voorspelde meervoudige reflecties, gebruikt. Voor het trainen zijn synthetische and velddata primaire reflectieresponsies als bekende uitkomsten gebruikt. Merk op dat de data verdeling tussen training en test data een significante rol speelt in deze U-Net toepassingen. Trainen op velddata en testen op nabije velddata laat de beste prestatie zien, vanwege overeenkomsten in de dataverdeling.

Ondiep water is heel uitdagend voor oppervlakte-gerelateerde meervoudige reflectievoorspelling. Fysisch-gebaseerde, deterministische aanpakken, zoals FWM-gebaseerde data reconstructie en LPMO, kunnen geofysici helpen om de essentie van het probleem beter te begrijpen en deels op te lossen. Voor slecht omschreven deterministische problemen, zoals adaptieve aftrekking en meervoudige reflectie de-aliasering, kan DL de onderliggende relaties vinden, wat niet eenvoudig haalbaar is via deterministische methodes. Het combineren van deterministische methodes en DL zal resulteren in een optimale prestatie. Dit is waar toekomstig onderzoek zich op zou moeten richten.

1

INTRODUCTION

1.1. OVERVIEW OF SEISMIC PROCESSING: ROLE OF PRIMARIES AND MULTIPLES

Seismic exploration is one of the best-known methods for exploring the subsurface with high resolution and large areal coverage, especially in the field of natural resource exploration and underground storage monitoring. The dynamite or vibrator lorry on land or the airgun at sea are used as a source to generate strong acoustic/elastic waves that can propagate through the earth. These waves are reflected back when they hit the boundary between layers with different physical properties, e.g., velocity and density. The reflected energy is then recorded by receivers deployed on the surface. In this way, the recorded seismic signals can be used to infer the structure of the subsurface and the properties of the media, and scientists can reveal hidden natural resources or changes in the subsurface. [1–3].

When seismic waves propagate through the earth, they follow the physical rules of acoustic/elastic waves, more specifically, acoustic waves in water and elastic waves in solids. Multiple scattering is a significant wave phenomenon in which we are interested in this thesis. Ideally, the energy that bounced back only once from the subsurface are extremely important for the conventional seismic data processing methods and the subsequent interpretation. This reflected energy is called seismic primaries. Current industry seismic processing workflows are basically primary-oriented, which include direct wave removal, random and swell noise removal, deghosting, wavelet deconvolution, multiple removal, velocity analysis, imaging and characterization [2]. However, due to the physics of multiple scattering, there always exists much energy that is reflected multiple times in the recorded data. These multiple reflected energy are seismic multiples, which consists of two categories [4]: surface-related multiples and internal multiples. Figure 1.1 demonstrates a simple illustration of seismic primaries and multiples. Surface-related multiples have bounced downward at the earth's surface at least once. Thus, they are those multiples that would disappear when the sea surface becomes transparent. Internal multiples have all downward bounces below the surface. Alternatively, surface-related multiples

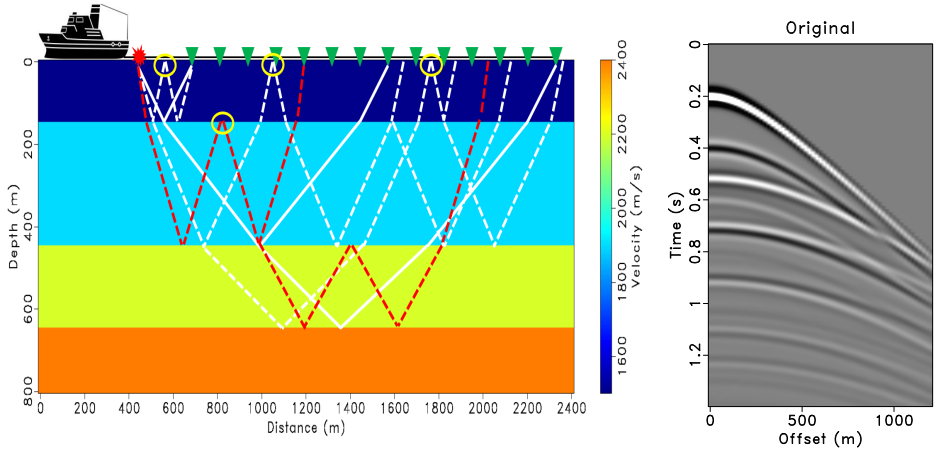

(a) (b)

Figure 1.1: Simple illustration of seismic primaries and multiples using a layered model (a) and its corresponding recorded original seismic data (b). Note that the seismic waves are generated via the air-gun (i.e., the red star) and recorded via the receivers (i.e., the green triangles) after propagation through the subsurface, where the white solid, the white dashed, and the red dashed lines represent primaries, surface-related multiples, and internal multiples, respectively.

and internal multiples can be distinguished via the shallowest interface where a downward reflection takes place as marked by the yellow circles. As indicated by the layered velocity model in Figure 1.1(a), seismic primaries are represented by the white solid lines while surface-related multiples are noted by the white dashed lines. Note that the red dashed lines describe internal multiples, which are not the priority of this thesis. Therefore, what we call "primaries" in this thesis also includes internal multiples. The corresponding recorded original seismic data including both primaries and surface-related multiples are shown in Figure 1.1(b). For better understanding and comparison, Figure 1.2 displays the double-sided original total data, the ground truth primaries and surface-related multiples (where the source is positioned in the middle of the receivers). In fact, the goal is to estimate both primaries and surface-related multiples directly from the original recorded total data (Figure 1.2(a)).

1.2. MULTIPLE REMOVAL OR MULTIPLE IMAGING

Surface-related multiples have been regarded as coherent noise and are removed before the subsequent processing workflows for decades [5–9]. Meanwhile, exploration geophysicists gradually realized that these multiples (note that we refer multiples to only surface-related multiples in this thesis and the internal multiples are beyond the scope of this research) are able to see through the earth multiple times and, therefore, carry valuable physical information about the subsurface [4]. Multiples are nowadays treated

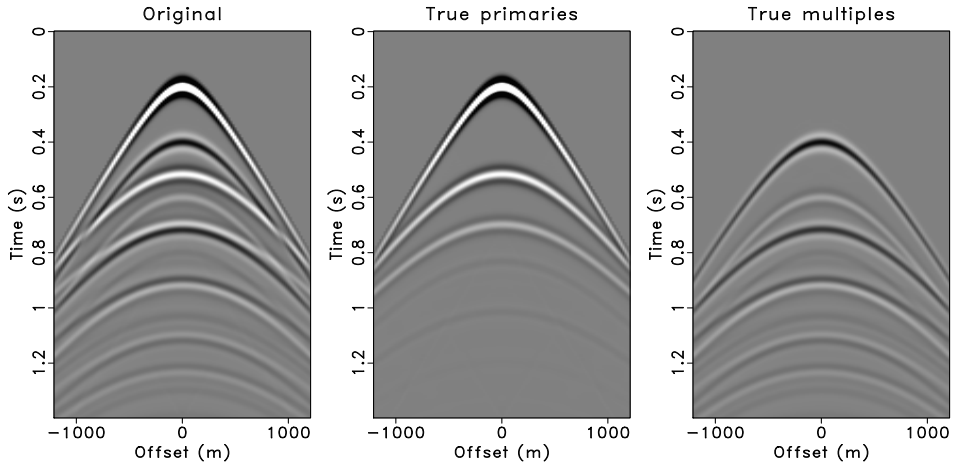

(a) (b) (c)

Figure 1.2: (a) Repeated original total data, but double sided. Ground truth primaries (b) and surface-related multiples (c) generated from the layered model in Figure 1.1(a).

as useful signals as well and can be directly included into imaging algorithms [10–15]. Although full wavefield imaging (including both primaries and all types of multiples) can be achieved, it is still desired to estimate primaries and multiples first and then image them separately, due to the crosstalk of multiples during imaging [14, 16], the challenges in shallow-water scenarios [17] and the benefits for conventional primary-oriented processing.

1.2.1. SURFACE-RELATED MULTIPLE ELIMINATION

Surface-related multiple elimination (SRME) has already been proved to be a powerful tool for multiple removal with the help of its data-driven engine and strong physics behind [18, 19]. Specifically, SRME first predicts the multiples based on a multidimensional convolution process from data itself without any prior knowledge about the subsurface, and then adaptively subtracts the predicted multiples from the original data using the minimum-energy criterion [7]. This is usually problematic in shallow water, and therefore, a full waveform inversion-based primary and multiple estimation scheme was proposed by [20, 21], which is known as estimation of primaries by sparse inversion (EPSI). [22] further proposed a robust version of EPSI based on L1-norm minimization. Concretely, the multiple prediction and adaptive subtraction process is replaced by a full waveform inversion process, in which the primary impulse response and source wavelet are the unknowns. Another inversion approach called closed-loop SRME (CL-SRME) with different parameterization, being primary and surface operator, was proposed by [23, 24], which combines the robustness of SRME with EPSI. Although the inversion schemes enjoy more physical consistency, they lack the computational efficiency, which is the bottle-neck for wide industry applications. SRME, in many cases, will still be the preferable choice in

terms of the computational cost.

Among all the difficulties for SRME, surface-related multiple leakage is a long-standing problem for primary and multiple estimation [4]. The leaked multiple energy will undoubtedly damage the subsequent migration and interpretation accuracy. Furthermore, this leaked energy is even more challenging for the already difficult shallow-water scenario due to the strong impact of missing near offsets [17, 20, 21, 24–28]. Both multiple prediction and adaptive subtraction parts are indispensable ingredients for SRME, and both of them could lead to the multiple leakage issue. In fact, multiple prediction is the most robust part in SRME because of its fulfillment of strong physics, but it still requires densely sampled data (near-offsets data for 2D situation and both under-sampling in crossline direction and near-offsets missing for 3D data), which is always difficult to satisfy in the real world [29]. Otherwise, the sampling issue results in both phase and amplitude errors for the predicted multiples. Thus, with the inaccurate predicted multiple model, it is more likely to limit the performance of adaptive subtraction and leave some amount of multiple leakage afterwards. Lots of efforts on data interpolation are spent to feed densely sampled data to SRME. [30] proposed to restore the missing offsets by parabolic Radon transform based on partial normal moveout corrected common-midpoint gathers. With unrecorded primary information hidden in the multiples, interferometric interpolation methods are available and effective to extract these hidden information for most 2D data interpolation cases [31, 32]. [20] also took advantage of the interferometry and presented an EPSI-based approach to reconstruct near-offsets data by utilizing multiples. Rather than the sparse constraint on the impulse response, [24] proposed to use the focal domain constraint to interpolate the missing data within the CL-SRME framework. An extreme version of focal constraint with many focal points actually is migration, therefore, [28] proposed to utilize the data reconstruction power of full wavefield migration as a better input for CL-SRME. As for the 3D case, [33] introduced a sparse inversion interpolation approach for 3D surface-related multiple prediction. A more general 3D SRME industry application with on-the-fly interpolation, which is called general surface multiple prediction (GSMP), is described by [34] and reviewed by [35].

Beside accurate prediction, adaptive subtraction is another problematic step in SRME, or other prediction and subtraction methods, due to its harsh assumption that primaries and multiples should not correlate in local windows [36]. The multiple leakage happens when primaries and multiples partially correlate, which is usually unavoidable. The core of adaptive subtraction is estimating a matching filter to correct for the amplitude and phase distortions. A dilemma between multiple leakage and multiple damage often occurs during adaptive subtraction, in which data processing practitioners usually reluctantly embrace the leakage rather than the damage that cannot be recovered anymore. [37] indicated the pitfalls of the L2-norm adaptive subtraction process where some part of the multiples is not orthogonal to the primaries. Many researchers have reported different approaches to improve the adaptive subtraction by relaxing its original assumption or replacing it. [38] proposed to utilize L1-norm instead of L2-norm adaptive subtraction when the primaries are much stronger than the multiples. Building on the work of [37], [39] showed on field data that the pattern-based subtraction method is less sensitive to this overlap between primaries and multiples, however, this method has difficulties when multiples and primaries are parallel to each other [4]. [40] proposed regularized

nonstationary regression-based adaptive subtraction without breaking the data into local windows. [41] introduced a nonlinear adaptive multiple subtraction method using the amplitude-preserving high-order sparse Radon transform. [42] presented a sparse curvelet-domain subtraction approach by iteratively shrinking the curvelet coefficients. Attracted by its effectiveness, a number of extended curvelet-based techniques are proposed [43–45]. However, the computational efficiency is currently the main drawback of sparsity-driven curvelet-based methods, and they also suffer the risk of dimming the primaries while removing multiples. In addition to the marine acquisition, [46] introduced a very detailed and much more difficult application of the adaptive subtraction for land seismic data.

Note that many non-SRME-type multiple removal approaches are also developed during the last several decades, e.g., Radon domain demultiple, which is able to attenuate multiples via the moveout difference between primaries and multiples [6], inverse-scattering series that can predict all possible internal multiples [8], Marchenko multiple elimination derived from projected Marchenko equations that can retrieve the primary response without any model information or adaptive subtraction [47], model-based water-layer demultiple method that is capable of removing the most difficult and dominant water-layer related multiples via modeling the Green's functions [48], etc. In addition, due to the advance of deep learning (DL)-based technology on seismic data processing and interpretation, multiple adaptive subtraction dilemma can be partially alleviated with the help from strong data fitting power of DL [49–51].

1.2.2. FULL-WAVEFIELD MIGRATION

A huge advantage of using surface-related multiples in imaging is extending the illumination for every single shot, which is able to overcome the limitations of the deployed acquisition geometry [52]. Since the sea surface can be regarded as a strong reflector, the surface-related multiples work as the secondary sources to better illuminate the subsurface via multiple scattering. More vertical propagation angles are achieved at the surface for a fixed source-receiver pair, which can also improve the angle coverage of the imaging. Meanwhile, more vertical multiple scattering rays are not only capable of enhancing the vertical resolution, but also providing an extra sensitivity for velocity estimation [53, 54]. Besides, surface multiple imaging can be extremely helpful when primary illumination is not enough, e.g., in the shadow zone.

Many efforts have been made to investigate the imaging with surface-related multiples for the last three decades [10, 14, 55–60]. Based on the initial concept of imaging multiples using up-down wavefield imaging principle proposed by [55], the early industry implementations have been developed for practical applications. Generally, surface-related multiples are migrated via re-injecting the recorded full wavefield as the illuminating source wavefield [60, 61]. Still, the crosstalk from unrelated orders of multiples becomes the most critical issue in imaging using surface-related multiples. To better deal with the problematic crosstalk issue, the inversion-based least-squares migration/imaging approach has been introduced to straightforwardly solve for the accurate solution [11, 12, 14, 16]. Despite the intensive computational cost, the inversion-based least-squares migration is presently the most optimal method for addressing the crosstalk issue in the imaging using surface-related multiples.

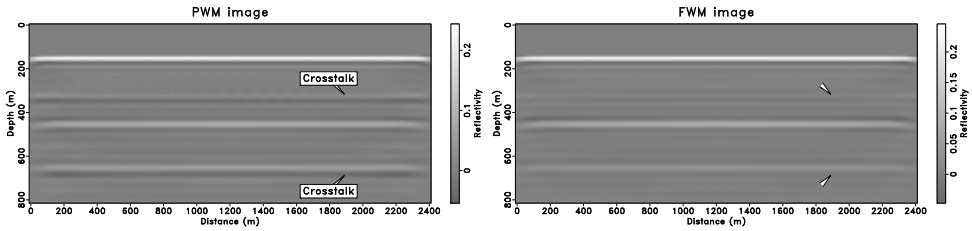

(a) (b)

Figure 1.3: Imaging comparison between PWM (a) and FWM (b). Note that the crosstalk comes from the multiple scattering energy.

Full-wavefield migration (FWM) is one of the aforementioned inversion-based least-squares migration methods taking multiples into the imaging process, which is initially proposed by [62]. Its robust capability for handling multiples comes from the core modeling engine, i.e., full-wavefield modeling (FWMod) [63]. Both multiple scattering and transmission effect are automatically taken into account via FWMod. [14] introduce the practical FWM implementations using both surface and internal multiples, and various imaging conditions and crosstalk attenuation mechanism are also discussed. [64] propose imaging with surface-related multiples via FWM to overcome large acquisition gaps, in which the modeled full wavefield are re-injected in the forward modeling process. Note that internal multiples can be automatically taken into consideration in FWM process, and a detailed field data example is provided by [15]. Figure 1.3 shows a simple demonstration of FWM compared to the traditional primary wavefield migration (PWM) using the same layered model from Figure 1.1(a). The crosstalk can be clearly observed from the PWM image due to its incapability of taking multiple scattering into account. However, FWM can easily attenuate such crosstalk via its more advanced modeling engine as shown in Figure 1.3(b).

1.3. INFLUENCE FROM WATER DEPTH

The water depth of the survey area is an extremely important factor on the option of multiple removal or/and multiple imaging. Seismic event curvature, the lateral amplitude variation, the overlap between primaries and multiples, the effect of missing near offsets, and the added benefits of multiple imaging are all related to water depth. Among them, the seismic event curvature and its lateral amplitude variation strongly affects the performance of the near-offset reconstruction required by SRME-type multiple estimation approaches. Note that the issue with missing near offsets is mainly caused by the practical logistic reason during the acquisition step. In addition, the overlap between primaries and multiples leads to severe difficulties for the multiple adaptive subtraction during the conventional SRME methods. Figure 1.4 demonstrates a direct field shot record comparison between a deep and shallow water environment. The corresponding zoom-in field shot records can be found in Figure 1.5. It can be clearly observed that the seismic event curvature, the lateral amplitude variation and the arrival time of surface multiples are their

fundamental differences. Note that the missing near offsets appear in both scenarios. It is extremely important to be aware of the fact that the water depth is simply a more straightforward and intuitive concept for helping us define our challenge. In fact, many different factors are combined together to determine whether it is "shallow" or "deep" water for the specific data. Such factors include the data frequency bandwidth, the size of the missing data gap and the medium contrasts. For example, 100 m water depth seems shallow for seismic data with ~ 100 Hz frequency bandwidth, however, it would be deep for high-frequency data with ~ 1000 Hz bandwidth.

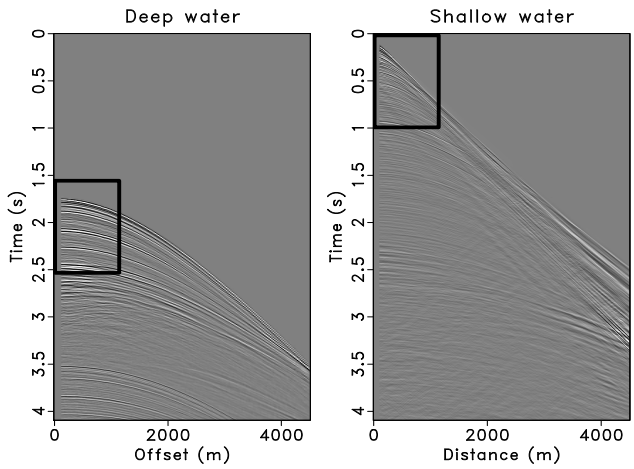

Figure 1.4: Seismic field shot records with missing near offsets from (a) deep water and (b) shallow water environment. Please note the fundamental differences between deep and shallow water environment, i.e., the event curvature, the lateral amplitude variation and the arrival time of surface multiples.

1.3.1. MEDIUM-DEPTH AND DEEP WATER ENVIRONMENT

A medium-depth and deep water environment for seismic exploration frequency range indicates that the water depth is usually more than 200 m. With such water depth, it is fairly convenient and straightforward to implement multiple removal due to the relative simplicity of the data. One example of seismic record from a deep water environment is shown in Figure 1.4(a) and 1.5(a), which is from the Norwegian Sea with approximately 1300 m water depth. More specifically, we can easily see that the earlier seismic events have relatively small curvature and their lateral amplitude variation is also small. The aforementioned event features will result in almost perfect near-offset reconstruction that is significant for SRME-type multiple estimation methods. Besides, due to the deep water depth, the water bottom reflection are generated at around 1.7 s, and thus, the surface-related multiples start to appear at around 3.5 s, which already have less influence on the target events above. Less primary and multiple overlaps are also extremely helpful to the

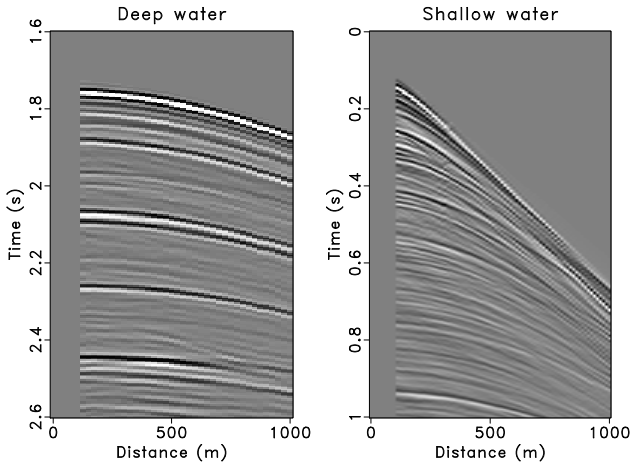

(a) (b)

Figure 1.5: The corresponding zoom-in field shot records indicated by the black boxes in Figure 1.4.

adaptive subtraction process, in which the more aggressive subtraction can be applied without worrying too much on primary damage. Note that in this part we broadly refer to non-shallow water environment since "deep water" has its own definition and challenges.

1.3.2. SHALLOW WATER ENVIRONMENT AND CHALLENGES

A shallow water environment in this thesis refers to a water depth between 50 to 200 m with respect to seismic exploration frequency range. The Nelson North Sea data used in this thesis are regarded as shallow-water data due to the combined factors, i.e., 5-80 Hz bandwidth, 225 m missing gap size, and 95 m water depth. Note that water depth smaller than 50 m conventionally refers to ultra-shallow water environment, which is beyond the scope of this research. As shown in Figure 1.4(b) and 1.5(b), the Nelson field seismic data are recorded at the British North Sea with average 95 m water depth. Because of the shallow water depth, it can be observed that the seismic events are highly curved, which can lead to strong stretching effects for the conventional near-offset reconstruction methods that employ normal moveout correction as an intermediate step [30]. Meanwhile, strong lateral amplitude variation displayed in the shallow water seismic data makes the data reconstruction even more difficult. In addition, we can notice that the surface-related multiples arrive much earlier (i.e., approximately 0.1 s) compared to the deep water scenario. Thus, shallow water depth also results in more complex overlap between primaries and multiples, which poses severe challenges for the adaptive subtraction process.

Sometimes in a shallow water environment, the multiples are so strong that they dominate the data, while only providing limited extra information of the target area. Therefore, primary and multiple separation is desired for shallow water environment. Two most important challenges for shallow water multiple estimation are introduced in detail:

- **Data coverage on multiple estimation**
  In a shallow water environment, the missing near-offsets have a strong negative effect on the ability of SRME-type methods to provide reliable results [4, 29]. Acquiring such near-offsets is usually difficult due to the operational constraints. There are many reports on acquiring near-offsets and decreasing crossline sampling in 3D. [65] introduce shooting over the seismic spread to record the important near-offsets. [66] propose to also include the negative offsets in 2D for surface multiple estimation. [67] demonstrate the shallow-water free-surface multiple attenuation on multimeasurement data under dense crossline sampling. Optimizing acquisition parameters for one-sided towed streamer in 3D is discussed by [68] and [69]. The aforementioned efforts in acquisition illustrate clearly the concerns due to near-offset gaps. However, when provided with accurately reconstructed near-offset data, the SRME-based approaches are shown to provide more consistent multiple suppression results [70]. Therefore, alternatives for handling shallow water multiples are being considered that rely on modeling/reconstructing the reverberations and water layer multiples with model-driven components to partly overcome the incomplete data acquisition issue [48, 71–74]. Besides, [24] introduce an inversion component by considering sparseness in the focal domain [75] as a constraint for shallow water data interpolation. [35] introduce on-the-fly interpolation for 3D SRME as an industry standard. Still, the data coverage remains as the most challenging issue for multiple estimation. With the help of imaging multiple scattering, FWM might achieve an accurate data reconstruction (i.e., including both near-offsets and crossline undersampling) using the FWM image as a strong constraint. This will be proposed in this thesis.

- **Adaptive subtraction dilemma**
  Despite all the efforts mentioned above to provide better reconstructed data for multiple estimation, surface-related multiple leakage or primary damage after the adaptive subtraction still can be seen in the results of SRME predicted primaries. The reasons behind are simply because: first, the data reconstruction can never be perfect, which leads to both phase and amplitude errors in the predicted multiples. Second, the assumption of adaptive subtraction that primaries and multiples do not correlate is often not met. Third, 2D prediction methods are applied on 3D data [4]. Essentially, the imperfections of adaptive subtraction directly lead to multiple leakage in the estimated primaries. It tends to be either underfitting or overfitting for the subtraction step regardless of the forced constraint. Underfitting results in more severe multiple leakage while overfitting can alleviate multiple leakage to some extent. However, overfitting is unfortunately the main cause for primary energy damage, as removing more multiples usually comes along with damaging primaries. This so-called adaptive subtraction dilemma between multiple leakage and primary damage usually occurs. The ability of least-squares adaptive subtraction strongly depends on the size of local windows and the filter length [18]. A small window size and a relatively long filter length, which is called “standard SRME” in this thesis, leads to better multiple removal, but at the same time causes more primary damage. For the primary-oriented processing, the best one can achieve during the trade-off is to protect the primaries as much as possible and, as a result, leave some amount of mul-

tiple leakage. That is to say, the local windows for SRME should be relatively large and the filter length for adaptive subtraction should be relatively short. We name this type of SRME as the "conservative SRME". More specifically, note that in this thesis, conservative SRME indicates the L2-norm adaptive subtraction step in the last iteration with large local windows or even global windows and a relatively short filter length, in which the primaries are not damaged while surface-related multiple leakage is more severe. In contrast, standard SRME means the L2/L1-norm adaptive subtraction step in the last iteration with small local windows and a relatively long filter length, in which the multiple leakage is alleviated while the primary damage is more severe. Instead of solving the leakage issue within the SRME itself, it might be much easier and more effective if another external multiple leakage extraction step is included after the conservative SRME to compensate for the multiple leakage. Meanwhile, DL, with its strong data fitting ability, might also have the potential to solve the adaptive subtraction dilemma.

1.4. RESEARCH QUESTIONS AND THESIS OUTLINE

Accordingly, the most important research questions that need to be investigated in this thesis are listed below:

- Can we take advantage of multiple imaging to alleviate the data coverage problem, especially the near-offset missing in shallow water, from all of the SRME-type approaches? (Chapter 2)
- Can we overcome the large computation cost and data storage of multiple imaging for data reconstruction and the inversion-type SRME in real 3D acquisition? (Chapter 3)
- Is there a fast, simple but effective recipe to relieve the multiple adaptive subtraction dilemma in industry? (Chapter 4 & Chapter 5)
- How can DL-based technology help us solve the exact same issues mentioned above from a very non-linear perspective? (Chapter 6 & Chapter 7)

Correspondingly, a list of our prime contributions is presented in advance before diving into the remaining chapters:

- We propose an integrated CL-SRME and FWM framework for accurate surface-related multiple estimation to tackle the unrecorded data reconstruction issue, which is further extended to a 3D scenario for SRME-type methods.
- We introduce local primary-and-multiple orthogonalization (LPMO) and its fast version for surface-related multiple leakage extraction, which mitigates the typical dilemma between primary damage and multiple leakage for standard adaptive subtraction.
- We investigate DL neural network with both total full wavefield and predicted surface multiples as two input channels to overcome the adaptive subtraction dilemma, and introduce DL-based multiple de-aliasing to attack the data sampling issue.

Finally, a general outline of the thesis will be given in the following:

- **Chapter 2:**
  In this chapter, an integrated framework is proposed to partially overcome the data coverage problem for the inversion-based CL-SRME. The crucial missing near offsets are reconstructed via FWM, which are combined with the original recorded data to form the complete data for multiple estimation. Both 2D synthetic and field data from the North Sea demonstrate the good performance of the integrated framework for reconstructing more accurate missing near offsets and estimating surface-related multiples in a shallow water environment.

- **Chapter 3:**
  This chapter further extends the proposed integrated framework in chapter 2 to a realistic 3D scenario. However, due to the limited data storage and computing power, it is very difficult to reconstruct the full sampling data set in 3D. Inversion-based CL-SRME also has a large computational cost. Based on our initial investigation, GSMP with FWM-reconstructed near offsets seems to be the most feasible and affordable solution. Two 3D synthetic examples are used to test the performance of FWM-aided GSMP in shallow water.

- **Chapter 4:**
  The multiple adaptive subtraction dilemma is first discussed and then alleviated by a simple but effective framework in this chapter. Primary damage is more severe than multiple leakage because the distorted primaries can hardly be recovered. Accordingly, more conservative adaptive subtraction is preferred, which mainly results in multiple leakage. LPMO is then proposed to extract the leaked multiples from the initially estimated primaries. This two step framework, i.e., first the initial conservative primary/multiple estimation and then the multiple leakage extraction via LPMO, is tested on two different synthetic examples with good accuracy. A 2D field data on the North Sea further proves the effectiveness of the proposed LPMO framework.

- **Chapter 5:**
  This chapter introduces a fast version of the previous proposed LPMO framework for higher efficiency. The original LPMO involves a large computational cost due to many conjugate-gradient iterations within the shaping regularization-based inversion framework. A scaled point-by-point division is used to avoid the iterative inversion in the original LPMO, which is called fast LPMO (FLPMO) framework. Two field data examples from the North Sea are used to prove the FLPMO performance compared to the original LPMO.

- **Chapter 6:**
  In this chapter, DL-based technology is brought forward to tackle the exact same issue mentioned in chapter 4, i.e., the multiple adaptive subtraction dilemma, from the perspective of a non-linear data mapping process. Due to the imperfections of the estimated multiples, the adaptive subtraction becomes a highly non-stationary and non-linear step, which is actually a very suitable task for DL. More specifically,

the U-Net is one of the most stable and powerful image-to-image mapping tool in the field of DL. Instead of directly mapping the full wavefield to the estimated primaries via any advanced multiple estimation approach, both full wavefield and the initially estimated multiples are used as two input channels, and the U-Net is trained on synthetic modeled primaries only. By including the estimated multiples in the second input channel of U-Net, the robust physics is taken into consideration by the deep neural network. Besides, the synthetic modeled true primaries are extremely helpful to the training, and thus, the adaptive subtraction dilemma can be partially overcome. Three different examples are used to demonstrate the performance of DL-based adaptive subtraction.

- **Chapter 7:**
  This chapter investigates another possibility of DL-based technology on helping the data coverage issue mentioned in chapter 2. The multidimensional convolution process inside the SRME-type methods requires dense data sampling on both source and receiver side. In real 3D marine acquisition, the source sampling is far from ideal, which leads to strong aliasing effect in the estimated multiples. Thus, the corresponding primaries are also severely affected. Instead of the nontrivial source interpolation, dealiasing on the estimated multiples with limited number of sources might be a potential alternative. DL is capable of handling this non-linear dealiasing task. The neural network (i.e., U-Net) can be trained on the pairs of the aliased multiples and the corresponding non-aliased multiples. This proposed DL framework is tested on a 2D field data from the North Sea.

- **Chapter 8:**
  The final conclusions of this thesis and some further recommendations for the future research are given in this chapter.

- **Appendix A:**
  Appendix in the end introduces a technical study related to seismic internal multiples, which is beyond the scope of this surface multiples-related thesis. However, the similar LPMO framework is applied on the FWM image as a post-processing step to further reduce the leaked internal multiple crosstalk.

REFERENCES

[1] A. J. Berkhout, *Seismic migration: Imaging of acoustic energy by wave field extrapolation, A: Theoretical aspects* (Elsevier (second edition), 1982).

[2] Ö. Yilmaz, *Seismic data analysis* (Society of Exploration Geophysicists, 2001).

[3] A. Gisolf and D. J. Verschuur, *The principles of quantitative acoustical imaging* (EAGE Publications, 2010).

[4] D. J. Verschuur, *Seismic multiple removal techniques : past, present and future* (EAGE Publications, 2013).

[5] J. V. Ryu, *Decomposition (DECOM) approach applied to wave field analysis with seismic reflection records*, Geophysics **47** (1982), pp. 869–883.

[6] D. Hampson, *Inverse velocity stacking for multiple elimination,* in *56th SEG Technical Program Expanded Abstracts* (Society of Exploration Geophysicists, 1986).

[7] D. J. Verschuur and A. J. Berkhout, *Estimation of multiple scattering by iterative inversion, Part II: Practical aspects and examples,* Geophysics **62** (1997), pp. 1596–1611.

[8] A. B. Weglein, F. A. Gasparotto, P. M. Carvalho, and R. H. Stolt, *An inverse-scattering series method for attenuating multiples in seismic reflection data,* Geophysics **62** (1997), pp. 1975–1989.

[9] W. Chen, J. Xie, S. Zu, S. Gan, and Y. Chen, *Multiple-reflection noise attenuation using adaptive randomized-order empirical mode decomposition,* IEEE Geoscience and Remote Sensing Letters **14** (2017), pp. 18–22.

[10] M. P. Brown and A. Guitton, *Least-squares joint imaging of multiples and primaries,* Geophysics **70** (2005), pp. S79–S89.

[11] D. Zhang and G. T. Schuster, *Least-squares reverse time migration of multiples,* Geophysics **79** (2014), pp. S11–S21.

[12] S. Lu, D. N. Whitmore, A. A. Valenciano, and N. Chemingui, *Separated-wavefield imaging using primary and multiple energy,* The Leading Edge **34** (2015), pp. 770–778.

[13] A. Nath and E. Verschuur, *Using surface-related multiples in imaging for data with large acquisition gaps,* in *87th SEG Technical Program Expanded Abstracts* (Society of Exploration Geophysicists, 2017).

[14] M. Davydenko and D. J. Verschuur, *Full-wavefield migration: using surface and internal multiples in imaging,* Geophysical Prospecting **65** (2016), pp. 7–21.

[15] M. Davydenko and D. J. Verschuur, *Including and using internal multiples in closed-loop imaging — Field data examples,* Geophysics **83** (2018), pp. R297–R305.

[16] S. Lu, L. Qiu, and X. Li, *Addressing the crosstalk issue in imaging using seismic multiple wavefields,* Geophysics **86** (2021), pp. S235–S245.

[17] C. Kostov, F. Xavier de Melo, A. Raj, A. Zarkhidze, A. Cooke, G. Miers, and J. Bacon, *Multiple attenuation for shallow-water surveys: Notes on old challenges and new opportunities,* The Leading Edge **34** (2015), pp. 760–768.

[18] D. J. Verschuur, A. J. Berkhout, and C. P. A. Wapenaar, *Adaptive surface-related multiple elimination,* Geophysics **57** (1992), pp. 1166–1177.

[19] A. J. Berkhout and D. J. Verschuur, *Estimation of multiple scattering by iterative inversion, Part I: Theoretical considerations,* Geophysics **62** (1997), pp. 1586–1595.

[20] G. J. van Groenestijn and D. J. Verschuur, *Estimating primaries by sparse inversion and application to near-offset data reconstruction,* Geophysics **74** (2009), pp. A23–A28.

[21] G. J. A. van Groenestijn and D. J. Verschuur, *Estimation of primaries and near-offset reconstruction by sparse inversion: Marine data applications,* Geophysics **74** (2009), pp. R119–R128.

[22] T. T. Y. Lin and F. J. Herrmann, *Robust estimation of primaries by sparse inversion via one-norm minimization,* Geophysics **78** (2013), pp. R133–R150.

[23] G. A. Lopez and D. J. Verschuur, *Closed-loop SRME — A new direction in surface multiple removal algorithms,* in *76th EAGE Conference and Exhibition* (European Association of Geoscientists & Engineers, 2014).

[24] G. A. Lopez and D. J. Verschuur, *Closed-loop surface-related multiple elimination and its application to simultaneous data reconstruction,* Geophysics **80** (2015), pp. V189–V199.

[25] N. Hargreaves, *Surface multiple attenuation in shallow water and the construction of primaries from multiples,* in *76th SEG Technical Program Expanded Abstracts* (Society of Exploration Geophysicists, 2006).

[26] H. Jin and P. Wang, *Model-based water-layer demultiple (MWD) for shallow water: from streamer to OBS,* in *82nd SEG Technical Program Expanded Abstracts* (Society of Exploration Geophysicists, 2012).

[27] B. Hung, M. Wang, K. Yang, and X. Wu, *Enhanced internal multiple attenuation in shallow water environment,* in *84th SEG Technical Program Expanded Abstracts* (Society of Exploration Geophysicists, 2014).

[28] D. Zhang and E. Verschuur, *Integration of closed-loop surface-related multiple estimation and full wavefield migration for shallow water,* in *81st EAGE Conference and Exhibition* (European Association of Geoscientists & Engineers, 2019).

[29] W. H. Dragoset and Ž. Jeričević, *Some remarks on surface multiple attenuation,* Geophysics **63** (1998), pp. 772–789.

[30] M. M. N. Kabir and D. J. Verschuur, *Restoration of missing offsets by parabolic radon transform,* Geophysical Prospecting **43** (1995), pp. 347–368.

[31] Y. Wang, Y. Luo, and G. T. Schuster, *Interferometric interpolation of missing seismic data,* Geophysics **74** (2009), pp. SI37–SI45.

[32] S. M. Hanafy and G. T. Schuster, *Interferometric interpolation of sparse marine data,* Geophysical Prospecting **62** (2013), pp. 1–16.

[33] E. J. van Dedem and D. J. Verschuur, *3D surface-related multiple prediction: A sparse inversion approach,* Geophysics **70** (2005), pp. V31–V43.

[34] I. Moore and B. Dragoset, *General surface multiple prediction: a flexible 3D SRME algorithm,* First Break **26** (2008), pp. 89–100.

[35] B. Dragoset, E. Verschuur, I. Moore, and R. Bisley, *A perspective on 3D surface-related multiple elimination,* Geophysics **75** (2010), pp. 75A245–75A261.

[36] M. M. N. Kabir and K. J. Marfurt, *Toward true amplitude multiple removal,* The Leading Edge **18** (1999), pp. 66–73.

[37] S. Spitz, *Pattern recognition, spatial predictability, and subtraction of multiple events,* The Leading Edge **18** (1999), pp. 55–58.

[38] A. Guitton and D. J. Verschuur, *Adaptive subtraction of multiples using the L1-norm,* Geophysical Prospecting **52** (2004), pp. 27–38.

[39] A. Guitton, *Multiple attenuation in complex geology with a pattern-based approach,* Geophysics **70** (2005), pp. V97–V107.

[40] S. Fomel, *Adaptive multiple subtraction using regularized nonstationary regression,* Geophysics **74** (2009), pp. V25–V33.

[41] Y. Xue, J. Yang, J. Ma, and Y. Chen, *Amplitude-preserving nonlinear adaptive multiple attenuation using the high-order sparse radon transform,* Journal of Geophysics and Engineering **13** (2016), pp. 207–219.

[42] F. J. Herrmann and E. Verschuur, *Curvelet-domain multiple elimination with sparseness constraints,* in *74th SEG Technical Program Expanded Abstracts* (Society of Exploration Geophysicists, 2004).

[43] F. J. Herrmann, D. Wang, and D. J. Verschuur, *Adaptive curvelet-domain primary-multiple separation,* Geophysics **73** (2008), pp. A17–A21.

[44] D. Wang, R. Saab, Ö. Yilmaz, and F. J. Herrmann, *Bayesian wavefield separation by transform-domain sparsity promotion,* Geophysics **73** (2008), pp. A33–A38.

[45] R. N. Neelamani, A. Baumstein, and W. S. Ross, *Adaptive subtraction using complex-valued curvelet transforms,* Geophysics **75** (2010), pp. V51–V60.

[46] P. G. Kelamis and D. J. Verschuur, *Surface-related multiple elimination on land seismic data—Strategies via case studies,* Geophysics **65** (2000), pp. 719–734.

[47] L. Zhang and E. Slob, *Free-surface and internal multiple elimination in one step without adaptive subtraction,* Geophysics **84** (2019), pp. A7–A11.

[48] P. Wang, H. Jin, S. Xu, and Y. Zhang, *Model-based water-layer demultiple,* in *81st SEG Technical Program Expanded Abstracts* (Society of Exploration Geophysicists, 2011).

[49] A. Siahkoohi, D. J. Verschuur, and F. J. Herrmann, *Surface-related multiple elimination with deep learning,* in *89th SEG Technical Program Expanded Abstracts* (Society of Exploration Geophysicists, 2019).

[50] A. Siahkoohi, M. Louboutin, and F. J. Herrmann, *The importance of transfer learning in seismic modeling and imaging,* Geophysics **84** (2019), pp. A47–A52.

[51] A. Kumar, H. Gary, and T. Rayment, *Adaptive subtraction using a convolutional neural network,* First Break **39** (2021), pp. 35–45.

[52] M. Davydenko, *Full wavefield migration: Seismic imaging using multiple scattering effects*, Ph.D. thesis (2016).

[53] A. J. Berkhout and D. J. Verschuur, *Enriched seismic imaging by using multiple scattering,* The Leading Edge **35** (2016), pp. 128–133.

[54] A. J. Berkhout, *Review paper: An outlook on the future of seismic imaging, Part III: Joint migration inversion,* Geophysical Prospecting **62** (2014), pp. 950–971.

[55] A. J. Berkhout and D. J. Vershuur, *Multiple technology: Part 2, Migration of multiple reflections,* in *64th SEG Technical Program Expanded Abstracts* (Society of Exploration Geophysicists, 1994).

[56] R. Muijs, J. O. Robertsson, and K. Holliger, *Prestack depth migration of primary and surface-related multiple reflections: Part I — Imaging,* Geophysics **72** (2007), pp. S59–S69.

[57] Y. Liu, X. Chang, D. Jin, R. He, H. Sun, and Y. Zheng, *Reverse time migration of multiples for subsalt imaging,* Geophysics **76** (2011), pp. WB209–WB216.

[58] N. Tu and F. J. Herrmann, *Fast imaging with surface-related multiples by sparse inversion,* Geophysical Journal International **201** (2015), pp. 304–317.

[59] M. Wong, B. Biondi, and S. Ronen, *Imaging with multiples using least-squares reverse time migration,* The Leading Edge **33** (2014), pp. 970–976.

[60] S. Lu, *Migration using sea surface-related multiples: Challenges and opportunities,* Geophysics **86** (2021), pp. WC11–WC19.

[61] D. J. Verschuur and A. J. Berkhout, *Seismic migration of blended shot records with surface-related multiple scattering,* Geophysics **76** (2011), pp. A7–A13.

[62] A. J. Berkhout, *Review paper: An outlook on the future of seismic imaging, Part II: Full-wavefield migration,* Geophysical Prospecting **62** (2014), pp. 931–949.

[63] A. J. Berkhout, *Review paper: An outlook on the future of seismic imaging, Part I: forward and reverse modelling,* Geophysical Prospecting **62** (2014), pp. 911–930.

[64] A. Nath and D. J. Verschuur, *Imaging with surface-related multiples to overcome large acquisition gaps,* Journal of Geophysics and Engineering **17** (2020), pp. 742–758.

[65] V. Vinje, J. E. Lie, V. Danielsen, P. E. Dhelle, R. Silliqi, C. Nilsen, E. Hicks, and A. Camerer, *Shooting over the seismic spread,* First Break **35** (2017), pp. 97–104.

[66] M. Majdański, C. Kostov, E. Kragh, I. Moore, M. Thompson, and J. Mispel, *Attenuation of free-surface multiples by up/down deconvolution for marine towed-streamer data,* Geophysics **76** (2011), pp. V129–V138.

[67] F. Xavier de Melo, C. Kostov, and A. Cooke, *Shallow-water free-surface multiple attenuation on multimeasurement data - A case study from the North Sea,* in *78th EAGE Conference and Exhibition* (European Association of Geoscientists & Engineers, 2016).

[68] L. T. Goss, U. Egozi, B. Ong, S. Sahai, M. Simon, and X. Meng, *Shallow water 3D SRME - A case study from West Africa,* in *73rd EAGE Conference and Exhibition* (European Association of Geoscientists & Engineers, 2011).

[69] L. T. Goss, P. Wang, Z. Meng, N. Chazalnoel, C. Ting, S. Sahai, X. Meng, D. Maguire, and S. Knapp, *Shallow water 3D MWD - A case study from West Africa,* in *75th EAGE Conference and Exhibition* (European Association of Geoscientists & Engineers, 2013).

[70] R. H. Baardman, D. J. Verschuur, R. G. van Borselen, M. O. Frijlink, and R. F. Hegge, *Estimation of primaries by sparse inversion using dual-sensor data,* in *80th SEG Technical Program Expanded Abstracts* (Society of Exploration Geophysicists, 2010).

[71] D. Lokshtanov, *Suppression of water-layer multiples and peg-legs by wave-equation approach,* in *63rd EAGE Conference and Exhibition* (European Association of Geoscientists & Engineers, 2001).

[72] A. Pica, G. Poulain, B. David, M. Magesan, S. Baldock, T. Weisser, P. Hugonnet, and P. Herrmann, *3D surface-related multiple modeling,* The Leading Edge **24** (2005), pp. 292–296.

[73] K. Yang and B. Hung, *Shallow water demultiple with seafloor reflection modeling using multichannel prediction operator,* in *82nd SEG Technical Program Expanded Abstracts* (Society of Exploration Geophysicists, 2012).

[74] H. Jin, M. Yang, P. Wang, Y. Huang, M. J. Parry, and Y. Paisant-Allen, *Application of MWD for shallow water demultiple - Hibernia case study,* in *74th EAGE Conference and Exhibition* (European Association of Geoscientists & Engineers, 2012).

[75] A. J. Berkhout and D. J. Verschuur, *Focal transformation, an imaging concept for signal restoration and noise removal,* Geophysics **71** (2006), pp. A55–A59.

2

CLOSED-LOOP SRME WITH FWM-RESTORED NEAR OFFSETS

Reliably separating primary and multiple reflections in a shallow water environment (i.e., 50 m to 200 m water depth) still remains a challenge. The success of previously published closed-loop surface-related multiple estimation (CL-SRME) depends heavily on the data coverage, i.e., the near-offset reconstruction. Therefore, we propose the integrated framework of CL-SRME and full-wavefield migration (FWM). Multiples recorded in the data are capable of helping reduce the acquisition imprint of the FWM image. With this image as a strong constraint, we are able to reconstruct the data at near-offsets, which is essential for better primary and multiple estimation during CL-SRME. FWM applied in a non-linear way can avoid the negative influences from the missing data, and at the same time bring in more physics between primaries and multiples. The FWM image of the top part of the subsurface is also used to back-project the information from multiples to primaries with the physical constraint of all this information belongs to the same earth model, provided that a good description of the source wavefield and a reasonable velocity model are available. The proposed integrated framework first reconstructs near-offsets via the closed-loop imaging process of FWM and then feeds the complete reconstructed data to CL-SRME for better primary and multiple estimation. A good performance is demonstrated on both 2D synthetic and field data examples in a challenging shallow water environment.

This chapter is a slightly updated version of the published paper "D. Zhang and D. J. Verschuur, Closed-loop surface-related multiple estimation with full wavefield migration-reconstructed near-offsets for shallow water, Geophysics 86 (2021), pp. WC21–WC30".

2.1. INTRODUCTION

Closed-loop surface-related multiple estimation (CL-SRME) is an inversion-based and fully data-driven primary/multiple estimation method [1, 2], which still uses the core surface-related multiple elimination (SRME) engine [3, 4], i.e., the robust physics between primaries and multiples. Instead of updating the primary impulse response and source wavelet in the previously published inversion-based method (i.e., estimating primaries by sparse inversion (EPSI) [5]), CL-SRME directly estimates primaries and surface operator in a flip-flop manner. Although many successful applications have been achieved, data sampling still poses the biggest challenge for CL-SRME, especially the missing near-offsets for shallow water scenarios [6–9]. The definition of shallow water in this thesis ranges from 50 m to 200 m water depth for typical exploration seismic surveys. Note that what we call “primaries" in this thesis also includes internal multiples.

Despite all the efforts, shallow water still remains challenging for CL-SRME due to data coverage, and 3D shallow water will be even more challenging. More specifically, the acquisition geometry with coarse crossline sampling and large near-offset gaps, the geological discontinuities (e.g., small channels) and the highly-curved shallow seismic events with strong lateral amplitude variation all create huge challenges for surface multiple estimation. Note that both aforementioned EPSI and focal CL-SRME, although successful for 2D data, are difficult to extend to a 3D scenario due to their weak constraints and the challenging sampling issue. Thus, we need a stronger constraint on data reconstruction to help CL-SRME achieve a better primary and multiple estimation for a challenging shallow water environment. Imposing sparseness in the focal domain with only a few depth levels appears not enough for larger near-offset gaps [2]. Therefore, many more depth levels are needed in the focal domain and a more accurate velocity model is also required for keeping the reflection information close to the focal point. In the limit, with a focal domain at every depth level, the focal transform becomes a least-squares imaging algorithm. To further exploit data redundancy, simultaneous imaging of primaries and all multiples, the full wavefield migration (FWM) [10], will use all available data information in a consistent process. FWM belongs to the least-squares migration family, and its unique modeling engine (i.e., full wavefield modeling (FWMod) [11]) allows it to account for both multiple scattering and transmission effects. Many successful applications have been reported to confirm the multiple imaging and data reconstruction power of FWM [12–15]. Among them, the non-linear FWM is proposed to overcome the data with missing gaps [15]. Thus, we propose the integrated framework of CL-SRME and FWM for shallow water, i.e., CL-SRME with FWM-reconstructed near-offsets. Besides, in the proposed framework, we use the image to back-project the information from multiples to primaries with the physical constraint of all information related to the same earth model, provided that a good description of the source wavefield and a reasonable velocity model are available. This image only functions as some transformed domain, and its main purpose is to support a better near-offset reconstruction. However, the resulting image can also be seen as a valuable by-product of this method, as it is known that multiples considerably enhance the image of the shallow part of the subsurface [16, 17]. Thus, by accurately removing the multiples from the data to enable clearer imaging of the deep structures and simultaneously obtaining a high-resolution image of the shallow subsurface, this approach yields a strong dual output. By combining the primary estimation ability of CL-SRME [2] with the

strong reconstruction power of FWM [13, 15] we should be able to obtain a better primary and multiple estimation. The synthetic example in this chapter demonstrates the significant contribution of near-offset quality on primary and multiple estimation, while the field data example shows the reconstructed missing water bottom reflections are sensitive enough to steer the CL-SRME inversion process to a better primary/multiple separation. Although the missing part of water bottom reflections seem small in the time-offset domain, it has large coverage in terms of reflection angles. Please note that this chapter aims to confirm the proposed integrated CL-SRME and FWM framework on 2D cases, although the future benefits lies in 3D.

This chapter is arranged as follows: a short introduction of CL-SRME and FWM will be presented first. Then the proposed integration of CL-SRME and FWM framework will be described in details. Results with a synthetic and a field example are demonstrated to show the performance of the proposed framework. A discussion and conclusion will finalize the chapter.

2.2. THEORY AND METHODOLOGY

2.2.1. REVIEW OF CL-SRME

We present a brief review of CL-SRME in this section, which was originally proposed by [1]. Instead of estimating the primary impulse response and source wavelet in EPSI [5], CL-SRME directly estimates the desired primaries. The core objective function can be written as follows:

$$J_{\text{CL-SRME}} = \sum_{\omega} \|\mathbf{P} - \hat{\mathbf{P}}_0(\mathbf{I} + \hat{\mathbf{A}}\mathbf{P})\|^2, \tag{2.1}$$

where $\mathbf{P}$ represents the total upgoing full wavefield, $\hat{\mathbf{P}}_0$ indicates the estimated primaries, $\hat{\mathbf{A}}$ is the estimated surface operator. Note that all the notations follow the detail-hiding rules of [18], where the columns of the matrix represent monochromatic shot gathers. The CL-SRME inversion process is strictly data-driven and does not use adaptive subtraction. Without adaptive subtraction, the output is compatible with the physics of wavefield propagation. In CL-SRME, the recorded data are explained by the estimated parameters $\hat{\mathbf{P}}_0$ and $\hat{\mathbf{A}}$, which are alternately updated via a descent method. Besides, an extra sparseness constraint, e.g., focal domain constraint [2], can be imposed on the estimated primaries to achieve more robust primary and multiple separation in terms of reducing multiple leakage. The updates in $\hat{\mathbf{P}}_0$ are obtained by a multi-dimensional cross-correlation of the data residual $\mathbf{P} - \hat{\mathbf{P}}_0(\mathbf{I} + \hat{\mathbf{A}}\mathbf{P})$ and the input data. Note that primaries, surface multiples and internal multiples are included in the input data, and the direct arrival are removed during preprocessing steps.

2.2.2. NON-LINEAR FWM

FWM is an inversion-based imaging method that can effectively take internal multiples and transmission effects into account due to its modeling engine [11], which is based on the estimated image and a migration velocity model. That is, given a good velocity model and a source wavefield description, FWM uses the reflectivity as the parameterization of the medium for solving the one-way wave equation, which is different from the typical two-way wave equation-based parameterization (i.e., velocity and density). FWM also be-

longs to the category of least-squares based imaging methods, and its objective function can be expressed in the following form:

$$J_{\mathtt{FWM}} = \frac{1}{2}\sum_{\omega}\sum_{shots} \|\mathbf{d}^{-}_{\mathtt{obs}}(z_0) - \mathbf{p}^{-}_{\mathtt{mod}}(z_0,\hat{\mathbf{r}})\|_2^2, \tag{2.2}$$

where $\hat{\mathbf{r}}$ indicates the subsurface coordinate-related reflectivity to be estimated, $\mathbf{p}^{-}_{\mathtt{mod}}(z_0,\hat{\mathbf{r}})$ denotes a single shot monochromatic modeled upgoing wavefield recorded at the surface z_0, and $\mathbf{d}^{-}_{\mathtt{obs}}(z_0)$ represents the single shot monochromatic observed upgoing wavefield recorded at the surface z_0. An extra sparseness constraint can also be added to equation 2.2, and gradient-based methods can be used to minimize the aforementioned objective function [13].

To better illuminate the subsurface, surface-related multiples can be straightforwardly included in the FWM process by reinjecting the $\mathbf{d}^{-}_{\mathtt{obs}}(z_0)$ [12]:

$$\mathbf{q}^{+}(z_0) = \mathbf{s}^{+}(z_0) + \mathbf{R}^{\cap}(z_0)\mathbf{d}^{-}_{\mathtt{obs}}(z_0), \tag{2.3}$$

where $\mathbf{R}^{\cap}(z_0)$ represents the downward reflection matrix at the sea surface, usually considered as $\mathbf{R}^{\cap}(z_0) = -\mathbf{I}$, $\mathbf{s}^{+}(z_0)$ denotes the source wavefield, $\mathbf{q}^{+}(z_0)$ indicates the total downward wavefield. In this way, the total downgoing wavefield is considered as the incident wavefield for imaging, which is referred to regular/linear FWM. However, the required high receiver coverage is not usually met in reality, and the problem occurs when there exist acquisition gaps. Therefore, implementing FWM in a non-linear manner was proposed [15]:

$$[\mathbf{q}^{+}(z_0)]^{i+1} = \mathbf{s}^{+}(z_0) + \mathbf{R}^{\cap}(z_0)[\mathbf{p}^{-}_{\mathtt{mod}}(z_0,\hat{\mathbf{r}})]^{i}, \tag{2.4}$$

where i indicates the iteration number. In this way, the acquisition gaps can be alleviated during FWM using surface multiples not by reinjecting measured data, but by using the modeled upgoing wavefield after several roundtrips through the subsurface. The aforementioned way of using FWM is referred to non-linear FWM. Note that due to the unrecorded near-offset data we implement the non-linear FWM in our proposed integrated CL-SRME and FWM framework to overcome the missing near-offsets. Due to the sensitivity of non-linear FWM, good estimates of both source wavefield and velocity model are required. FWM as it appears in the examples all refer to as non-linear FWM. More details about non-linear FWM can be found in [15].

2.3. INTEGRATION OF CL-SRME AND FWM

CL-SRME itself is heavily influenced by the data coverage, especially by the missing near-offsets. FWM has already demonstrated its robust data reconstruction performance [13]. More specifically, the estimated reflectivity during FWM is used to synthetically model the complete data. Note that the estimated reflectivity makes use of both surface and internal multiples during imaging. Therefore, the integration of CL-SRME and FWM can effectively solve the data coverage requirement for CL-SRME, and produce more accurate estimated primaries. Our proposed workflow is presented in Figure 3.1. There are two important components in this flow chart: the data reconstruction engine (FWM) and the surface-related multiple estimation engine (CL-SRME). The general process works as follows: we first feed the incomplete recorded data (i.e., with missing near-offsets) into the

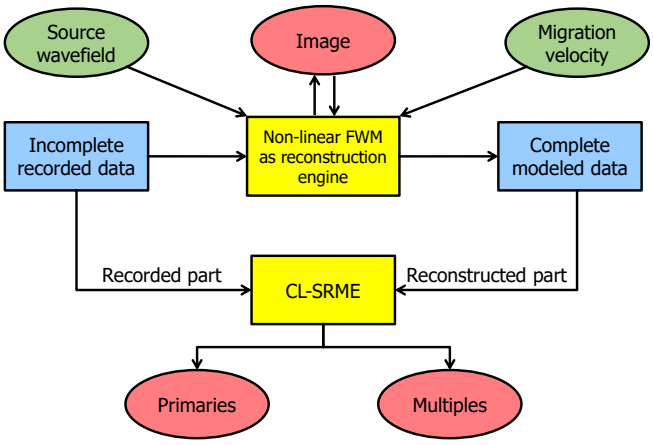

Figure 2.1: The proposed framework for integration of CL-SRME and FWM.

FWM engine provided that a source wavefield and a given migration velocity are available, from which the estimated image can be obtained. Note that a least-squares procedure is contained inside FWM, therefore, reflectivity is updated in the adjoint/migration stage, and the modeled data are generated in the forward modeling stage. Based on the estimated image, we can simultaneously demigrate the complete modeled data (i.e., with near-offsets included) during FWM. After we combine the recorded part from the original data and the reconstructed part from the modeled data, the combined data are fed into the CL-SRME to have a better estimated primaries and multiples. Note that due to the consistent waveform inversion during FWM the modeled data have matched well with the recorded data. Therefore, there is no need to apply an extra amplitude matching step, which might be necessary for other conventional approaches. The combination process can be expressed as follows:

$$\mathbf{d}^{-}_{\mathtt{CL-SRME}}(z_0) = \mathbf{d}^{-}_{\mathtt{obs}}(z_0) + \mathscr{M} \circ \mathbf{p}^{-}_{\mathtt{mod}}(z_0, \hat{\mathbf{r}}), \tag{2.5}$$

where $\mathbf{d}^{-}_{\mathtt{CL-SRME}}(z_0)$ indicates the final combined data that are fed into CL-SRME for primary estimation, $\mathscr{M}$ represents the sampling operator that contains the coordinates of the missing traces, and $\circ$ indicates the entry-wise product. In this workflow, the image only acts as a strong constraint for the modeled complete data. The FWM image may not be perfect and still contain cross-talk. However, it can still serve as a basis for data reconstruction, which is our main purpose for the FWM step.

2.4. RESULTS

To demonstrate the performance of the proposed integrated surface-related multiple estimation framework for shallow water, we will show one synthetic and one field data example. Both examples illustrate difficult shallow water scenarios with missing near-offsets.

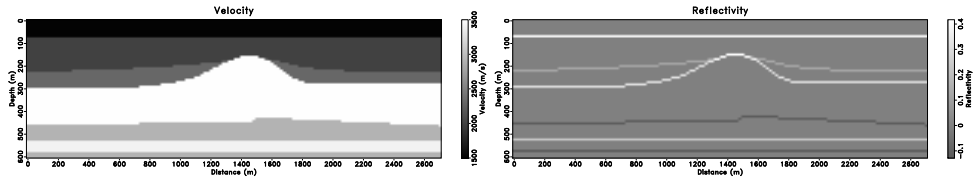

(a) (b)

Figure 2.2: Synthetic data example. (a) Velocity model. (b) Reflectivity model.

2.4.1. SYNTHETIC DATA EXAMPLE

We first test the proposed framework on the synthetic model as shown in Figure 2.2, which consists of a shallow water layer, an anticline structure, several tiny faults and two deep target layers. The water depth is 80 m. We model the fixed-spread streamer-type data with 136 sources and 136 receivers. Both source and receiver interval is 20 m. Note that the full wavefield modeling (FWMod) [11] is used to generate the synthetic data for demonstrating the best performance of the proposed framework. Both velocity model (Figure 2.2(a)) and reflectivity model (Figure 2.2(b)) are required for FWMod. The modeled ground truth data are shown in Figure 2.3. Surface-related multiples are clearly visible in modeled full wavefield in Figure 2.3(a). Due to a shallow water depth, the water bottom reflection event is highly curved and displays relatively strong energy; it is crucial for CL-SRME-based primary and multiple estimation [19]. From the primaries in Figure 2.3(b), a weak event related to an internal multiple can be observed around 0.3 s, which can be used as QC for comparing primary estimation results.

First, Figure 2.4 is dedicated to demonstrate the importance of the near-offsets for surface-related multiple estimation. The decimated data with missing near-offsets as shown in Figure 2.5(a) are directly fed to CL-SRME. The missing gap is 320 m (i.e., 160 m offsets to both sides and 15 missing traces in total). From the poorly estimated multiples in Figure 2.4(b) it is clear that only small potion of the later multiple events can be somehow predicted, and seems disastrous for the earlier events. Consequently, the corresponding primaries in Figure 2.4(a) are still severely interfered by the multiples, where very few multiples are removed. Therefore, accurate data reconstruction is necessary for good multiple estimation. Figure 2.5 demonstrates the data reconstruction performance comparison. The missing near-offset gap completely hides the curvature information of shallow event and makes data reconstruction extremely difficult. The parabolic Radon transform (PRT) is commonly used for near-offsets reconstruction in industry [20], and is regarded as a benchmark in this chapter. PRT reconstructed data and their corresponding reconstruction errors are shown in Figure 2.5(b) and 2.5(e), respectively. PRT achieves a good near-offset reconstruction performance in the later part of data. However, we can observe strong reconstruction errors in the shallow part, especially the water bottom reflection, due to the stretching effects during normal moveout correction (NMO) that is required in PRT-based reconstruction. Figure 2.5(c) and 2.5(f) present the FWM reconstructed data and their corresponding reconstruction errors, respectively. FWM reconstructed near-offsets are quite close to the ground truth from visual comparison. Further-

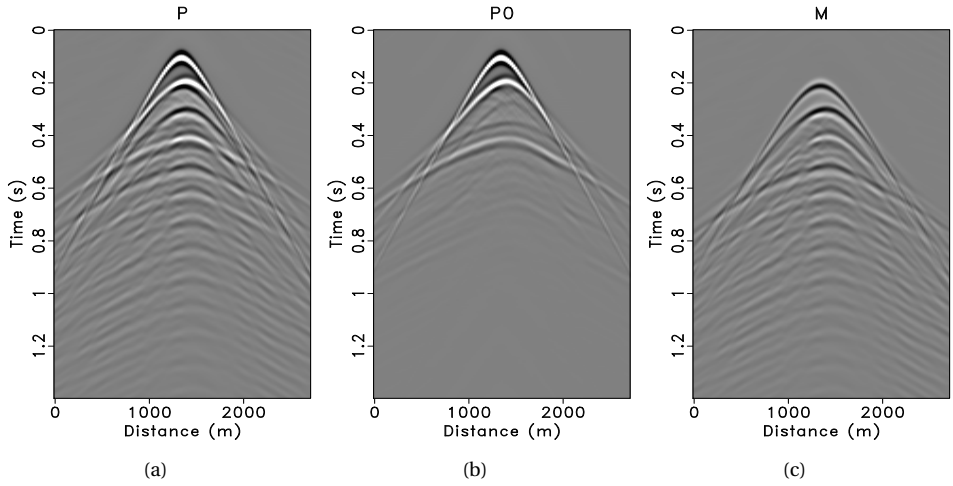

Figure 2.3: Modeled ground truth data via FWMod. (a) Full wavefield. (b) Primaries. (c) Surface-related multiples. Note that both full wavefield and primaries also contain internal multiples, which are considered as "primaries" by CL-SRME. Similarly, data in Figure 2.3(c) are (presumably) full data without primaries and their internal multiples, i.e., free-surface multiples and their internal multiples.

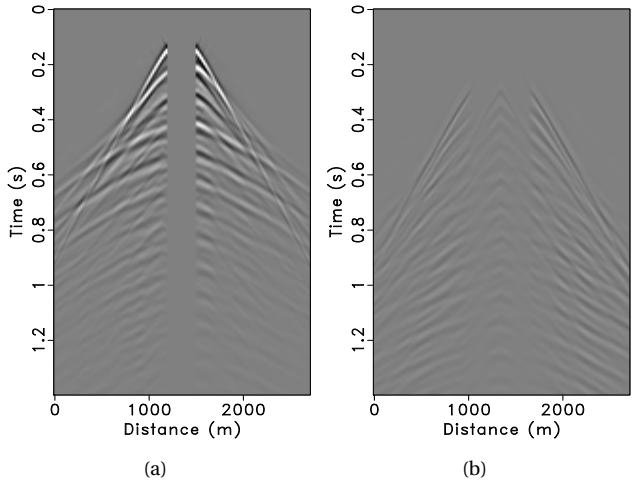

Figure 2.4: The effect of leaving out near-offsets on CL-SRME-based primary and multiple estimation. Estimated primaries (a) and multiples (b) without any near-offsets reconstruction, respectively.

more, the FWM reconstruction errors are much smaller compared with PRT reconstructed

data, which indicates a better reconstruction performance of FWM compared to PRT. For a better comparison, a single trace comparison at distance 1360 m is also provided. Note that black solid, red solid and blue dashed lines denote ground truth, PRT reconstructed and FWM reconstructed near-offset trace, respectively. It is clear that FWM reconstructed near-offsets are very close to the ground truth while the PRT reconstructed near-offsets have larger errors at the shallow part. It can be observed that shallow events are usually more curved, makes them more difficult to reconstruct by PRT.

The effect of data reconstruction on CL-SRME-based primary and multiple estimation for this synthetic example is shown in Figure 2.6. Estimated primaries and multiples from ground truth data are presented in Figure 2.6(a) and 2.6(d), respectively. Comparing with the ground truth primaries and multiples in Figure 2.3, CL-SRME achieves almost perfect performance. Estimated primaries and multiples from PRT reconstructed data are shown in Figure 2.6(b) and 2.6(e), respectively. As seen in Figure 2.6(b), many leaked multiples are visible in the estimated primaries indicated by the arrow, which prevents interpreters seeing the real structure. From estimated multiples in Figure 2.6(e), it seems that the first-order surface multiple from the water bottom reflection is much weaker than the ground truth. Estimated primaries and multiples from FWM reconstructed data are shown in Figure 2.6(c) and 2.6(f), respectively. We observe that the estimated primaries and multiples from FWM reconstructed data are very similar to the ideal case, which indicates the FWM reconstructed near-offsets are accurate enough for CL-SRME. Note that the internal multiple event in Figure 2.6(c) is noticeable, as internal multiples are considered as primaries in CL-SRME. The missing water bottom reflection at near-offsets are so crucial that it can steer the primary and multiple estimation to a physical-consistent direction. Note that the gap might be small in terms of space-time window, but it is not small in terms of reflection angles or amplitudes of the waveforms.

2.4.2. FIELD DATA EXAMPLE

The Nelson data set from the North Sea is used for demonstrating the proposed framework on primary and multiple estimation. The Nelson data set are originally extracted from a 2D streamer survey line with 25 m original source spacing. We can obtain a fixed-spread data set via reciprocity and source interpolation, arriving at 201 sources and 201 receivers. Both source and receiver intervals are 12.5 m. More details descriptions about the preprocessing steps, the original acquisition geometry and the survey background can be found in [21] and [22]. The maximum water depth is 95 m (90 m on average). The double-sided near-offset gap is 225 m (i.e., 17 missing traces in total), which is smaller than that of the synthetic data. Due to a good performance of PRT on the later part of the data, we only compare the data reconstruction performance on the shallow events, which only requires a constant water velocity. From the decimated data in Figure 2.7(a), it is worth mentioning that the deep part of the missing near-offsets are reconstructed by PRT. Figure 2.7(b) and 2.7(d) present PRT and FWM reconstructed data, respectively. The reconstruction differences from the shot gather are difficult to see. Therefore, we provide a single trace comparison in Figure 2.7(c) for convenience. Note that red solid and blue dashed lines denote the PRT reconstructed and the FWM reconstructed near-offset trace, respectively. The FWM reconstructed near-offset trace has stronger amplitude than its PRT counterpart, which agrees with the conclusion of the synthetic test. Besides, the PRT gives a slightly distorted

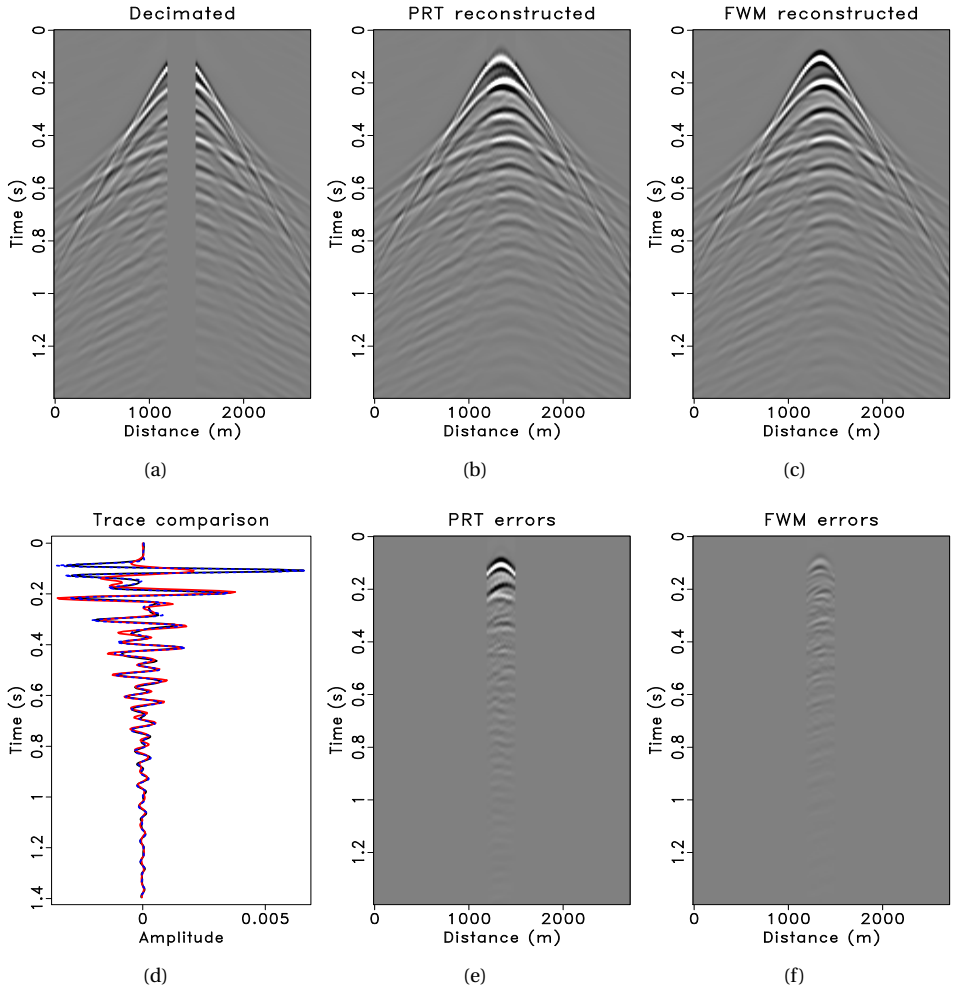

Figure 2.5: Data reconstruction performance comparison. (a) Decimated data with missing near-offsets. (b) & (e) PRT reconstructed data and their corresponding reconstruction errors, respectively. (c) & (f) FWM reconstructed data and their corresponding reconstruction errors, respectively. (d) Single trace comparison at Distance 1360 m. Note that black, red and blue lines denote ground truth, PRT reconstructed and FWM reconstructed near-offset trace, respectively.

wavelet due to the stretching effect of the involved NMO correction. Note that for the very critical shallow part of the data, we only use the FWM reconstructed water bottom reflection, while the rest is taken from the PRT reconstructed data.

Next, we evaluate the effect of data reconstruction on CL-SRME-based primary and multiple estimation. Figure 2.8(a) and 2.8(c) show the estimated primaries and multiples

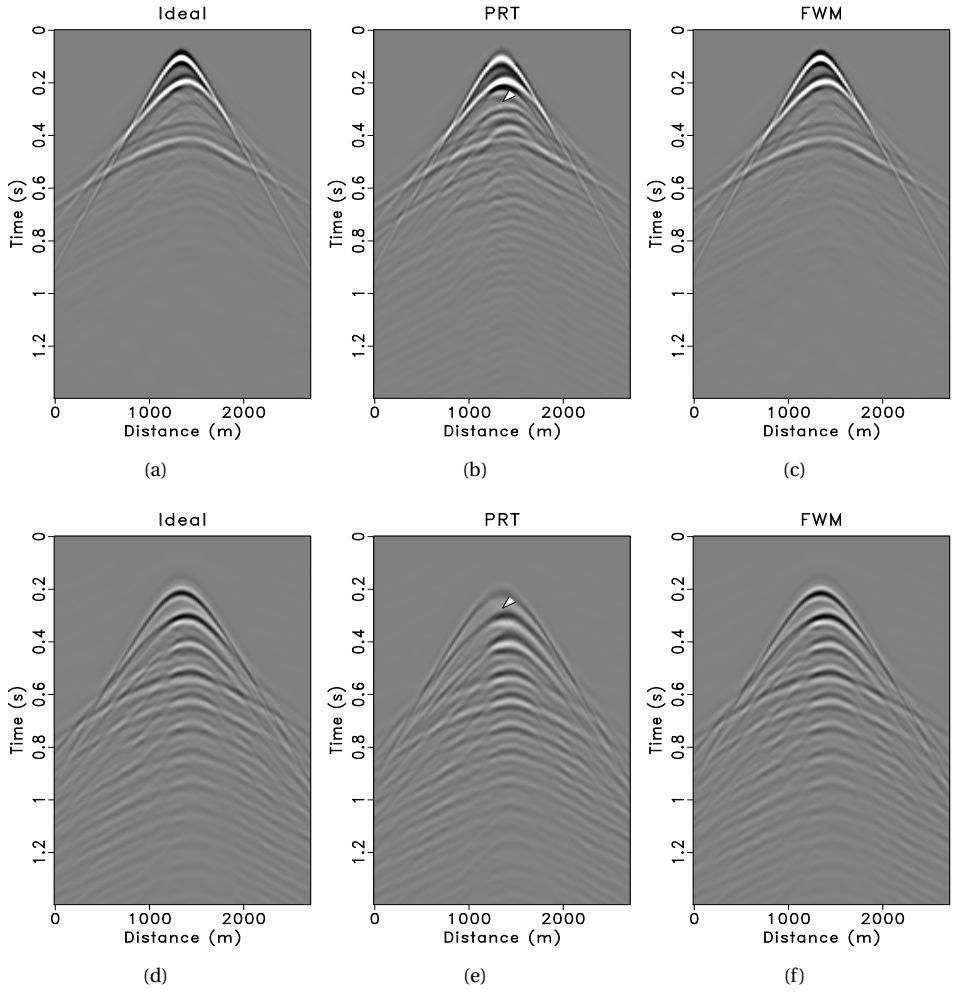

Figure 2.6: The effect of data reconstruction on CL-SRME-based primary and multiple estimation. (a) & (d) Estimated primaries and multiples from ground truth data, respectively. (b) & (e) Estimated primaries and multiples from PRT reconstructed data, respectively. (c) & (f) Estimated primaries and multiples from FWM reconstructed data, respectively.

from PRT reconstructed data, respectively. Figure 2.8(b) and 2.8(d) show the estimated primaries and multiples from FWM reconstructed data, respectively. From the estimated primaries, we can observe that there are visible multiple leakages indicated by the arrows from the PRT reconstructed data. Those two first-order multiple leakages can be easily confirmed. However, the same leakages are suppressed by using the FWM reconstructed data. Meanwhile, the estimated multiples using the FWM reconstructed data are slightly stronger than using PRT reconstructed data. Thus, the small update in the water-bottom

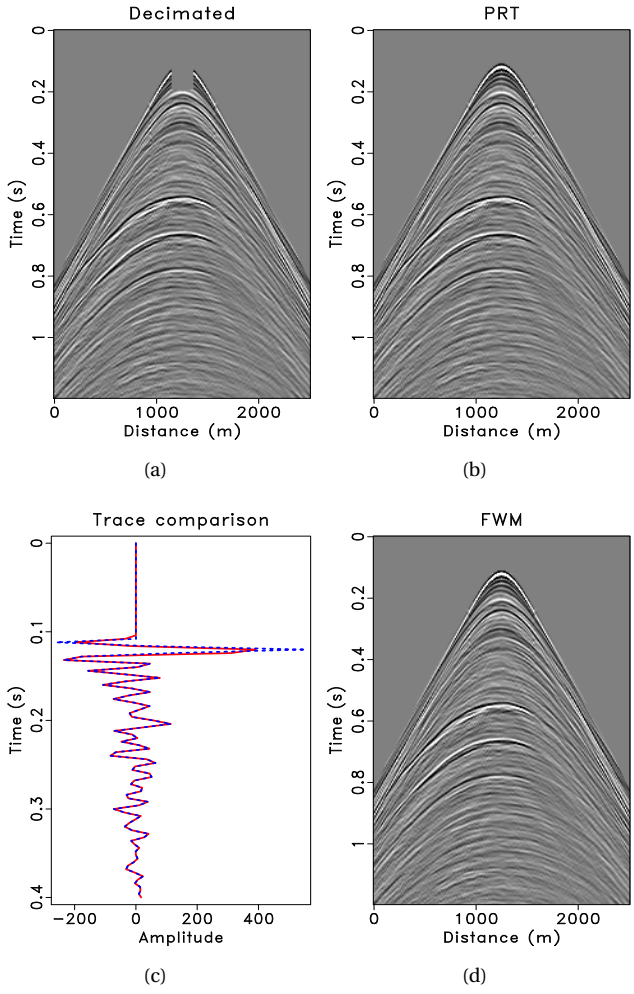

Figure 2.7: Data reconstruction comparison for the Nelson field data set. (a) Decimated data with top part of missing near-offsets. (b) & (d) PRT and FWM reconstructed data, respectively. (c) Single trace comparison at Distance 1250 m. Note that red and blue lines denote PRT reconstructed and FWM reconstructed near-offset trace, respectively.

reflection can drive the CL-SRME to a different solution.

Figure 2.9 presents the stacked section comparison, which shows the differences more clearly. The original full wavefield stacked section is shown in Figure 2.9(a). Visible surface multiples can be observed in the original full wavefield stack. Estimated primary stacked sections using PRT and FWM reconstructed data are displayed in Figure 2.9(b) and 2.9(c), respectively. Compared to the original stack, both results greatly attenuate the surface multiples. However, the primary stack using FWM reconstructed data presents less resid-

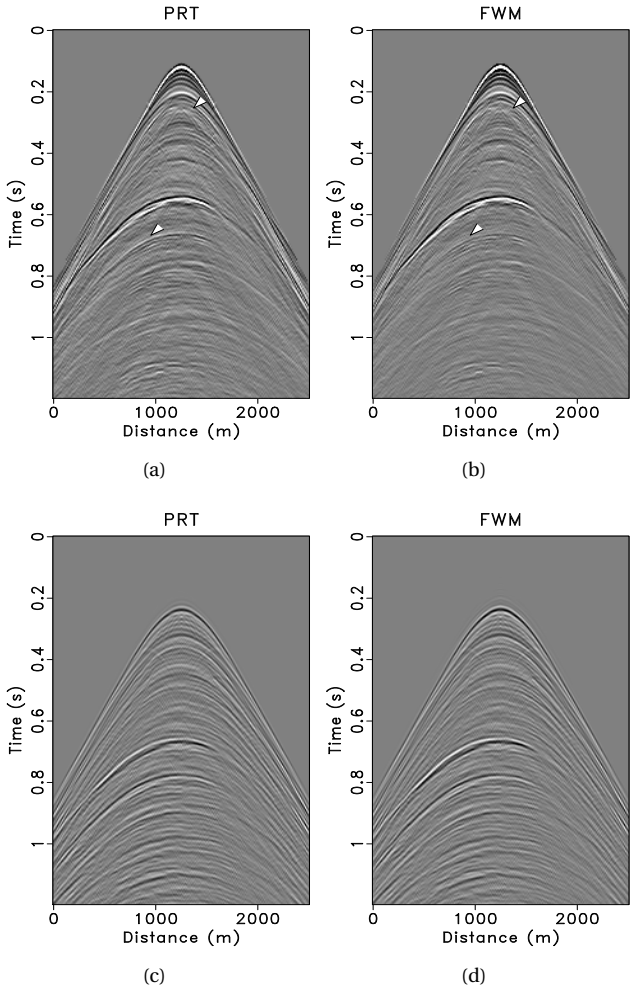

Figure 2.8: The effect of data reconstruction on CL-SRME-based primary and multiple estimation. (a) & (c) Estimated primaries and multiples from PRT reconstructed data, respectively. (b) & (d) Estimated primaries and multiples from FWM reconstructed data, respectively. Note that arrows indicate the location of residual multiples.

ual multiples compared to the primary stack using PRT reconstructed data, especially for the first-order multiples indicated by the arrows. Note that a slight primary dimming is present in the deep part of Figure 2.9(c), probably due to 3D effects.

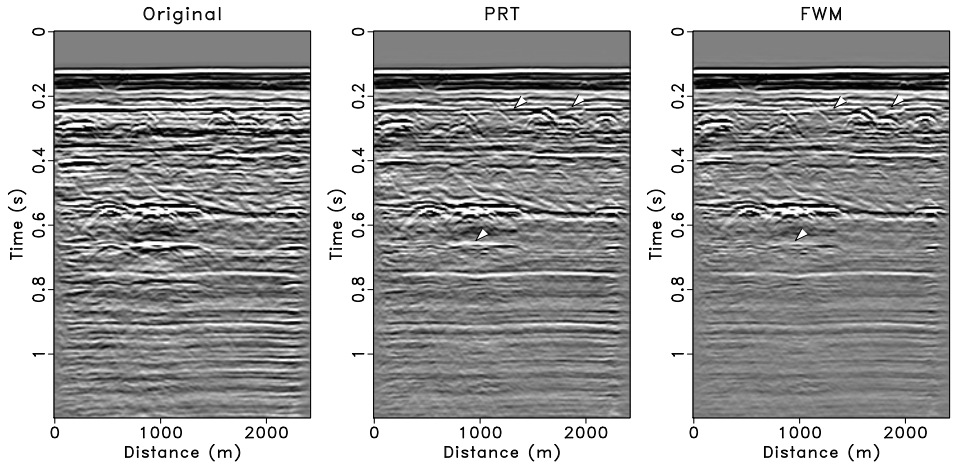

Figure 2.9: Stacked section comparison. (a) Original full wavefield. (b) Estimated primaries using PRT reconstructed data. (c) Estimated primaries using FWM reconstructed data.

2.5. DISCUSSION

Velocity information is essential for the integration of CL-SRME and FWM framework. Primaries typically need to be reconstructed from deeper reflectors than the water bottom, which is a function of near-offsets, geology and velocity. The data reconstruction power lies in FWM, however, FWM requires a decent velocity model and a good source wavefield description to function well. For example, we use the smoothed version of the true velocity in the synthetic example. To make most of the proposed framework, velocity estimation is usually necessary, where joint migration inversion (JMI) [23] can handle this, as it is based on the same foundations as FWM. Conventional velocity estimation methods usually require demultipled data beforehand, while JMI is able to take both surface and internal multiples into consideration. Missing data will pose difficulty on JMI for velocity estimation, however, most important velocity information come from far-offsets. Besides, conventional near-offsets reconstruction can be applied first, and then fed to JMI for better performance. Recently proposed pseudo-time JMI is more stable in terms of the velocity estimation [24]. In practice, only the shallow part of near-offsets need to be carefully described by FWM and the deep part can be solved by PRT. Therefore, shallow velocity estimation is a key pre-processing step for the proposed integrated framework. At least, it is important to have a correct water speed for field data application. As for the source estimation, we know the true source wavefield for synthetic data. Although it is challenging for field data, FWM is flexible on the source assumption. FWM is not limited by a point source, and in fact it can accommodate any source wavefield as long as the temporal and spatial properties are known. The more accurate the description of the source, the better the source estimation. In this chapter, we use EPSI to estimate the source signal for the Nelson field data. The merging of synthetic data estimated by FWM and the field data

requires consistency of the wavelets in the two data sets, with wavelet here including not only the source signature but also residual ghosts and effects from the (rough) sea surface reflection. Note that all kinds of source estimation methods utilize the consistency between primaries and multiples. More assumptions and ways to validate the assumptions are described in [25].

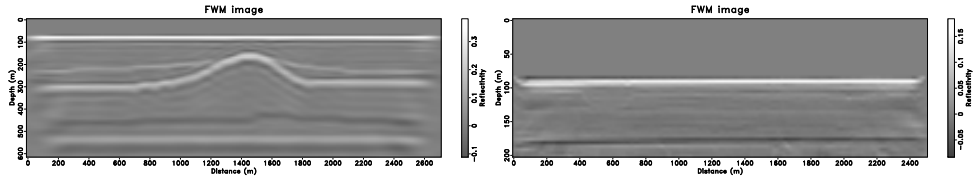

(a) (b)

Figure 2.10: The by-product images from the proposed integrated CL-SRME and FWM framework for the synthetic example (a) and the field data example (b).

The proposed integrated CL-SRME and FWM framework can provide a high-resolution shallow subsurface image as by-product. Figure 2.10 shows two FWM images corresponding to the previous examples. In fact, the by-product image in Figure 2.10(a) is quite acceptable with minimum crosstalks, and its estimated reflectivity is close to the true model in Figure 2.2(b). However, residual crosstalk for the field data is still visible as shown in Figure 2.10(b). It is probably due to applying a 2D method to real (3D) data, which creates some amplitude inconsistencies, mostly because of the 3D geometric spreading. Note that we do not need a perfect image for data reconstruction purpose; actually the crosstalk is required to build the correct amplitudes for data reconstruction. The interdependence between preprocessing (multiple estimation included), image estimation and velocity estimation makes processing of shallow water data challenging and distinct from the conventional scenarios, where these processing steps can be effectively separated. We show benefits by combining treatment of multiple estimation and subsurface imaging, given preprocessing and a velocity model.

At the same time, we need to mention that for 2D field data the primary model that has the least multiple leakage may not be the best model for primary amplitude preservation in the deeper area due to the fact that 3D data can never be perfectly represented by a 2D theory. The energy loss in the deeper area for the field example is probably due to the balancing process inside the CL-SRME inversion scheme. Therefore, the correct physics is difficult to retain in a 2D world, and sometimes it is acceptable to break the physics for achieving better performance. For the 2D data in shallow water, the main challenge is the near-offsets gap, which can be reconstructed with reasonable accuracy via EPSI, focal CL-SRME and the proposed method [2, 26, 27]. However, for the challenging 3D scenario (i.e., only 2% recorded data in a shallow water environment), both EPSI and focal CL-SRME will fail due to their weak constraint on the solution space. In other words, both EPSI and focal CL-SRME can not be easily scaled to the 3D case to handle near-offsets gap and large crossline undersampling. Conversely, FWM will be beneficial in the 3D case because of its much stronger constraints in the image. More specifically, the sparsity constraint

in EPSI is limited, and thus, focal constraint was introduced to help with more curved events. FWM achieves even stronger constraint via the image to be able to reconstruct the exact shape of highly curved events with strong lateral amplitude variation. Therefore, all methods (i.e., EPSI, focal CL-SRME and the proposed framework) can obtain acceptable results in 2D, while only the proposed integrated CL-SRME and FWM framework has the potential to overcome the extreme challenging 3D world.

FWM has already shown strong interpolation power for the missing near-offsets reconstruction although it requires acceptable model information. However, the undersampling issue is much more severe in reality, e.g., large source spacing and receiver side subsampling. Figure 2.11 demonstrates the FWM reconstruction performance on the same synthetic example with both source (1:5) and receiver (1:2) undersampling. It can be seen that FWM could still perform effectively with large parts of missing data. Thus, the main advantage of the proposed framework will be achieved in a full 3D scenario. Also there we can expect larger missing near-offset data, such that the PRT will perform very poorly. However, both CL-SRME and FWM consume heavy cost in 3D, which is still under research. Currently, an affordable solution is the 3D FWM-aided general surface multiple prediction approach (GSMP), in which FWM is only used to reconstruct near-offsets and GSMP solves the crossline undersampling issue [28].

We recognize that the computational cost of the proposed integrated framework of CL-SRME and FWM is a challenge. It is not easy to give a direct number for the cost, however, we can provide a rough idea compared to the standard SRME process. That is, CL-SRME roughly approximates to 50 times of SRME, while FWM is at least 1000 times. It is certainly not cheap, but we are currently pursuing a noticeable improvement on shallow water multiple estimation with a high-resolution shallow imaging result as a by-product. Besides, the utilized FWM algorithm is not fully optimized as it was implemented in Matlab, which leaves room for further reducing the cost in the future. In general, both FWM and CL-SRME cost increases linearly with source and/or receiver numbers. To limit computational costs, we realize that PRT is able to give acceptable results for time later than 0.3 s, and FWM is only applied for the top part of shallow subsurface. Note that in terms of iteration number used in this chapter, we apply 20 CL-SRME iterations for both synthetic and field examples. As for FWM, we use 80 iterations for the synthetic model because we would like to achieve the best possible performance. However, it is usually sufficient for field examples to use 20 FWM iterations.

Near-offset reconstruction performance using PRT depends on several parameters. The near-offset gap size and the water depth are the most important ones [2]. Both parameters heavily influence the curvature of the reflection data. Shallower water depth leads to higher curvature of water bottom reflection, which generates more severe stretching effects. Larger gap size results in missing curvature information, which leads to poorer reconstruction. In this chapter, the PRT reconstruction performance seems better for the field data example compared to the synthetic data. This is partly because of the smaller gap size (225 m) and the somewhat larger water depth (95 m) compared to the synthetic model (320 m and 80 m, respectively). An extra experiment of the proposed framework on the same synthetic model with 50 m water depth has been implemented in Figure 2.12. In this case, we can observe shorter time difference between primaries and its first-order multiples. Although there are slightly more reconstruction errors than the 80 m case, the

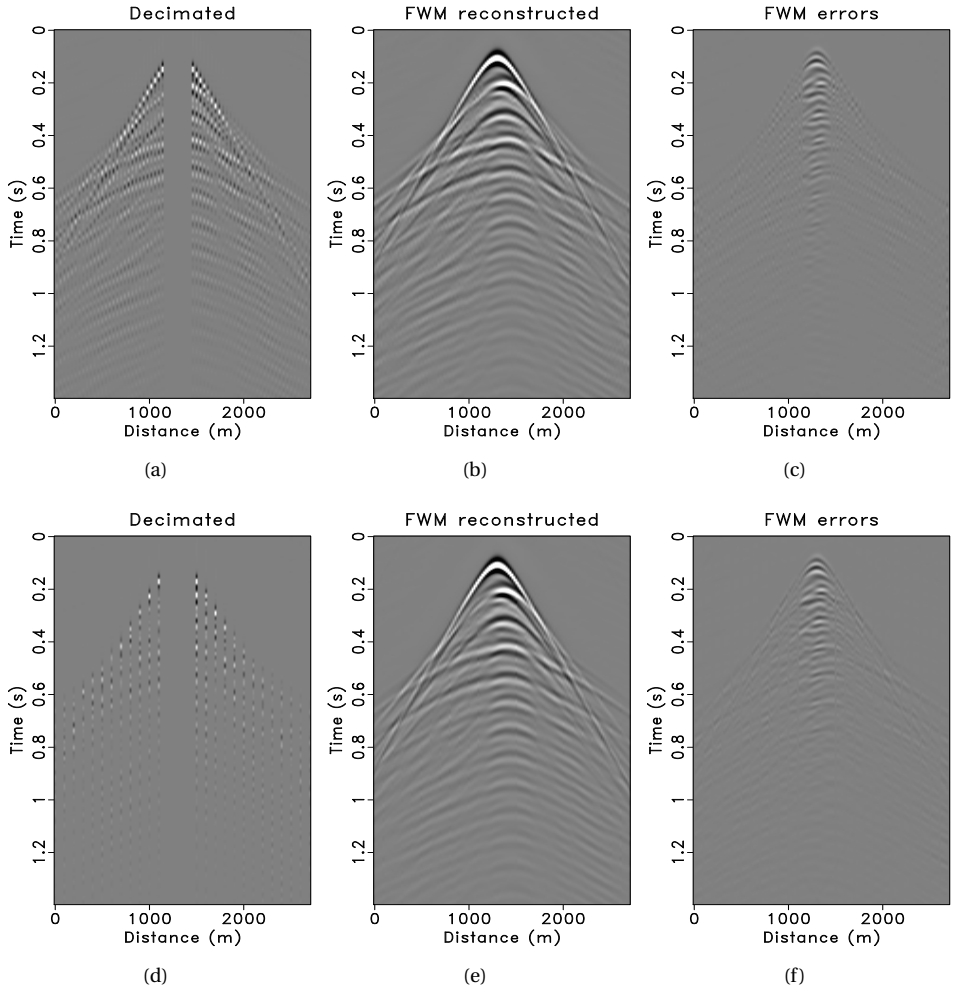

Figure 2.11: FWM reconstruction performance on the same synthetic example with both source (1:5) and receiver (1:2) undersampling. (a) Decimated shot gather with missing receivers and near-offsets. (b) & (c) FWM reconstructed shot gather and their corresponding reconstruction errors, respectively. (d) Decimated common-receiver gather with missing sources and near-offsets. (e) & (f) FWM reconstructed common-receiver gather and their corresponding reconstruction errors, respectively.

overall FWM reconstruction is acceptable. For the given bandwidth we expect that performance will decrease further with shallower water depth. Thus, combination of MWD [8] for extreme shallow and FWM for medium shallow might be a solution.

When the water depth is shallower than 50 m, the source array effect and the direct arrival might have seriously negative effects on the imaging process. Point-source approx-

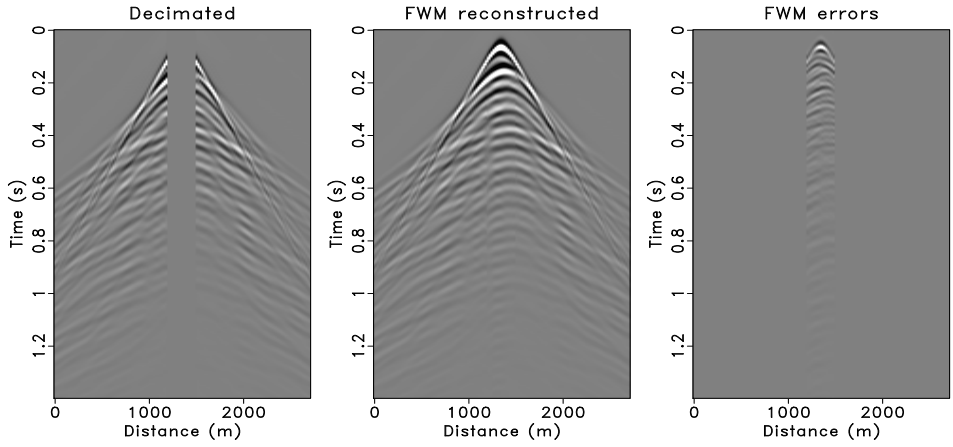

Figure 2.12: FWM reconstruction performance on the same synthetic example with shallower water depth (i.e., 50 m). (a) Decimated data with missing near-offsets. (b) FWM reconstructed data and (c) their corresponding reconstruction errors.

imation in imaging and demultiples are not valid anymore. Nevertheless, we can always take array effects into account when defining the source field during forward modeling. Note that a good estimate of source wavefield is required for the sensitive non-linear FWM. Extreme shallow water creates another big problem, being that the source signal and data interfere with each other. Thus, the proposed framework will break down as soon as we cannot get a good estimate of the source wavefield. In extreme shallow water scenarios (0-30 m), we suggest a combination of detailed high-resolution shallow subsurface model inversion for the very shallow part and our proposed framework for the medium shallow part. Note that this scenario is challenging and requires further research.

We always prefer the most logical reconstructed data, which can represent the physics. One of the advantages of FWM is its good link between primaries and multiples, and this is the physics that needs to be used and retained. In general, FWM has more physics and more flexibility without the danger of over-parameterization. Still, the shallow water environment is too complicated to be solved by a single approach. Alternatively, an even more integrated framework including refraction analysis, multiple estimation, and a dedicated near-surface model building/inversion might contribute to an ideal solution. We need these combinations of algorithms to maximally utilize the physical relations to solve the challenging shallow water problem.

2.6. CONCLUSIONS

We have proposed a new integrated CL-SRME and FWM framework for better primary and multiple estimation, which can support CL-SRME with good-quality near-offsets in order to avoid primary estimation failure that typically occurs in shallow-water environ-

ments. Using FWM - with its closed-loop simultaneous primaries and multiples imaging approach - as the reconstruction method and feeding the reconstructed near-offsets to CL-SRME are the key components to success. A 2D synthetic and a 2D field data example have shown the good performance of the proposed integrated framework for a shallow water environment. These 2D demonstrations will pave the road for a full 3D implementation with coarse sampling, where the proposed integrated framework will have its main impact.

2.7. ACKNOWLEDGMENTS

The authors thank PGS for providing the Nelson field data set.

REFERENCES

[1] G. A. Lopez and D. J. Verschuur, *Closed-loop SRME - A new direction in surface multiple removal algorithms,* in *76th EAGE Conference and Exhibition* (European Association of Geoscientists & Engineers, 2014).

[2] G. A. Lopez and D. J. Verschuur, *Closed-loop surface-related multiple elimination and its application to simultaneous data reconstruction,* Geophysics **80** (2015), pp. V189–V199.

[3] D. J. Verschuur, A. J. Berkhout, and C. P. A. Wapenaar, *Adaptive surface-related multiple elimination,* Geophysics **57** (1992), pp. 1166–1177.

[4] D. J. Verschuur and A. J. Berkhout, *Estimation of multiple scattering by iterative inversion, Part II: Practical aspects and examples,* Geophysics **62** (1997), pp. 1596–1611.

[5] G. J. van Groenestijn and D. J. Verschuur, *Estimating primaries by sparse inversion and application to near-offset data reconstruction,* Geophysics **74** (2009), pp. A23–A28.

[6] N. Hargreaves, *Surface multiple attenuation in shallow water and the construction of primaries from multiples,* in *76th SEG Technical Program Expanded Abstracts* (Society of Exploration Geophysicists, 2006).

[7] P. Plasterie, M. Gayne, M. Lange, I. Sarjono, A. Pica, S. Leroy, G. Poulain, R. Bril, C. Faulkner, and C. Mosher, *Shallow water 3D surface-related multiple modelling, case study,* in *78th SEG Technical Program Expanded Abstracts* (Society of Exploration Geophysicists, 2008).

[8] H. Jin and P. Wang, *Model-based water-layer demultiple (MWD) for shallow water: from streamer to OBS,* in *82nd SEG Technical Program Expanded Abstracts* (Society of Exploration Geophysicists, 2012).

[9] C. Kostov, F. Xavier de Melo, A. Raj, A. Zarkhidze, A. Cooke, G. Miers, and J. Bacon, *Multiple attenuation for shallow-water surveys: Notes on old challenges and new opportunities,* The Leading Edge **34** (2015), pp. 760–768.

[10] A. J. Berkhout, *Review Paper: An outlook on the future of seismic imaging, Part II: Full-wavefield migration,* Geophysical Prospecting **62** (2014), pp. 931–949.

[11] A. J. Berkhout, *Review Paper: An outlook on the future of seismic imaging, Part I: forward and reverse modelling,* Geophysical Prospecting **62** (2014), pp. 911–930.

[12] M. Davydenko and D. J. Verschuur, *Full-wavefield migration: using surface and internal multiples in imaging,* Geophysical Prospecting **65** (2016), pp. 7–21.

[13] M. Davydenko and D. J. Verschuur, *Including and using internal multiples in closed-loop imaging — Field data examples,* Geophysics **83** (2018), pp. R297–R305.

[14] A. Nath and E. Verschuur, *Using surface-related multiples in imaging for data with large acquisition gaps,* in *87th SEG Technical Program Expanded Abstracts* (Society of Exploration Geophysicists, 2017).

[15] A. Nath and D. J. Verschuur, *Imaging with surface-related multiples to overcome large acquisition gaps,* Journal of Geophysics and Engineering **17** (2020), pp. 742–758.

[16] S. Lu, D. N. Whitmore, A. A. Valenciano, and N. Chemingui, *Separated-wavefield imaging using primary and multiple energy,* The Leading Edge **34** (2015), pp. 770–778.

[17] D. J. Verschuur and A. J. Berkhout, *From removing to using multiples in closed-loop imaging,* The Leading Edge **34** (2015), pp. 744–759.

[18] A. J. Berkhout, *Seismic migration: Imaging of acoustic energy by wave field extrapolation, A: Theoretical aspects* (Elsevier (second edition), 1982).

[19] D. J. Verschuur, *Seismic multiple removal techniques : past, present and future* (EAGE Publications, 2013).

[20] M. M. N. Kabir and D. J. Verschuur, *Restoration of missing offsets by parabolic Radon transform,* Geophysical Prospecting **43** (1995), pp. 347–368.

[21] G. Cambois, D. Carlson, C. Jones, M. Lesnes, W. Söllner, H. Tabti, and A. Day, *Dual-sensor streamer data – calibration, acquisition QC and attenuation of seismic interferences and other noises,* in *71st EAGE Conference and Exhibition* (European Association of Geoscientists & Engineers, 2009).

[22] R. H. Baardman, D. J. Verschuur, R. G. van Borselen, M. O. Frijlink, and R. F. Hegge, *Estimation of primaries by sparse inversion using dual-sensor data,* in *80th SEG Technical Program Expanded Abstracts* (Society of Exploration Geophysicists, 2010).

[23] A. J. Berkhout, *Review Paper: An outlook on the future of seismic imaging, Part III: Joint migration inversion,* Geophysical Prospecting **62** (2014), pp. 950–971.

[24] S. Qu, Y. Van den Brule, and D. J. Verschuur, *A stable scheme of joint migration inversion in the pseudo-time domain,* in *EAGE Conference and Exhibition Online* (European Association of Geoscientists & Engineers, 2020).

[25] J. Rickett, *The variable projection method for waveform inversion with an unknown source function,* Geophysical Prospecting **61** (2013), pp. 874–881.

[26] G. J. A. van Groenestijn and D. J. Verschuur, *Estimation of primaries and near-offset reconstruction by sparse inversion: Marine data applications,* Geophysics **74** (2009), pp. R119–R128.

[27] D. Zhang and E. Verschuur, *Integration of closed-loop surface-related multiple estimation and full wavefield migration for shallow water,* in *81st EAGE Conference and Exhibition* (European Association of Geoscientists & Engineers, 2019).

[28] D. Zhang and E. Verschuur, *3D surface-related multiple estimation for shallow water aided by full wavefield migration,* in *EAGE Conference and Exhibition Online* (European Association of Geoscientists & Engineers, 2020).

3

3D FWM-AIDED SRME

Industry standard 3D surface-related multiple elimination (SRME) still faces challenges in shallow-water scenarios. Full wavefield migration (FWM) using surface-related multiples possesses a strong reconstruction power, especially for near-offsets, by using the image as a constraint. Therefore, we propose a 3D FWM-aided surface-related multiple estimation framework for shallow water, which includes a data reconstruction step via 3D FWM and a multiple estimation step via 3D SRME or general surface multiple prediction (GSMP). Specifically, the FWM reconstructed data are combined with the observed data as input for the 3D multiple estimation engine for better primary prediction. Application on data from a 3D synthetic model demonstrates a good reconstruction accuracy of 3D FWM and a good performance of the proposed framework for the challenging shallow-water scenario.

This chapter is an extended version of proceeding "D. Zhang and E. Verschuur, 3D Surface-related multiple estimation for shallow water aided by full wavefield migration, in EAGE Conference and Exhibition Online Expanded abstracts, (European Association of Geoscientists & Engineers, 2020)".

3.1. INTRODUCTION

3D surface-related multiple elimination (SRME) is an industry standard data-driven primary estimation method, which requires fully-sampled data set. To overcome the most difficult data sampling issue in 3D case, many efforts have been spent in both industry and academia. [1] proposed a sparse inversion interpolation approach on the multiple contribution gathers along the crossline direction after the inline summation. General surface multiple prediction (GSMP) using on-the-fly interpolation is described by [2] and reviewed by [3], which later became an industry standard for 3D due to its strong flexibility regarding the acquisition geometry. Generally, all the aforementioned methods work well for the deep-water scenarios, however, problems occur in the shallow-water towed-streamer scenarios. Both crossline undersampling and missing near-offsets are very common while at the same time there typically exist strong surface-related multiples. Especially, the highly-curved near-offsets missing data are extremely hard to reconstruct, while they actually contribute significantly to the prediction of surface-related multiples [4–7].

Currently, 3D multiple estimation for shallow-water scenario still remains very challenging although a lot of studies have been done in this particular field [8–13]. Therefore, more accurate data reconstruction approaches, especially for near-offsets, are desperately needed. [7] proposed the integration of closed-loop SRME and full wavefield migration (FWM) to solve the sampling issue for 2D shallow-water scenario, in which the FWM image is regarded as a strong constraint to better reconstruct the near-offsets data. The reason why we still prefer SRME to separate primaries and multiples is that data-driven methods in principle are more accurate than model-driven methods [14]. The FWM-based reconstruction method can be extended to 3D straightforwardly while, however, 3D inversion-based SRME currently is still not practical in terms of the computational efficiency. Therefore, in this chapter, we propose a 3D FWM-aided surface multiple estimation framework which consists of two cascaded steps: data reconstruction step via 3D FWM and multiple estimation via 3D SRME or GSMP. By integrating the strong data reconstruction power of 3D FWM and multiple estimation ability of 3D SRME or GSMP, we are able to obtain a better primary estimation even in a shallow-water scenario. A 3D synthetic model example is used to demonstrate our proposed framework.

3.2. 3D SRME AND GSMP

The 2D SRME concept can be extended to the 3D case straightforwardly. Assume seismic data with full coverage in sources and receivers at the surface, the desired multiple estimation can be achieved via summing all contributions for one source-receiver pair [4]:

$$M(x_r, y_r, x_s, y_s, \omega) = -\sum_{y_k}\sum_{x_k} P_0(x_r, y_r, x_k, y_k, \omega) P(x_k, y_k, x_s, y_s, \omega), \tag{3.1}$$

where $P_0(x_r, y_r, x_k, y_k, \omega)$ indicates the monochromatic primary wavefields from a source location at $(x_k, y_k, z = 0)$ to a receiver location at $(x_r, y_r, z = 0)$ and $P(x_k, y_k, x_s, y_s, \omega)$ denotes the monochromatic total upgoing wavefield from a source location at $(x_s, y_s, z = 0)$ to a receiver location at $(x_k, y_k, z = 0)$. Essentially, the 3D SRME process for estimating multiples M can be regarded as a multi-dimensional convolution between a 3D common receiver gather P_0 and a 3D common shot gather P in a pre-defined aperture, i.e., the domain of integration. Note that in practice P_0 is unknown and, therefore, it is replaced by P

in the first iteration. Equation 3.1 is adequate for the discussion in this chapter with focus on the spatial sampling of the data and the kinematics of the predicted multiples.

In reality, a major sampling issue (both in crossline and missing near-offset data) prevents 3D SRME from being successfully applied. Therefore, intensive data interpolation is highly demanded to overcome the sampling problem. GSMP, a flexible 3D SRME algorithm [2], incorporates on-the-fly interpolation within its multiple prediction framework, where every desired source-receiver pair combination is created from the existing traces [3]. These selected traces are then corrected via some form of differential NMO before they are fed into the prediction process. The fundamental difference between 3D SRME and GSMP is in the preprocessing, where the former is precomputing and storing all the required data, and the latter is fetching the required data on-the-fly. Although GSMP is very flexible on handling any acquisition geometry, it still suffers from the interpolation accuracy especially for near-offset reconstruction in shallow water.

3.3. FWM FOR DATA RECONSTRUCTION

With the help of surface-related multiples FWM is capable of better imaging and illuminating the shallow subsurface [15–17]. In order to achieve this, the total downgoing wavefield $\mathbf{Q}^+(z_0)$ as the incident wavefield for 3D migration, which is in the detail-hiding notation [18] with data matrices, where column vectors represent monochromatic shot records, should be modified as:

$$\mathbf{Q}^+(z_0) = \mathbf{S}^+(z_0) + \mathbf{R}^\cap(z_0, z_0)\mathbf{P}^-_{obs}(z_0), \tag{3.2}$$

where $\mathbf{S}^+(z_0)$ contains the source wavefields, $\mathbf{R}^\cap(z_0, z_0)$ represents the downward reflectivity usually considered as $\mathbf{R}^\cap = -\mathbf{I}$ and $\mathbf{P}^-_{obs}(z_0)$ denotes the observed wavefields with all of them at the acquisition surface after receiver deghosting. The total downward wavefields $\mathbf{Q}^+(z_0)$ are then forward extrapolated at every depth level z_m given by:

$$\mathbf{P}^+(z_m, z_0) = \mathbf{W}^+(z_m, z_0)\mathbf{Q}^+(z_0), \tag{3.3}$$

while the recorded total upgoing wavefields are inverse extrapolated to every depth level z_m by:

$$\mathbf{P}^-(z_m, z_0) = [\mathbf{W}^-(z_0, z_m)]^{-1}\mathbf{P}^-_{obs}(z_0) \approx [\mathbf{W}^+(z_m, z_0)]^*\mathbf{P}^-_{obs}(z_0), \tag{3.4}$$

where $\mathbf{W}^+$ and $\mathbf{W}^-$ are downgoing and upgoing propagation operators, respectively. Reflectivity is then extracted by the imaging condition, which is the cross-correlation of $\mathbf{P}^+(z_m, z_0)$ and $\mathbf{P}^-(z_m, z_0)$ shot by shot. In this way, the primaries and multiples are migrated simultaneously. Nevertheless, direct imaging by cross-correlation is not accurate enough, which can be improved by the inversion approach in FWM [16]. More specifically, FWM aims at explaining the full recorded data by the modeled one in terms of the predicted reflectivity. Therefore, the objective function can be described as:

$$J = \sum_\omega \|\mathbf{P}^-_{obs}(z_0) - \mathbf{P}^-_{mod}(z_0)\|_2^2, \tag{3.5}$$

where $\mathbf{P}^-_{mod}(z_0)$ is the modeled upgoing wavefield based on the estimated reflectivity at each depth level in the subsurface.

Note that using equation 3.2 requires a high receiver coverage and density, which is often not met in reality, due to missing near-offsets, coarse cross-line sampling and obstructions like a big platform gap. Therefore, we suggest using the surface-related multiples in a non-linear way [19]:

$$[\mathbf{Q}^{+}(z_0)]^{i} = \mathbf{S}^{+}(z_0) + \mathbf{R}^{\cap}(z_0, z_0)[\mathbf{P}^{-}_{mod}(z_0)]^{i-1}, \tag{3.6}$$

where i is the iteration number and $[\mathbf{P}^{-}_{mod}(z_0)]^{i-1}$ indicates the modeled upgoing wavefield from previous iterations.

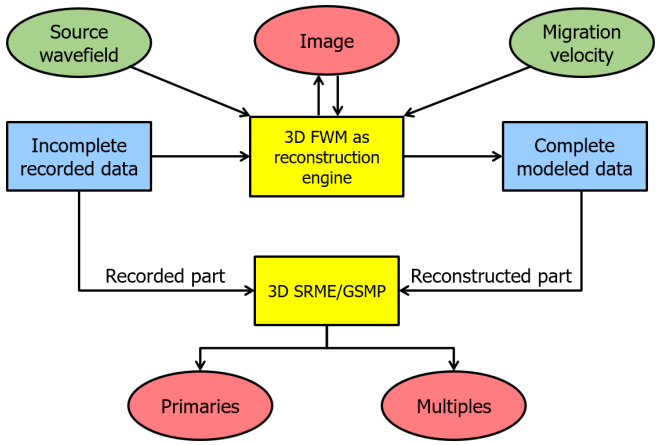

Figure 3.1: The proposed 3D FWM-aided SRME workflow for shallow water.

Using the migrated image as a constraint, FWM demonstrates a strong data reconstruction power [7]. Specifically, FWM uses the image to back-project the information from multiples to primaries with the physical constraint of all information belonging to the same earth model. Figure 3.1 demonstrates the proposed workflow for 3D FWM-aided SRME. The reconstructed data from $[\mathbf{P}^{-}_{mod}(z_0)]^{i-1}$ are combined with the observed data $\mathbf{P}^{-}_{obs}(z_0)$ to form the final complete data that will be fed into 3D multiple estimation engine, e.g., 3D SRME or GSMP. In this way, we propose a 3D FWM-aided surface-related multiple estimation framework to better estimate primaries for shallow-water scenarios.

3.4. EXAMPLE ON 3D LAYERED MODEL

We test our proposed FWM-aided surface-related multiple estimation framework on a 3D synthetic layered model shown in Figure 3.2(a), which includes a 80 m shallow water layer, a dipping plane and a deep horizontal plane. Figure 3.2(b) indicates the data acquisition details, where receivers are along the green lines with inline interval of 20 m and crossline interval of 100 m, and sources are along the red dotted lines with inline interval of 20 m and crossline interval of 200 m. For this 3D synthetic model, all numerical data are generated using full wavefield modeling (FWMod) [20]. Figure 3.3 shows the reference ground-truth 3D shot gathers at one specific source location (inline=1000 m, xline=900 m) for the full wavefield, primaries and multiples, respectively. Note that these complete

data are modeled on a full grid with 20 m in/crossline interval. Due to a coarse acquisition shown in Figure 3.2(b), the very limited data are actually recorded as shown in Figure 3.4(a). Note that all the near-offsets within a 200 m gap are also taken into account and removed. From the decimated data, it is obvious that less than 20 percent of the full grid is recorded because of the crossline undersampling and near-offsets missing. In order to fulfill the sampling requirement for 3D SRME, the recorded data need to be reconstructed before multiple prediction. In shallow-water scenarios, most data-driven reconstruction methods are not valid anymore due to highly-curved events, while FWM could still provide decent reconstruction results [7]. Figure 3.4(b) shows the complete reconstructed full-grid data via 3D FWM. The reconstruction errors are displayed in Figure 3.4(c), which demonstrates a good reconstruction performance.

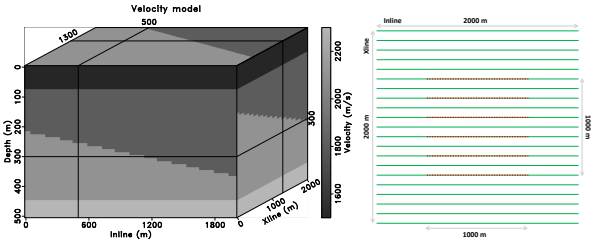

(a) (b)

Figure 3.2: 3D synthetic layered model. (a) Velocity model. (b) Top view of data acquisition geometry with green lines representing receivers and red lines representing sources.

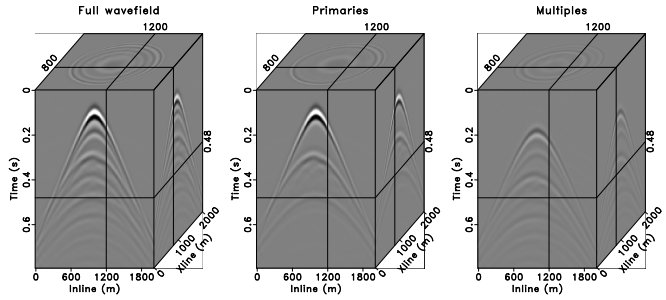

(a) (b) (c)

Figure 3.3: Reference ground-truth 3D shot gathers. (a) True full wavefield. (b) True primaries. (c) True multiples.

We then investigate the influence of data sampling issue on both 3D SRME and GSMP. Note that only one source line (Xline=900 m) ranging from 500 to 1500 m in the inline direction is compared in this study. To put better emphasis on the sampling issue, one iteration of multiple prediction and global adaptive subtraction with a short filter length are used for both the 3D SRME and GSMP process. All the results could be improved with

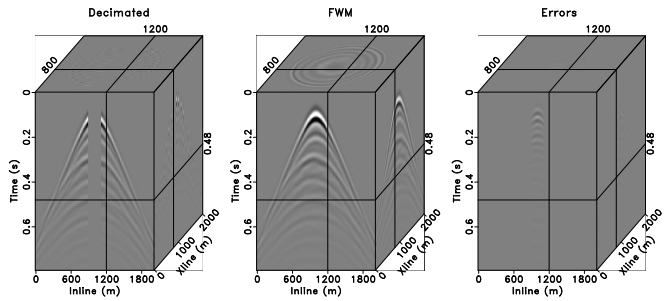

Figure 3.4: 3D FWM reconstruction performance. (a) Decimated data with only original existing traces. (b) FWM reconstructed data. (c) Reconstruction errors compared to Figure 3.3(a).

more iterations. Figure 3.5 shows the final comparison results for 3D SRME and GSMP by using the proposed 3D FWM-aided surface-related multiple estimation framework. True multiples and primaries are shown in Figures 3.5(f) and 3.5(l) for reference purpose. Multiples and primaries in Figures 3.5(e) and 3.5(k) are estimated via using the complete true full wavefield data in 3D SRME, which is considered as a benchmark in our study. This is theoretically the best result for 1 iteration.

We first feed original existing traces without any reconstruction to both 3D SRME and GSMP. Figures 3.5(a) and 3.5(g) show the estimated multiples and primaries for 3D SRME. These extremely poor results demonstrate the importance of data sampling for 3D SRME. Figures 3.5(b) and 3.5(h) show the estimated multiples and primaries for GSMP, which is slightly better than 3D SRME due to its on-the-fly interpolation engine. However, the missing near-offsets cannot be well approximated by on-the-fly interpolation based on differential NMO correction and still remain a challenge for GSMP. We then insert only the 3D FWM reconstructed near-offsets into the existing traces and feed them into GSMP, which gives much better estimated multiples and primaries as shown in Figures 3.5(c) and 3.5(i). Therefore, FWM reconstructed near-offsets are accurate enough to boost the quality of the overall GSMP results. Finally, we use the full 3D FWM reconstructed data demonstrated in Figure 3.4(b) as the input for 3D SRME to overcome the sampling challenges for both crossline direction and near-offsets missing. Figures 3.5(d) and 3.5(j) display the final estimated multiples and primaries, which are very similar to our benchmark results in Figures 3.5(e) and 3.5(k). These results also indicate a good reconstruction performance for 3D FWM. Although FWM-aided 3D SRME can overcome the sampling issue and provide the closest result to the benchmark, it requires more computational resources and data space than FWM-aided GSMP that could also provide an acceptable result.

3.5. EXAMPLE ON EAGE 3D OVERTHRUST MODEL

The proposed 3D FWM-aided GSMP framework has already been demonstrated on a simple layered 3D model, in which a promising multiple estimation result has been achieved

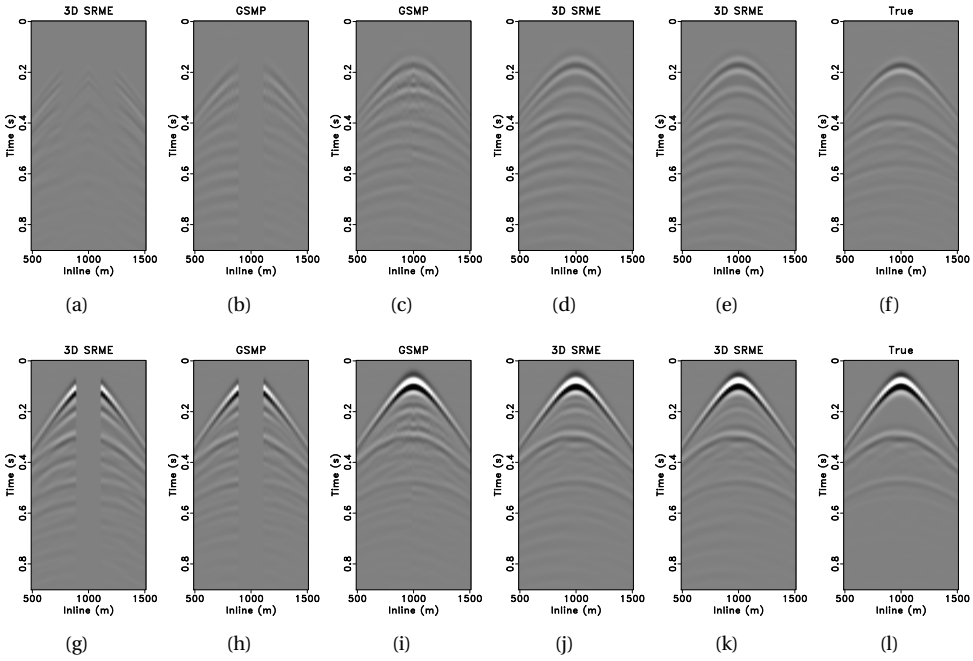

Figure 3.5: 1st iteration 3D SRME and GSMP comparison based on the proposed 3D FWM-aided surface-related multiple estimation framework. (a) & (g) 3D SRME Estimated multiples and primaries, respectively, using decimated data. (b) & (h) GSMP estimated multiples and primaries, respectively, using original existing traces. (c) & (i) GSMP estimated multiples and primaries, respectively, using existing traces together with 3D FWM reconstructed near-offsets. (d) & (j) 3D SRME estimated multiples and primaries, respectively, using 3D FWM reconstructed data. (e) & (k) 3D SRME estimated benchmark multiples and primaries, respectively, using complete true full wavefield. (f) & (l) Reference true multiples and primaries, respectively.

[21]. However, on the one hand, the previous model is not general enough. On the other hand, we wish to reduce the number of sources so that it is closer to reality. We thus applied our proposed framework on a part of EAGE 3D Overthrust model to further investigate its performance. The velocity model is shown in Figure 3.6(a). The size of the model is 4000 m by 4000 m in both inline and crossline direction, and the depth is 1000 m. We manually add a water layer on top of the model with 100 m water depth, thus, a shallow water environment is created. Figure 3.6(b) presents the acquisition geometry, in which the red stars represent sources and the black dashed lines represent receivers. Note that there are only three source lines for this geometry, and the crossline source spacing is 420 m. The inline source spacing is 100 m, and the inline receiver spacing is 20 m ranging from 1000 m to 3000 m. Each source line includes 9 receiver lines with 100 m crossline spacing, which is one patch. There are three patches overlapping in total. The number of

sources are 63, which is quite limited. Note that the near-offset gap is 120 m, and the data are modeled via FWMod [20].

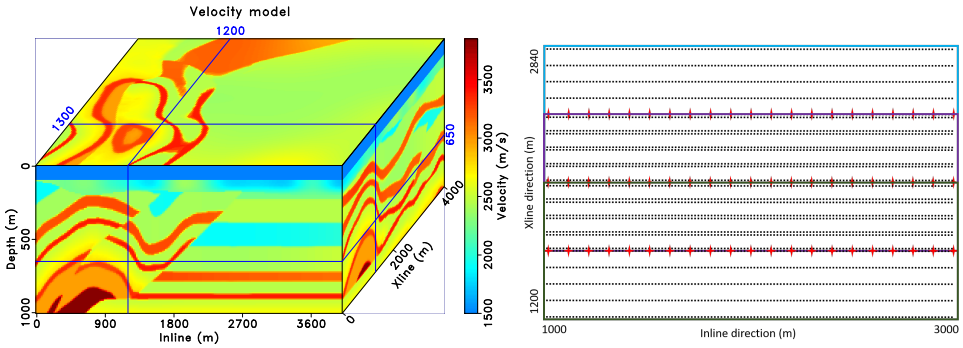

(a) (b)

Figure 3.6: EAGE 3D Overthrust model. (a) Velocity model. (b) Acquisition geometry with three patches (red stars representing sources and black dashed lines representing receivers).

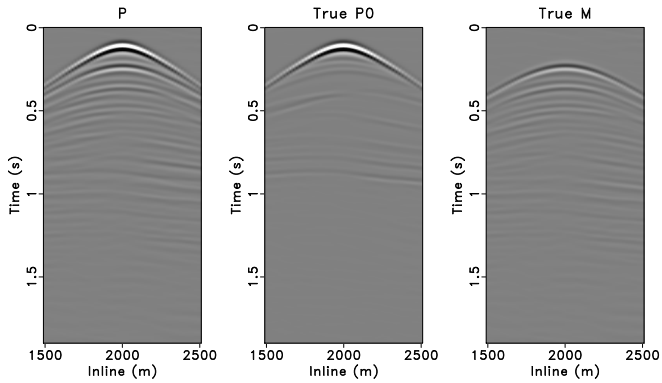

(a) (b) (c)

Figure 3.7: Reference ground-truth shot gathers (one middle shot slice from a center 3D shot gather). (a) True full wavefield. (b) True primaries. (c) True multiples.

For convenience, we only demonstrate one middle slice of a 3D center shot for comparison. Figures 3.7(a), 3.7(b) and 3.7(c) show the original full wavefield, the true primaries and the true multiples, respectively. Note that the weak primary event around 0.25 s in Figure 3.7(b) completely overlaps with the first order water-bottom related surface multiple, as shown in Figure 3.7(a). Data from the receiver side are reconstructed (both missing near-offsets and undersampled crossline direction) by 3D FWM. More specifically, the recorded data are first fed to FWM. Constrained by the images (or the image can be regarded as a transform domain), FWM are capable of reconstructing all the missing

data at the receiver side. The reconstruction performance and its accuracy have been discussed in [21].

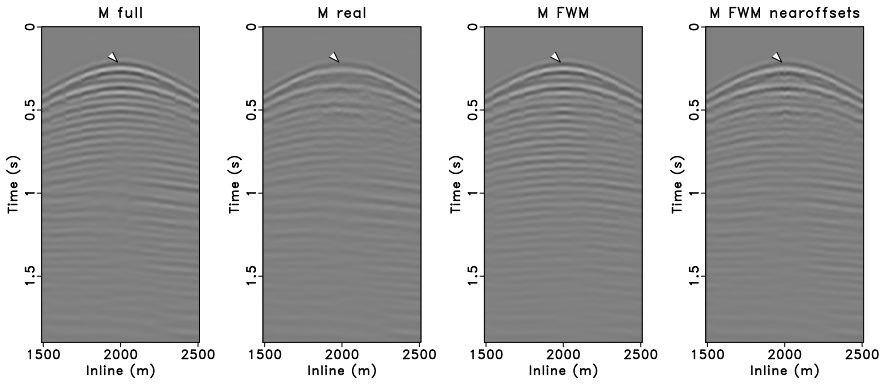

Figure 3.8: GSMP estimated multiples based on (a) a full receiver coverage, (b) a real world receiver coverage, (c) a FWM reconstructed full receiver coverage, and (d) a real world plus FWM reconstructed nearoffset receiver coverage. Crossline source sampling is 420 m in all these tests.

After 3D FWM-aided reconstruction, the fully sampled receiver side data can be obtained. A set of different input data scenarios are implemented for GSMP, and the results are shown in Figure 3.8. The current ideal situation indicates a full receiver coverage, therefore, we feed the original full sampled (only receiver side) data to GSMP. Note that this "ideal" situation is still not perfect, as sources are still undersampled. First, Figure 3.8(a) shows the full receiver coverage estimated multiple model without adaptive matching, which resembles to the true multiples. Next, a real world receiver coverage, which is the worst scenario, is fed to GSMP. The corresponding result is displayed in Figure 3.8(b). It can be seen that due to the missing near-offsets and undersampling along the crossline direction the estimated multiples have much weaker amplitude and wrong phase (event indicated by the arrow), which could lead to a failed subtraction. Next, we feed FWM reconstructed full receiver coverage to GSMP, which results in the estimated multiples in Figure 3.8(c). Visually it is very similar to the full receiver coverage result for the shallow part, however, there might be some errors for the deeper part. In the end, we only feed the FWM reconstructed near-offsets plus the recorded data to GSMP, and the estimated multiples are shown in Figure 3.8(d). FWM reconstructed near-offsets are crucial for improving the shallow multiples compared to the worst case in Figure 3.8(b) although it performs worse than the FWM reconstructed full receiver coverage.

Figure 3.9 presents the corresponding primaries after a global adaptive subtraction of the estimated multiples in Figure 3.8. Compared to Figure 3.7(b) it is clear that all results show residual multiples as this is the first SRME iteration and sources are still undersampled. More iterations and inversion-type 3D multiple estimation is our further research. It can be noticed the multiple leakage for the real world scenario indicated by the arrows is

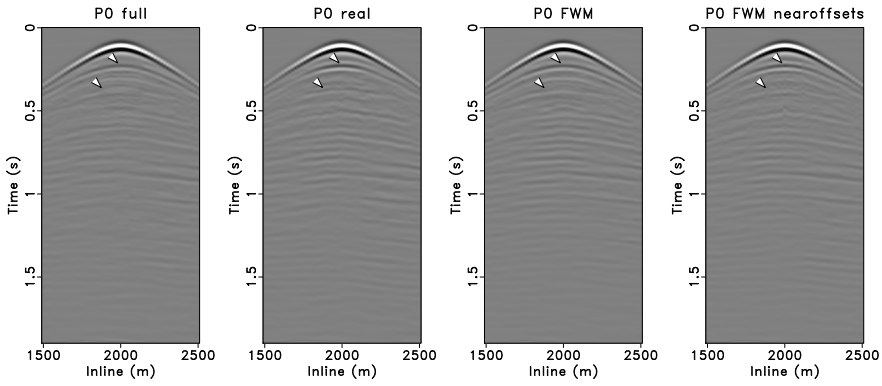

Figure 3.9: Post-subtraction primaries based on (a) a full receiver coverage, (b) a real world receiver coverage, (c) a FWM reconstructed full receiver coverage, and (d) a real world plus FWM reconstructed nearoffset receiver coverage.

much worse than the rest. The FWM reconstructed full receiver case (Figure 3.9(c)) is the closest to the ideal full receiver case (Figure 3.9(a)), while the near-offsets are crucial for less multiple leakage.

3.6. DISCUSSION

In this chapter we mainly investigate the influence of the receiver side data reconstruction on multiple estimation. We recover the receiver side by FWM and use GSMP for the source side due to logistics, i.e., large data storage. In theory, we prefer a full sampling data in both receiver and source sides, and then full 3D SRME is even available. We tested this ideal sampling case for the first simple and smaller 3D layered model, and full 3D SRME is still feasible. In the presented 3D Overthrust example, however, both memory and computational cost surge significantly for data reconstruction oriented 3D FWM (i.e., the proposed application), which is our current dilemma. Therefore, we only utilize 63 shots for efficiency, which is also close to real world. Still, more shots are preferred, and at least double the number of sources along crossline direction is our next step.

As for the reconstruction accuracy, it is very promising for the simple 3D layered model. However, as for the 3D Overthrust model, we noticed that due to the model complexity FWM performs worse for the deep part, which could lead to a undesired multiple estimation. The limited number of sources might also degrade the FWM performance despite of taking multiples into account. Therefore, it would be more robust to apply the proposed framework on the shallow part of the data.

3.7. CONCLUSIONS

We have proposed a cascaded framework for 3D multiple estimation in shallow-water scenarios, which includes a data reconstruction step via 3D FWM and a multiple estimation

step via 3D SRME or GSMP. The strong data reconstruction power of FWM is crucial for better near-offset reconstruction and the subsequent multiple prediction. 3D FWM has demonstrated its strong data reconstruction power through two different shallow-water 3D synthetic data sets. Besides, FWM-aided 3D SRME could deliver the best primary and multiple estimation due to fully taking advantages of the FWM reconstruction power. Nevertheless, FWM-aided 3D SRME is currently not affordable due to the huge data storage issue and the intensive computational cost. FWM-aided GSMP only utilizes partial reconstruction power of FWM (i.e., near-offset reconstruction), however, it can provide acceptable results with less computational resources. Application on two different 3D synthetic data demonstrate the good performance of the proposed framework in a shallow-water scenario.

REFERENCES

[1] E. J. van Dedem and D. J. Verschuur, *3D surface-related multiple prediction: A sparse inversion approach,* Geophysics **70** (2005), pp. V31–V43.

[2] I. Moore and B. Dragoset, *General surface multiple prediction: a flexible 3D SRME algorithm,* First Break **26** (2008), pp. 89–100.

[3] B. Dragoset, E. Verschuur, I. Moore, and R. Bisley, *A perspective on 3D surface-related multiple elimination,* Geophysics **75** (2010), pp. 75A245–75A261.

[4] D. J. Verschuur, *Seismic multiple removal techniques : past, present and future* (EAGE Publications, 2013).

[5] G. J. van Groenestijn and D. J. Verschuur, *Estimating primaries by sparse inversion and application to near-offset data reconstruction,* Geophysics **74** (2009), pp. A23–A28.

[6] C. Kostov, F. Xavier de Melo, A. Raj, A. Zarkhidze, A. Cooke, G. Miers, and J. Bacon, *Multiple attenuation for shallow-water surveys: Notes on old challenges and new opportunities,* The Leading Edge **34** (2015), pp. 760–768.

[7] D. Zhang and E. Verschuur, *Integration of closed-loop surface-related multiple estimation and full wavefield migration for shallow water,* in *81st EAGE Conference and Exhibition* (European Association of Geoscientists & Engineers, 2019).

[8] N. Hargreaves, *Surface multiple attenuation in shallow water and the construction of primaries from multiples,* in *76th SEG Technical Program Expanded Abstracts* (Society of Exploration Geophysicists, 2006).

[9] P. Plasterie, M. Gayne, M. Lange, I. Sarjono, A. Pica, S. Leroy, G. Poulain, R. Bril, C. Faulkner, and C. Mosher, *Shallow water 3D surface-related multiple modelling, case study,* in *78th SEG Technical Program Expanded Abstracts* (Society of Exploration Geophysicists, 2008).

[10] P. Wang, H. Jin, S. Xu, and Y. Zhang, *Model-based water-layer demultiple,* in *81st SEG Technical Program Expanded Abstracts* (Society of Exploration Geophysicists, 2011).

[11] H. Jin, M. Yang, P. Wang, Y. Huang, M. J. Parry, and Y. Paisant-Allen, *Application of MWD for shallow water demultiple - Hibernia case study,* in *74th EAGE Conference and Exhibition* (European Association of Geoscientists & Engineers, 2012).

[12] H. Jin and P. Wang, *Model-based water-layer demultiple (MWD) for shallow water: from streamer to OBS,* in *82nd SEG Technical Program Expanded Abstracts* (Society of Exploration Geophysicists, 2012).

[13] B. Hung, M. Wang, K. Yang, and X. Wu, *Enhanced internal multiple attenuation in shallow water environment,* in *84th SEG Technical Program Expanded Abstracts* (Society of Exploration Geophysicists, 2014).

[14] D. J. Verschuur and A. J. Berkhout, *From removing to using multiples in closed-loop imaging,* The Leading Edge **34** (2015), pp. 744–759.

[15] D. J. Verschuur and A. J. Berkhout, *Seismic migration of blended shot records with surface-related multiple scattering,* Geophysics **76** (2011), pp. A7–A13.

[16] A. J. Berkhout, *Review paper: An outlook on the future of seismic imaging, Part II: Full-wavefield migration,* Geophysical Prospecting **62** (2014), pp. 931–949.

[17] M. Davydenko and D. Verschuur, *Full-wavefield migration: using surface and internal multiples in imaging,* Geophysical Prospecting **65** (2016), pp. 7–21.

[18] A. J. Berkhout, *Seismic migration: Imaging of acoustic energy by wave field extrapolation, A: Theoretical aspects* (Elsevier (second edition), 1982).

[19] A. Nath and E. Verschuur, *Using surface-related multiples in imaging for data with large acquisition gaps,* in *87th SEG Technical Program Expanded Abstracts* (Society of Exploration Geophysicists, 2017).

[20] A. J. Berkhout, *Review paper: An outlook on the future of seismic imaging, Part I: forward and reverse modelling,* Geophysical Prospecting **62** (2014), pp. 911–930.

[21] D. Zhang and E. Verschuur, *3D surface-related multiple estimation for shallow water aided by full wavefield migration,* in *EAGE Conference and Exhibition Online* (European Association of Geoscientists & Engineers, 2020).

4

LOCAL PRIMARY-AND-MULTIPLE ORTHOGONALIZATION

Accurate multiple removal remains an important step in seismic data processing sequences. Most multiple removal methods, like surface-related multiple elimination (SRME), consist of a multiple prediction step and an adaptive subtraction step. Due to imperfect circumstances (e.g. coarse data sampling) or built-in assumptions (e.g. 2D method versus 3D data), multiple leakage is commonly observed in the results. More aggressive adaptive multiple subtraction can reduce the leakage problem, for example, by using small local windows and a long filter length, but at risk of severely damaging the primaries due to overfitting. In contrast, conservative adaptive subtraction with large or global windows and a short filter length can preserve most primary energy while tending to have more multiple leakage because of underfitting. Assuming that the primaries and multiples do not correlate locally in the time-space domain, a proposed solution to this problem is to extract the leaked multiples from the initially estimated primaries using local primary-and-multiple orthogonalization (LPMO) rather than restoring the damaged primaries. The proposed framework consists of two steps: an initial primary estimation step and a multiple leakage extraction step. The initial step corresponds to conservative SRME (or equivalent method) that produces the initially estimated primary and multiple models. The second step is based on LPMO to retrieve the leaked multiples from the estimated primaries via a time- and space-varying weight function that is estimated from the local correlation of predicted multiples and residual multiples in the estimated primaries with the help of shaping regularization. In this way we can obtain a better primary model that has much less leaked multiple energy and less primary damage at the same time. We demonstrate a good performance of this proposed framework via two synthetic data examples and one field data example.

This chapter is a slightly modified version of the published paper "D. Zhang, D. J. Verschuur, S. Qu, and Y. Chen, Surface-related multiple leakage extraction using local primary-and-multiple orthogonalization, Geophysics 85 (2020), pp. V81–V97". Note that all figures have been replotted in a consistent manner to other chapters.

4.1. INTRODUCTION

Surface-related multiples have been regarded as coherent noise and removed before the subsequent processing workflows for decades [1–5]. Meanwhile, exploration geophysicists gradually realized that these multiples (note that we refer multiples to only surface-related multiples in this thesis and the internal multiples are beyond the scope of this research) are able to see through the earth multiple times and, therefore, carry valuable physical information about the subsurface [6]. Multiples are nowadays treated as useful signals as well and can be directly included into the imaging algorithms [7–12]. Although full wavefield imaging (including both primaries and all types of multiples) can be achieved, it is still desired to estimate primaries and multiples first and then image them separately, due to the crosstalk of multiples during imaging, the challenges in shallow-water scenarios and the benefits for conventional primary-oriented processing.

Surface-related multiple elimination (SRME) is the standard tool for primary and multiple estimation for decades. However, dilemma between primary damage and surface-related multiple leakage usually occurs due to the inaccurate data reconstruction and the overlapping events. Despite all the efforts mentioned in Chapter 1, surface-related multiple leakage still can be seen in the results of SRME predicted primaries. The reasons behind are simply because: first, the data reconstruction can never be perfect, which leads to both phase and amplitude errors in the predicted multiples. Second, the assumption of adaptive subtraction that primaries and multiples do not correlate is often not met. Essentially, the imperfections of adaptive subtraction directly lead to multiple leakage in the estimated primaries. It tends to be either underfitting or overfitting for the subtraction step regardless of the forced constraint. Underfitting results in more severe multiple leakage while overfitting can alleviate multiple leakage to some extent. However, overfitting is unfortunately the main cause for primary energy damage, as removing more multiples usually comes along with damaging primaries. The ability of least-squares adaptive subtraction strongly depends on the size of local windows and the filter length. A small window size and a long filter length, which is called standard SRME in this thesis, lead to better multiple removal, but at the same time causes more primary damage. For the primary-oriented processing, the best one can achieve during the trade-off is to protect the primaries as much as possible and, as a result, leave some amount of multiple leakage. That is to say, the local windows for SRME should be relatively large and the filter length for adaptive subtraction should be relatively short. We name this type of SRME as the conservative SRME. More specifically, note that in this thesis, conservative SRME indicates the L2-norm adaptive subtraction step in the last iteration with large local windows or even global windows and a short filter length, in which the primaries are not damaged while surface-related multiple leakage is relatively more severe. In contrast, standard SRME means the L2/L1-norm adaptive subtraction step in the last iteration with small local windows and a long filter length, in which the multiple leakage is alleviated while the primary damage is relatively more severe. Instead of solving the leakage issue within the SRME itself, it might be much easier and more effective if another external extraction step is included after the conservative SRME to compensate for the multiple leakage.

To this end, multiple leakage can also be seen as one type of signal leakage if we temporarily treat multiples as our useful signal. Signal leakage is a long-standing problem in the field of random noise attenuation [13, 14]. Most studies try to propose more ad-

vanced denoising algorithm by introducing more solid assumptions. However, the fact that signal leakage always exists should be kept in mind regardless of the algorithms. An extra external step to compensate for the signal leakage might therefore be preferable. [15] proposed to extract the leaked signal from random noise using an extra local signal-and-noise orthogonalization step and showed very promising results, in which traditional f-x deconvolution is used as the initial denoising operator. In addition, successful applications on removing ground-roll noise and blending noise based on local orthogonalization are reported [16, 17]. Inspired by the concept of local orthogonalization, we propose a new framework for primary estimation and surface-related multiple leakage extraction using local primary-and-multiple orthogonalization (LPMO) to complement the conservative SRME. This local orthogonalization assumption is equivalent to assuming that the primaries and multiples do not correlate locally in the time-space domain. In this chapter, we focus on both standard and conservative SRME with least-squares adaptive subtraction. The proposed framework mainly consists of two steps: an initial primary estimation step and a multiple leakage extraction step. The initial step corresponds to the conservative SRME (or equivalent method), which produces the initially estimated primary and multiple models. The second step is based on LPMO to extract the leaked multiples from the estimated primaries via a time- and space-varying weight function that is estimated from the local correlation of predicted multiples and residual multiples in the estimated primaries with the help of shaping regularization, which can be regarded as an external remedy for correcting the initially predicted primaries and multiples from the conservative SRME. Thus, we can obtain better primary and multiple models for subsequent processing steps. Preliminary results are shown in [18]. Fair comparisons with standard SRME are also provided to display their different behaviors in this chapter. We demonstrate a good performance of our proposed two-step framework on two synthetic and one field data set. Above all, the proposed framework could make the conventional adaptive subtraction process easier to parameterize and also be beneficial for the subsequent quality control (QC) step.

We organize this chapter as follows: First, we present a brief review of SRME and some important aspects for the adaptive subtraction. The LPMO is then introduced in detail, which together with a conservative SRME primary estimation approach forms our proposed two-step framework. Two synthetic examples are provided to describe and compare the proposed approach with the standard SRME. In addition, a comprehensive investigation on shallow-water field data is presented to demonstrate the effectiveness of the proposed framework. A discussion part on the important aspects of the algorithm is also included at the end.

4.2. REVIEW OF SRME

SRME or specifically iterative SRME is briefly reviewed in this section. Let $\mathbf{P}$ represent the monochromatic total upgoing wavefields from all sources recorded at the surface, and $\mathbf{P}_0$ denote primary wavefields. Both $\mathbf{P}_0$ and $\mathbf{P}$ are in the detail-hiding notation [19], where vectors (the columns of the matrix) represent monochromatic shot records. The core engine used for all SRME-based algorithms can be expressed as follows:

$$\mathbf{P}_0 = \mathbf{P} - \mathbf{P}_0\mathbf{A}\mathbf{P} = \mathbf{P} - \mathbf{M}, \tag{4.1}$$

where **A** is the surface operator, being defined as $\mathbf{S}^{-1}\mathbf{R}^{\cap}$, i.e., the surface reflectivity from below combined with the inverse source properties. Surface multiples **M** can be predicted based on $\mathbf{P}_0\mathbf{AP}$. The traditional SRME based on equation 4.1 is an iterative approach [20] in the way that $\mathbf{P}_0^{k+1} = \mathbf{P} - \mathbf{P}_0^k\mathbf{A}^{k+1}\mathbf{P}$, where k represents the iteration number, which is typically 2 or 3.

The adaptive subtraction step for SRME is implemented in the time domain using a minimum-energy constraint:

$$\mathbf{E} = \sum_{t,x_r,x_s} [p(t,x_r,x_s) - a^{(k+1)}(t) * \hat{m}^{(k+1)}(t,x_r,x_s)]^2, \tag{4.2}$$

where $p(t,x_r,x_s)$, $\hat{m}^{(k+1)}(t,x_r,x_s)$ and $a^{(k+1)}(t)$ represent the estimated primaries, the unadapted multiples (i.e. $-\mathbf{P}_0\mathbf{P}$) and the surface operator in the time domain, respectively. The length of the surface operator is also known as the filter length, which is capable of controlling the trade-off between underfitting and overfitting. x_r and x_s are the source and receiver locations of seismic data. For the standard SRME, the predicted multiples are first matched and subtracted in a global window during the first 1 or 2 iterations. Small local windows and a long filter length are then utilized for adaptive subtraction in the last iteration to better remove the multiples [3]. It is worth noting that small local windows and a long filter length for standard SRME can damage the primaries though more multiples are removed due to overfitting. On the other hand, for conservative SRME when the last iteration of adaptive subtraction is still implemented in a global window or large local windows with a short filter length, it leads to a more conservative result with much less primary damage and relatively more multiple leakage due to underfitting. However, we suggest and utilize the conservative SRME for primary-oriented processing to avoid hurting the primaries although there are more multiple leakage. Then, the leaked multiples can be further extracted by the algorithm discussed in the next section.

4.3. LOCAL PRIMARY-AND-MULTIPLE ORTHOGONALIZATION

The proposed LPMO should directly follow the initial primary and multiple estimation step and can be regarded as an external remedy for correcting the initially predicted primaries and multiples from the conservative SRME. Now, we rewrite the initial estimated primary and multiple relation in the time domain using the vector notation:

$$\mathbf{p} = \mathbf{p}_0 + \mathbf{m}, \tag{4.3}$$

where **p** is total upgoing wavefield. $\mathbf{p}_0$ and **m** represent the initial estimated primaries and multiples using any prediction method (conservative SRME in this thesis), respectively. Based on the assumption that the final estimated primaries $\tilde{\mathbf{p}}_0$ and multiples $\tilde{\mathbf{m}}$ should be orthogonal, we are capable of orthogonalizing them by:

$$\tilde{\mathbf{m}} = \mathbf{m} + \mathbf{w} \circ \mathbf{m}, \tag{4.4}$$

$$\tilde{\mathbf{p}}_0 = \mathbf{p}_0 - \mathbf{w} \circ \mathbf{m}, \tag{4.5}$$

where **w** is the LPMO weight and $\circ$ denotes the Hadamard product (i.e. sample-by-sample multiplication). This local orthogonalization assumption is equivalent to assuming that

the primaries and multiples do not correlate locally in the time-space domain:

$$\sum \tilde{\mathbf{p}}_0 \circ \tilde{\mathbf{m}} \approx 0. \tag{4.6}$$

The LPMO weight can be estimated by solving the following unconstrained minimization problem:

$$\min_{\mathbf{w}} \| \overbrace{\mathbf{p}-\mathbf{m}}^{\mathbf{p}_0} - \mathbf{w} \circ \mathbf{m} \|_2^2. \tag{4.7}$$

The above minimization problem utilizes weighted multiples to match the leaked multiples in the initially estimated primary model in a least-squares sense. By forcing a smooth constraint to the unconstrained minimization problem in equation 4.7, we thus obtain a constrained optimization problem:

$$\hat{\mathbf{w}} = \arg\min_{\mathbf{w}} \|\mathbf{p}_0 - \mathscr{M}\mathbf{w}\|_2^2 + \mathbf{S}(\mathbf{w}), \tag{4.8}$$

where $\mathscr{M} = diag(\mathbf{m})$ and $\mathbf{S}(\mathbf{w})$ denotes a smooth constraint operator. Furthermore, with the power of shaping regularization [21] we are able to solve the least-squares problem:

$$\hat{\mathbf{w}} = [\lambda^2 \mathbf{I} + \mathscr{T}(\mathscr{M}^T \mathscr{M} - \lambda^2 \mathbf{I})]^{-1} \mathscr{T} \mathscr{M}^T \mathbf{p}_0, \tag{4.9}$$

where λ is a scaling parameter and $\mathscr{T}$ represents a triangle smoothing operator that fulfills the role of smooth constraint operator $\mathbf{S}(\mathbf{w})$. $[\cdot]^T$ denotes matrix transpose. In order to make our solution more stable and to avoid unphysical results, we apply an additional thresholding operator and median filter to the estimated LPMO weight:

$$\bar{\mathbf{w}} = \mathbf{FT}(\hat{\mathbf{w}}), \tag{4.10}$$

where $\mathbf{T}$ is a thresholding operator that forces the weight to have values within 0 to 1, and $\mathbf{F}$ is a median filtering operator. The current LPMO weight range is very robust and more detailed description will be shown in the discussion part. Therefore, we can substitute our final estimated weight $\bar{\mathbf{w}}$ back into equations 4.4 and 4.5 to obtain the final results.

4.4. RESULTS

We have investigated our proposed two-step framework on two synthetic data sets and one field data set. For all the examples, a conservative SRME followed by the LPMO is applied to obtain the best result. In contrast, we also provide the standard SRME results as the comparison.

4.4.1. LENS-SHAPED SYNTHETIC DATA EXAMPLE

We first test our proposed two-step framework, namely conservative SRME followed by LPMO, on a 2D synthetic lens-shaped model, which consists of a water layer, a high velocity lens-shaped body overlying a target layer. Sources and receivers are placed covering the whole surface with a lateral interval of 20 m. For this 2D synthetic model, full wavefield numerical data are produced using full wavefield modeling (FWMod) [22] based on the velocity model in Figure 4.1(a) and the reflectivity model in Figure 4.1(b). Figure 4.2

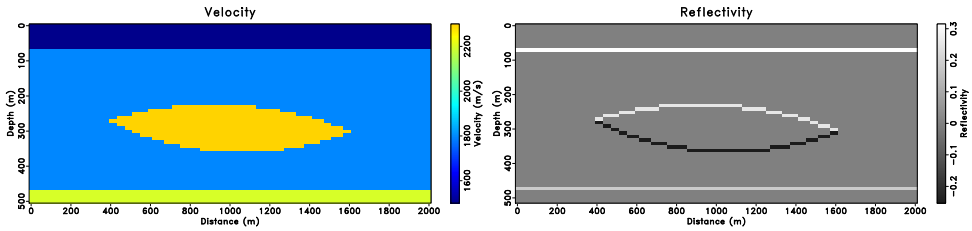

(a) (b)

Figure 4.1: 2D lens-shaped synthetic model. (a) Velocity model. (b) Reflectivity model.

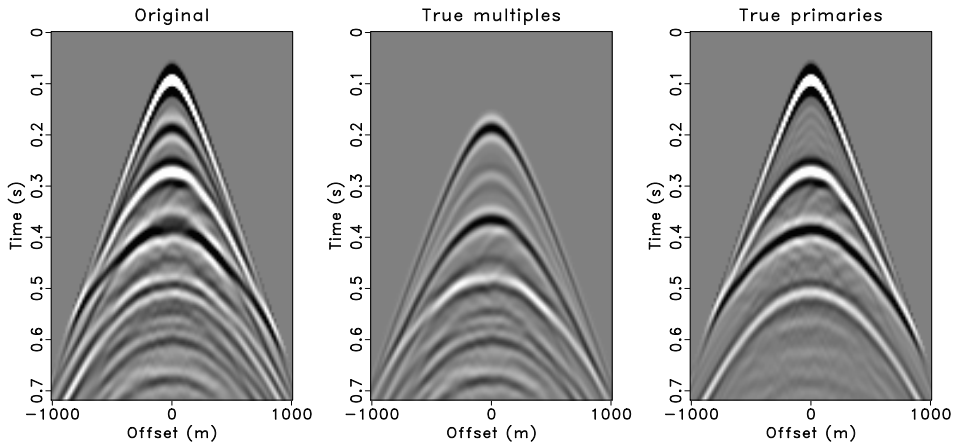

(a) (b) (c)

Figure 4.2: Modeled reference data. (a) True full wavefield. (b) True multiples. (c) True primaries.

presents the modeled ground-truth wavefields, in which the true multiples and primaries are used as reference data.

Initially predicted multiples and primaries using conservative SRME with a global subtraction window are displayed in Figures 4.3(a) and 4.3(b), respectively. The filter length for the global adaptive subtraction is 28 ms. Note that due to some overlapping energy between multiples and primaries and global window adaptive subtraction, there exists obvious multiple leakage in the initially estimated primary model shown in Figure 4.3(b). Also, the amplitude of the estimated multiples in Figure 4.3(a) is weaker than the true multiples in Figure 4.2(b) due to this leakage. However, these leaked multiples can be well detected by the proposed LPMO where in this example the smoothing radii of the triangle smoothing operator is 2 time samples, the thresholding ranges from 0 to 1, and the size of the median filter is 5 time samples $*$ 5 traces. The final estimated LPMO weight according to equation 4.10 is shown in Figure 4.3(c). We can clearly recognize the shape of leaked mul-

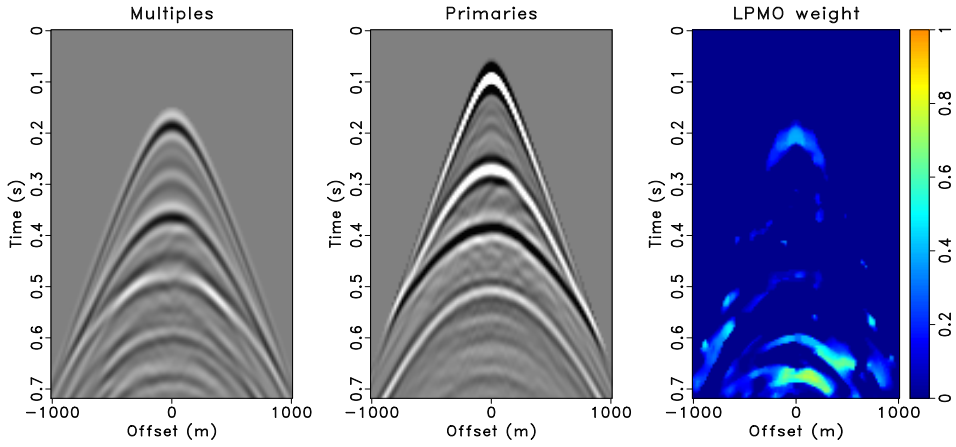

(a) (b) (c)

Figure 4.3: Initially predicted multiples (a) and primaries (b) using conservative SRME with a global subtraction window. (c) The estimated LPMO weight based on (a) and (b). Surface-related multiple leakage can be effectively detected by the LPMO weight.

tiples from the estimated weight. Thus, we utilize the estimated LPMO weight to extract these leaked multiple energy. After LPMO, the final estimated multiples and primaries are presented in Figure 4.4. Figures 4.4(a) and 4.4(b) are exactly the same conservative SRME results as Figures 4.3(a) and 4.3(b), and are only used for better comparison. The most obvious multiple leakage spots indicated by the arrows are successfully extracted in the final primary model as shown by Figure 4.4(e). At the same time, we can also observe the final estimated multiples in Figure 4.4(d) extract back their leaked energy, and thus, they are now more accurate and close to the true multiples in Figure 4.2(b). In order to test the improvement of our proposed framework, we propose to utilize the so-called local similarity map [23] as an effective measure to evaluate surface-related multiple leakage extraction performance. After calculating the local similarity between estimated primaries and multiples before and after LPMO, we are able to better judge whether the surface-related multiple leakage is extracted or not. A high similarity value means high correlation between the two data sets. From the local similarity maps, shown in Figures 4.4(c) and 4.4(f), it can be concluded that the leaked multiple energy around 0.2 s and 0.6 s has been successfully extracted due to the low similarity observed around these areas after LPMO. At the same time, it is worth noting that there still exist some high similarity areas between the final predicted multiples and primaries after the proposed LPMO step in Figure 4.4(f). The reason behind is that these high similarity areas indicate the local overlapping areas between multiples and primaries. Although the overlapping areas cannot be solved due to the violation of the initial assumption, they are well protected from damage by the proposed method through the thresholding process and the smoothing operator. We also provide a single trace comparison at offset -60 m in Figure 4.5. The black line denotes the modeled true primaries. The green and the red lines represent the conservative SRME primaries

and its primaries after LPMO, respectively. It is clear that the leaked multiples visible in the green line are effectively extracted and the red line is closer to the true primaries.

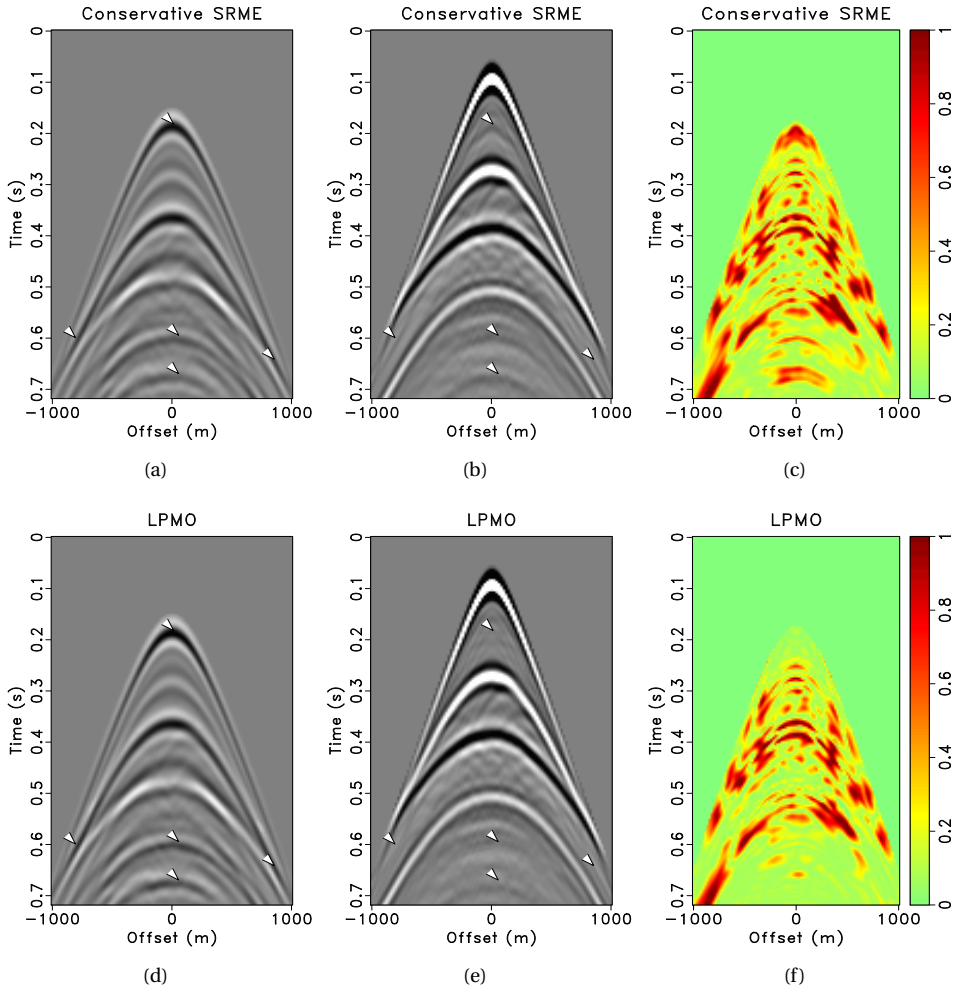

Figure 4.4: (a) & (b) Initially predicted multiples and primaries using conservative SRME with a global subtraction window, respectively. (d) & (e) Final estimated multiples and primaries after LPMO, respectively. (c) & (f) Local similarity maps before and after LPMO, respectively. The arrows indicate where the leaked multiples are extracted.

Next, we will introduce a fair comparison between the proposed framework and the standard SRME. In detail, we provide two standard SRME results: L2-norm standard SRME with 240 ms $*$ 25 traces local subtraction window size and L1-norm standard SRME with 240 ms $*$ 25 traces local subtraction window size [24]. The filter length for local subtraction windows is 28 ms. Although this filter length is the same with the global subtraction

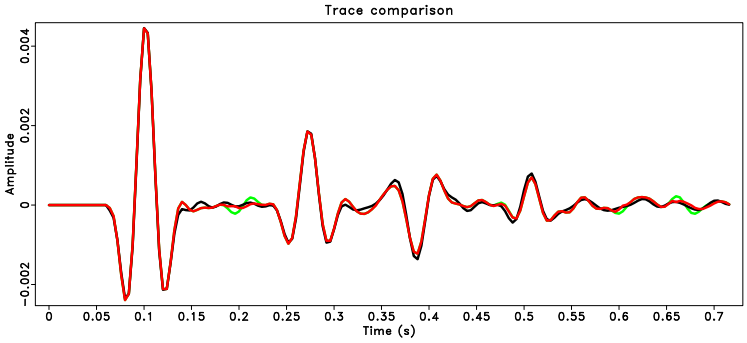

Figure 4.5: Single trace comparison before and after LPMO. The black line denotes the true modeled primaries, the green line denotes the conservative SRME primaries, and the red line denotes the proposed primaries after LPMO.

4

window case, it is actually much more powerful due to the utilization of small local windows. The estimated primary results are shown in Figures 4.6(a) and 4.6(b), respectively. For comparison, the final estimated primaries from the proposed framework is also displayed in Figure 4.6(c). From Figure 4.6 we can see that compared to the proposed primaries, both L2-norm and L1-norm standard SRME results exhibit more multiple leakage indicated by the arrows and at the same time more primary damage indicated by the rectangles. Note that the L1-norm result seems to be slightly better than the L2-norm result in terms of preserving primaries, and also better at extracting multiple leakage at around 0.2 s and 0.6 s. Essentially, small local subtraction windows and a long filter length in standard SRME lead to more primary damage for the adaptive subtraction although the multiple leakage of standard SRME is better than the conservative SRME result. The proposed two-step framework to extract surface-related multiple leakage, however, exhibits both less primary damage and less multiple leakage.

4.4.2. COMPLEX SALT SYNTHETIC DATA EXAMPLE

The second synthetic example is a more complex salt model, which has 201 shots and 201 receivers with a lateral interval of 15 m. The velocity model is shown in Figure 4.7 and it consists of a shallow water layer, shallow layers, a high velocity salt layer and deep target layers. The data set is generated by acoustic finite difference modeling. Figures 4.8(a) and 4.8(b) show the true full wavefield and the reference primaries, respectively. It is obvious that the surface-related multiples are strong and the deep primaries are severely interfered by the multiples. Note that the amplitude of the primaries in the full wavefield is slightly smaller than the reference primaries due to the deghosting process that was applied to the full wavefield.

The proposed two-step framework is applied to this data set. Initially estimated multiples and primaries by the conservative SRME with a global subtraction window are displayed in Figures 4.9(a) and 4.9(b), respectively. The filter length is 40 ms. Compared to the reference primaries in Figure 4.8(b), the multiple leakage is very obvious in the initially estimated primary model. Figure 4.9(c) demonstrates the final estimated LPMO weight that

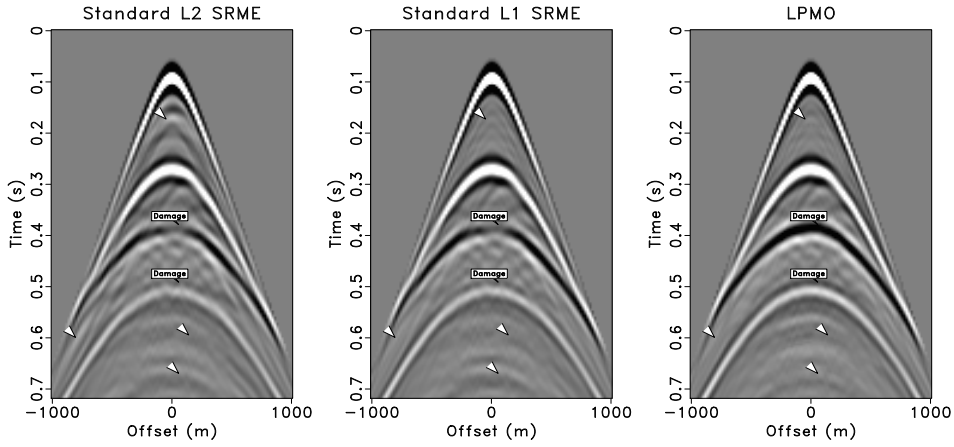

Figure 4.6: Comparison with the standard SRME. (a) L2-norm standard SRME primaries with 240 ms ∗ 25 traces local subtraction window size. (b) L1-norm standard SRME primaries with 240 ms ∗ 25 traces local subtraction window size. (c) The proposed primaries after LPMO (for comparison purpose). The arrows in (a) and (b) denote the more severe multiple leakage compared to (c). The rectangles in (a) and (b) denote the primary damage compared to (c).

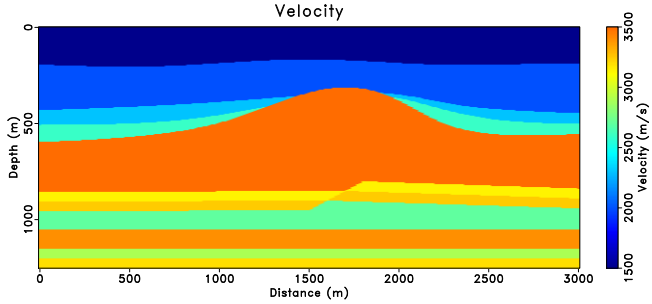

Figure 4.7: Complex salt velocity model.

shows good correlation with the leaked multiples. In this example, the smoothing radii of the triangle smoothing operator is 2 time samples, the thresholding ranges from -0.5 to 0.8, and the size of the median filter is 5 time samples ∗ 5 traces. Interestingly, the negative weight in this example means that there exist phase-shift errors during conservative SRME, and therefore, this part of the leaked multiple needs to be extracted by negative weights. Figure 4.10 displays the surface-related multiple leakage extraction results before and after LPMO. The conservative SRME predicted multiples and primaries shown in Figures 4.10(a) and 4.10(b) are only displayed for better comparison. The final estimated primaries after LPMO are presented in Figure 4.10(e), in which the leaked multiples are

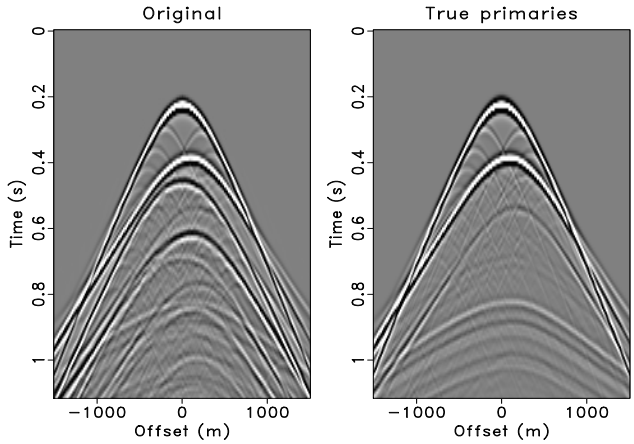

Figure 4.8: Modeled reference data. (a) True full wavefield after deghosting. (c) Reference primaries.

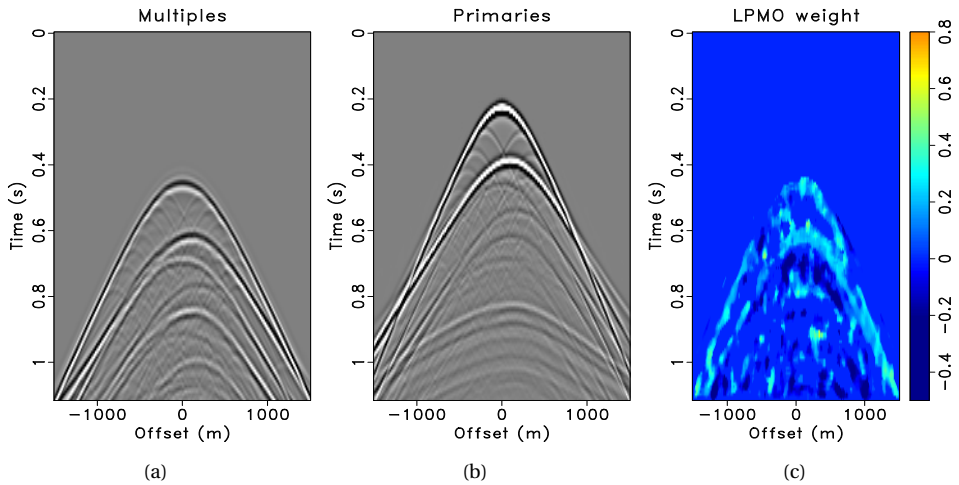

Figure 4.9: Initially predicted multiples (a) and primaries (b) using conservative SRME with a global subtraction window. (c) The estimated LPMO weight based on (a) and (b). Surface-related multiple leakage can be effectively detected by the LPMO weight. Note that the negative weights come from phase-shift errors during conservative SRME.

extracted indicated by the arrows. The rectangles indicate the extracted multiple leakage with phase-shift errors. Also, the final estimated multiples in Figure 4.10(d) show restoration of leaked energy compared to Figure 4.10(a). Similarly, the local similarity maps in

Figures 4.10(c) and 4.10(f) are used to better demonstrate the multiple leakage extraction improvement before and after LPMO. Moreover, a single trace comparison at offset 0 m as shown in Figure 4.11 is provided to display the effect of the proposed framework in detail. The black line indicates the reference primaries, the green line indicates the conservative SRME estimated primaries, and the red line indicate the primaries from the proposed two-step framework. It can be seen that these primaries (red line) are closer to the reference primaries (black line) and the larger amplitude of the leaked multiples (green line) around 0.6 s can be easily misinterpreted as primary energy.

A fair comparison with the standard SRME is carried out in Figure 4.12. L2-norm and L1-norm standard SRME primaries with 320 ms $*$ 25 traces local subtraction window size are shown in Figures 4.12(a) and 4.12(b), respectively. The filter length for both L2 and L1-norm cases is 56 ms, which is longer than the global subtraction case. For better comparison reason, the proposed two-step framework primaries are presented in Figure 4.12(c). Compared to the proposed primaries, the arrows indicate more leaked multiples in Figures 4.12(a) and 4.12(b). However in terms of the amount of multiple leakage, the standard SRME results all seem better than the conservative SRME result in Figure 4.10(b) due to overfitting. Meanwhile, the rectangles in standard SRME results denote more primary damage than the proposed primaries, which is the main drawback of the standard SRME. Still, we can find that the L1-norm standard result seems better than the L2-norm standard result with respect to the primary preservation.

4.4.3. FIELD DATA EXAMPLE

We present an example of the proposed two-step framework applied to a North Sea data set from the Nelson field as shown in Figure 4.13, and a comprehensive investigation is shown in this section. The data are extracted from a 2D dual-sensor towed-streamer line with 25 m source spacing and 12.5 m receiver spacing. From the dual-sensor data the upgoing wavefield was obtained [25]. By using reciprocity, shot interpolation and near-offset reconstruction [26], a split-spread dataset is obtained, from which a fixed-spread subset is selected with 201 sources and 201 receivers. Both source and receiver spacing are 12.5 m, where sources were interpolated from the original 25 m grid. The water depth is around 100 m, which is relatively shallow. The same data were used in [27] for inversion-type SRME. From Figure 4.13, it can be seen that the surface-related multiples are clearly present and the primaries are strongly interfered by the multiples.

Initially predicted multiples and primaries using conservative SRME with large local subtraction windows (500 ms $*$ 80 traces) are displayed in Figures 4.14(a) and 4.14(b), respectively. The filter length is 20 ms. Due to the fact that 3D data can never be perfectly represented by a 2D theory and given unavoidable interpolation errors, surface-related multiple leakage is obvious in the initially predicted primary model. Besides, the shallow-water scenario makes the problem even more difficult. The proposed LPMO weight is displayed in Figure 4.14(c), in which we are able to effectively detect the shape and position of the leaked multiples. In this example, the smoothing radii of the triangle smoothing operator is 2 time samples, the thresholding ranges from 0 to 1, and the size of the median filter is 3 time samples $*$ 3 traces. After LPMO, the final estimated multiples and primaries are presented in Figures 4.15. We are confident about the first-order surface-related multiple leakages indicated by the arrows. Therefore, the most obvious multiple leakages around

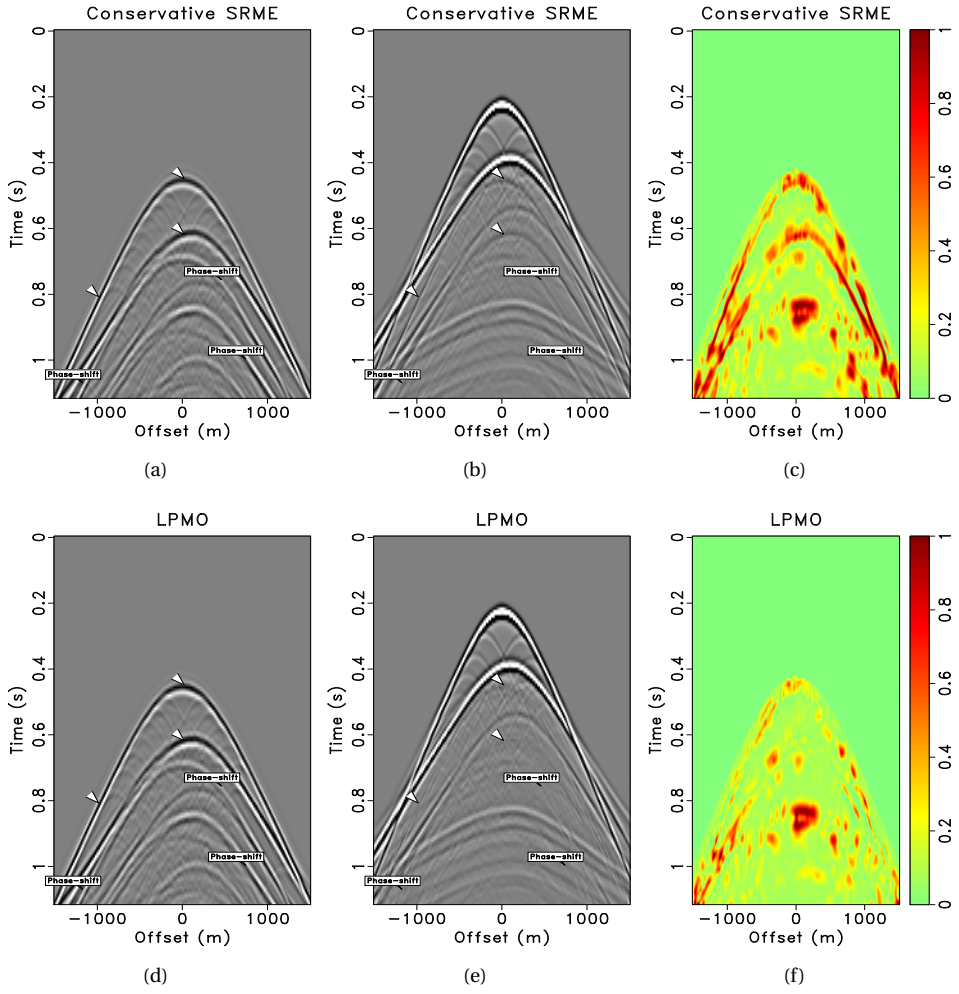

Figure 4.10: (a) & (b) Initially predicted multiples and primaries using conservative SRME with a global subtraction window, respectively. (d) & (e) Final estimated multiples and primaries after LPMO, respectively. (c) & (f) Local similarity maps before and after LPMO, respectively. The arrows indicate where the leaked multiples are extracted, and the rectangles indicate where the phase-shift leaked multiples are extracted.

0.7 s are effectively extracted in the final primary model shown in Figure 4.15(e), while we can also observe the final estimated multiples retrieved some of their leaked multiple energy shown in Figure 4.15(d). Here, we also utilize local similarity maps to measure whether the leaked multiples are extracted or not. From the local similarity maps shown in Figures 4.15(c) and 4.15(f), it can be seen that we have successfully extracted the leaked multiples especially around 0.7 s. A detailed single trace comparison at 87.5 m is shown

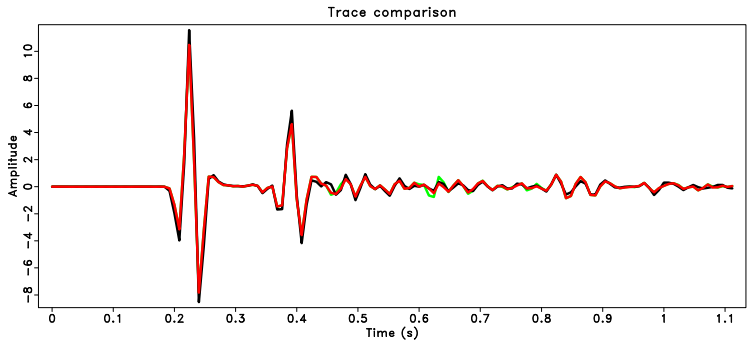

Figure 4.11: Single trace comparison before and after LPMO. The black line denotes the reference primaries, the green line denotes the conservative SRME primaries, and the red line denotes the proposed primaries after LPMO.

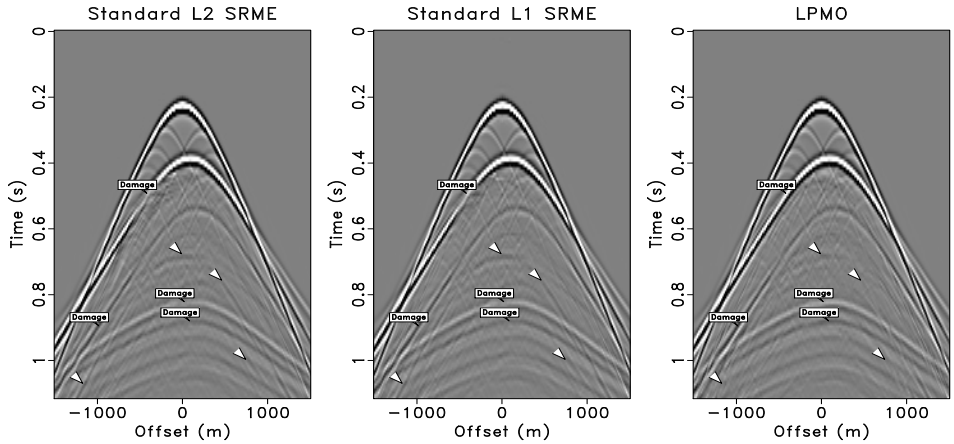

Figure 4.12: Comparison with the standard SRME. (a) L2-norm standard SRME primaries with 320 ms ∗ 25 traces local subtraction window size. (b) L1-norm standard SRME primaries with 320 ms ∗ 25 traces local subtraction window size. (c) The proposed primaries after LPMO (for comparison purpose). The arrows in (a) and (b) denote the more severe multiple leakage compared to (c). The rectangles in (a) and (b) denotes the primary damage compared to (c).

in Figure 4.16. The blue line denotes the full wavefield, the green line denotes the conservative SRME primaries and the red line denotes the primaries from the proposed framework. We can clearly see that the conservative SRME primaries (green line) around 0.7 s contain strong leaked multiples which can be easily misinterpreted as primaries. After LPMO, the proposed primaries (red line) around 0.7 s become much smaller than the con-

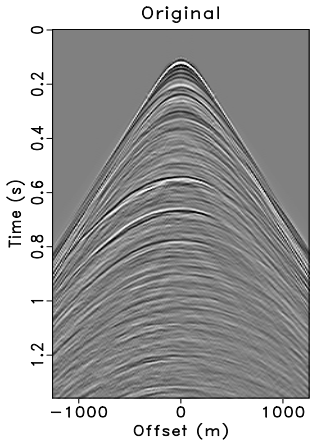

Figure 4.13: Field data shot record with surface-related multiples.

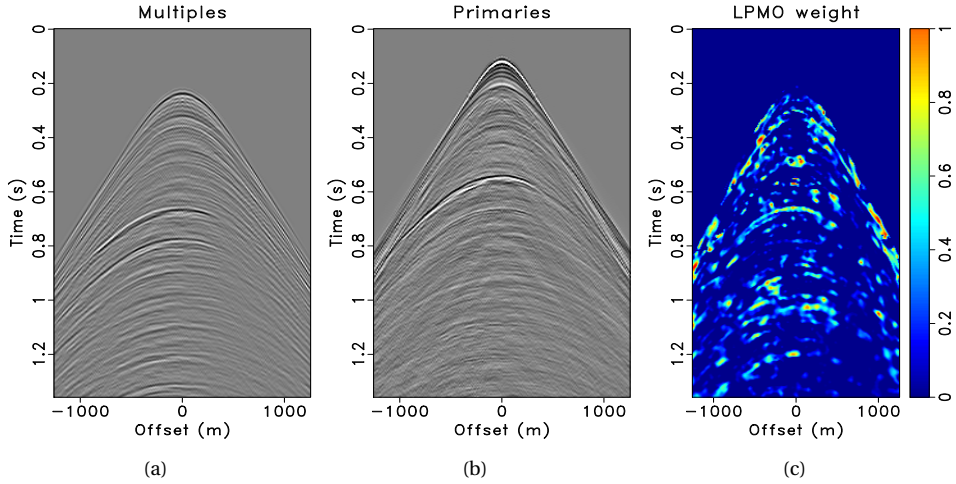

Figure 4.14: Initially estimated multiples (a) and primaries (b) using conservative SRME with large subtraction windows. (c) The estimated LPMO weight based on (a) and (b). Surface-related multiple leakage can be effectively detected by the LPMO weight.

servative SRME primaries (green line). Similar observations can be made when selecting the -150 m common-offset gathers as presented in Figure 4.17. All the arrows in Figures 4.17(b) and 4.17(c) represent the improvement of the leaked multiples for the proposed framework. Moreover, a stacked section comparison before and after LPMO is provided in Figure 4.18 to demonstrate the effectiveness of the proposed method. Compared to the stacked section of the full wavefield shown in Figuer 4.18(a), the conservative SRME primaries in Figure 4.18(b) have already removed lots of multiple energy, but some amount

of leaked multiples indicated by the arrows are still there. After LPMO, the proposed primaries in Figure 4.18(c) display much less multiple leakage, which is better for accurate interpretation.

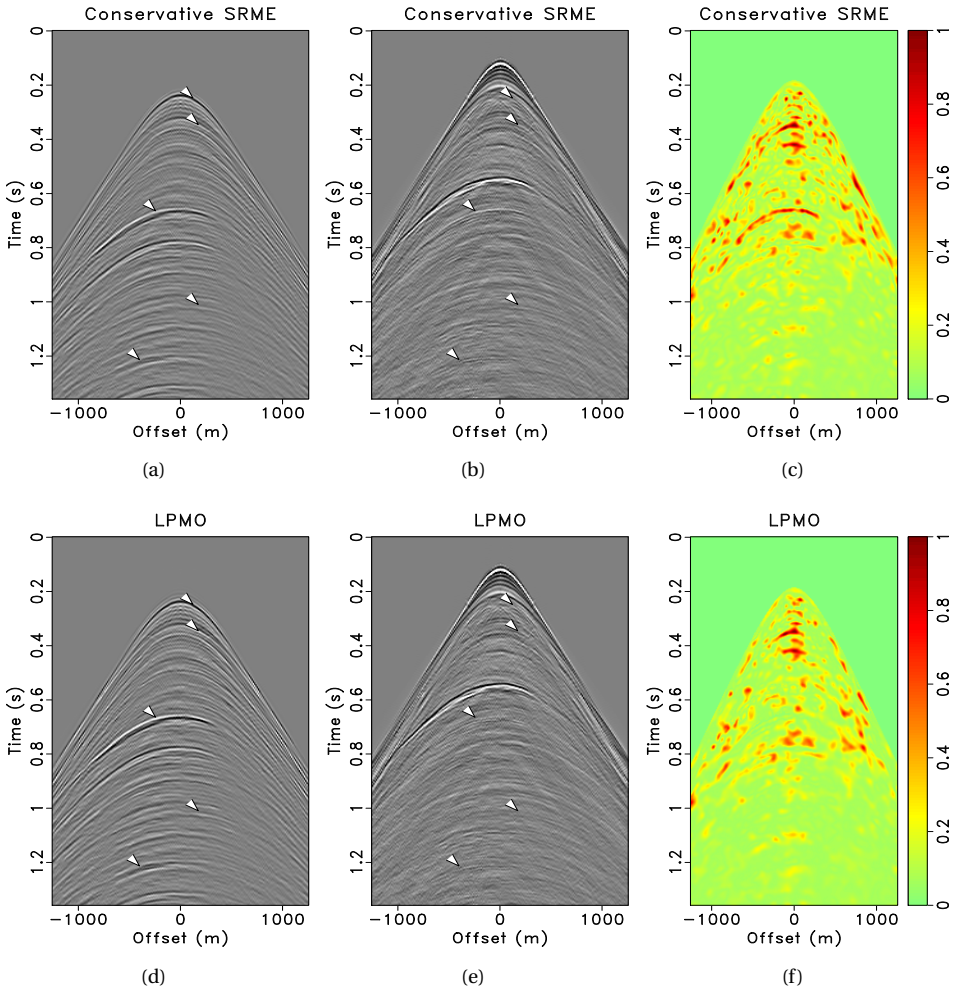

Figure 4.15: (a) & (b) Initially predicted multiples and primaries using conservative SRME with large subtraction windows, respectively. (d) & (e) Final estimated multiples and primaries after LPMO, respectively. (c) & (f) Local similarity maps before and after LPMO, respectively. The arrows indicate where the leaked multiples are extracted.

We also demonstrate the advantages of the proposed framework by providing a fair comparison with both standard SRME shot gathers and stacked sections in Figures 4.19 and 4.20. The local subtraction window size is 160 ms $*$ 25 traces for standard SRME and a longer filter length 44 ms is used. From the shot gather comparison, it can be seen that

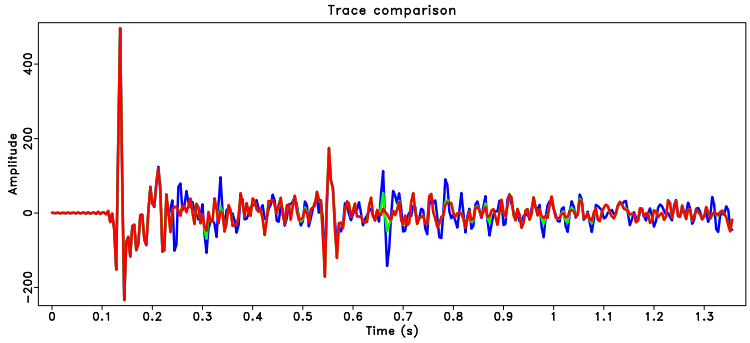

Figure 4.16: Single trace comparison at offset 87.5 m before and after LPMO. The blue line denotes the full wavefield, the green line denotes the conservative SRME primaries, and the red line denotes the proposed primaries after LPMO.

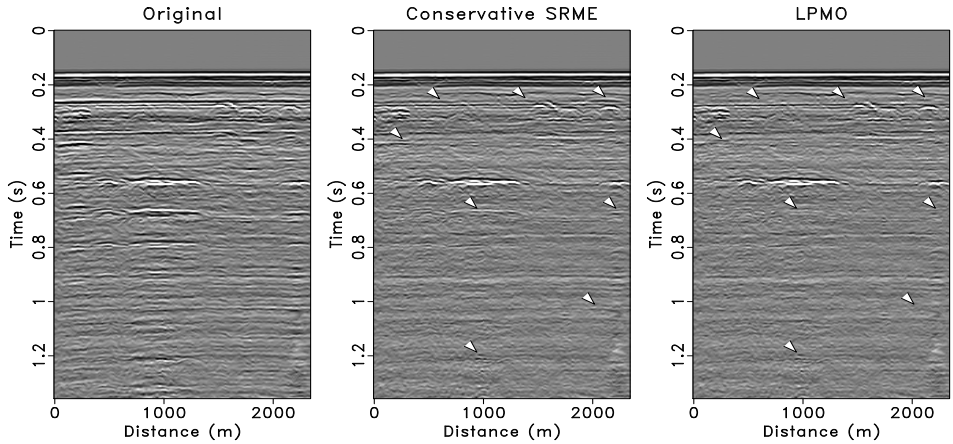

Figure 4.17: Common-offset gather comparison at offset -150 m. (a) Common-offset gather of the input. (b) Common-offset gather of the initially predicted primaries by the conservative SRME with large subtraction windows. (c) Common-offset gather of the final estimated primaries after LPMO.

both standard L2-norm SRME primaries in Figure 4.19(a) and L1-norm SRME primaries in Figure 4.19(b) display slightly more multiple leakage than the proposed primaries indicated by the arrows. Because of the small local subtraction windows and a long filter length, they are definitely better than the conservative SRME primaries shown in Figure 4.14(b) in terms of multiple leakage. Furthermore, the obvious primary damage indicated by the rectangles in both L1 and L2 norm standard SRME results reveals the overfitting of standard SRME, which can severely affect the subsequent imaging and interpretation

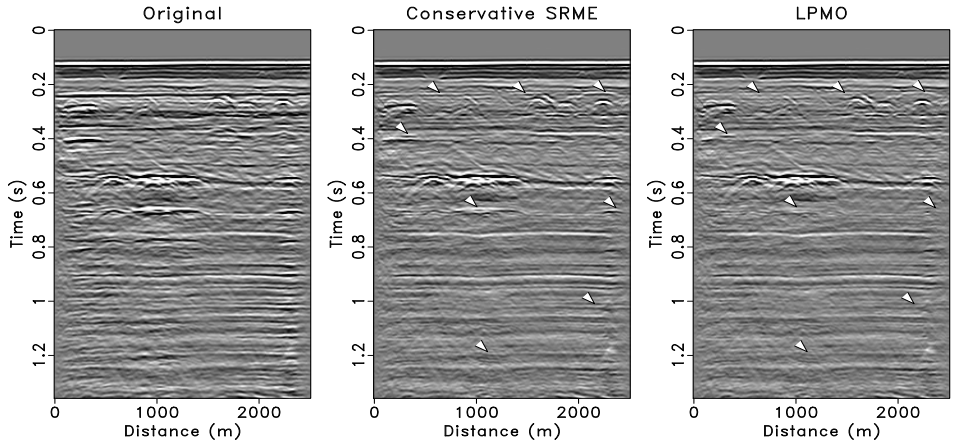

Figure 4.18: Stacked section comparison. (a) Stacked section of the input. (b) Stacked section of the initially predicted primaries by the conservative SRME with large subtraction windows. (c) Stacked section of the final estimated primaries after LPMO.

accuracy. The standard SRME stacked sections in Figures 4.20(a) and 4.20(b) show the negative influences of the damaged primaries as indicated by the rectangles, in which the primary energy is dimmed in general compared to the proposed primaries in Figure 4.20(c). Besides, the multiple leakage in the standard SRME results are still slightly more than the proposed result, as indicated by the arrows, although they are already better than the conservative SRME.

4.5. DISCUSSION

The essential differences between a one-point matching filter and the proposed LPMO step is more broadly discussed here including the computation of weights subject to smoothing, scaling, thresholding and median filtering. First, the proposed framework can be considered as a one-point non-stationary matching filter, which is capable of adapting to the complex non-stationary seismic data. Second, obtaining a one-point non-stationary filter requires solving a highly under-determined inverse problem. For this type of inverse problem, the shaping regularization is able to control the smoothness and deliver a fast convergence, which is indicated by equation 4.9. The smoothing radii used in the constraint operator $\mathbf{S}(w)$ contributes to the final resolution of the estimated weights. Furthermore, the scaling parameter λ usually can be set as $\|\mathcal{M}^T\mathcal{M}\|_2$. Both the thresholding and median filtering operators in equation 4.10 are especially designed for the multiple leakage extraction problem, which is not needed for the random noise removal case. Thresholding of the estimated LPMO weights is highly necessary, due to the complex behavior of multiples and primaries, while median filtering is purely for obtaining more stable result and avoiding outliers.

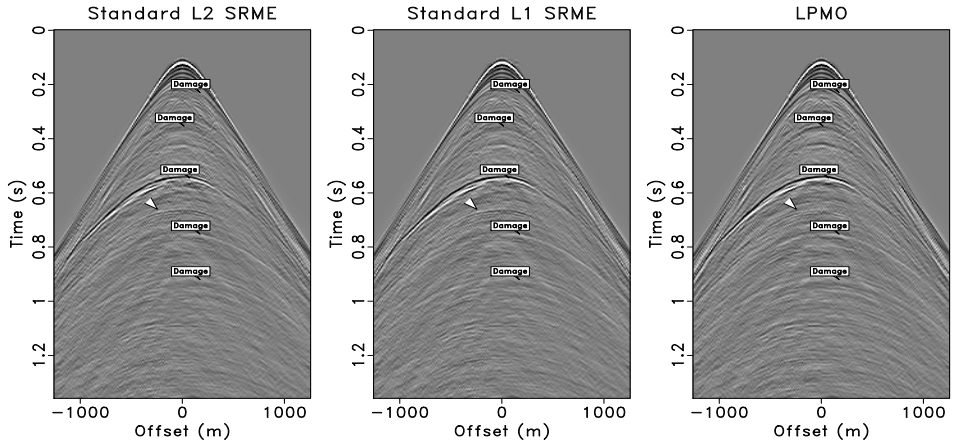

Figure 4.19: Shot gather comparison with the standard SRME. (a) L2-norm standard SRME primaries with 160 ms ∗ 25 traces local subtraction window size. (b) L1-norm standard SRME primaries with 160 ms ∗ 25 traces local subtraction window size. (c) The proposed primaries after LPMO (for comparison purpose). The arrows in (a) and (b) denote the more severe multiple leakage compared to (c). The rectangles in (a) and (b) denote more primary damage compared to (c).

The thresholding range is the very key parameter in the proposed framework. In the theory part, we mention that after shaping regularization we obtain the estimated LPMO weights and then we apply a thresholding operator $\mathbf{T}$ on the weights to force them to usually have values within 0 to 1. The logic behind it is shown in Figure 4.21. The yellow line indicates the estimated multiples from the conservative SRME. Usually, we can safely assume that the amplitude of the leaked multiple should be smaller than that of the estimated multiple, which means the estimated weights should be smaller than 1. As mentioned before, the overall LPMO can be seen as a one-point non-stationary matching filter [15] and the objective function only cares about the minimum energy after matching and subtraction. More importantly, the algorithm itself cannot tell the difference between leaked multiples and primaries. Therefore, there is a tendency for the algorithm to use estimated multiples to match the primaries, which will result in quite large weights (i.e. $\mathbf{w} > 1$) due to the fact that primaries usually have much higher amplitude than the estimated multiples. Thus, a thresholding operator can help the algorithm focus on the interested leaked multiple energy. It is necessary to be aware of other special situations regarding the thresholding operator. First, as mentioned in the complex salt model example, the estimated LPMO weight introduces some negative values as shown in Figure 4.9(c). This is because of the phase-shift errors when predicting the multiple model. Thus, in this case, the multiple leakage and the estimated multiple model might have opposite polarity, which can be compensated by introducing negative weights. Secondly, real data always have some sampling issues (e.g. near offsets missing and crossline under-sampling). Even

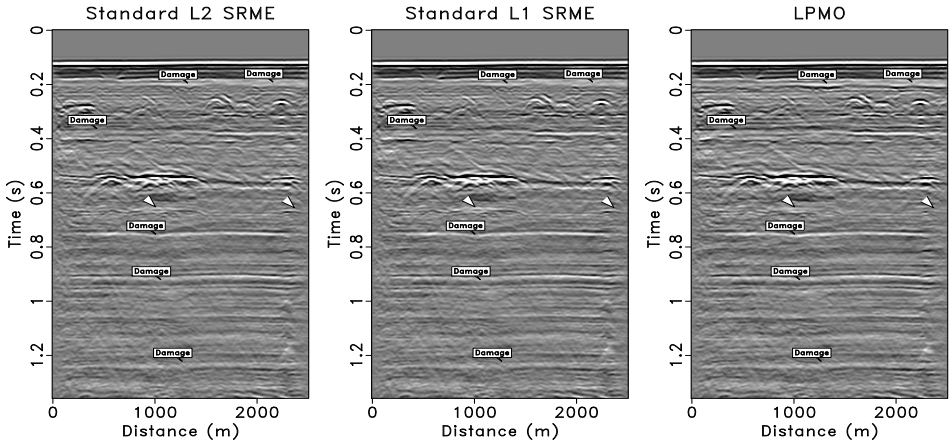

(a) (b) (c)

Figure 4.20: Stacked section comparison with the standard SRME. (a) Stacked section of the L2-norm standard SRME primaries with 160 ms ∗ 25 traces local subtraction window size. (b) Stacked section of the L1-norm standard SRME primaries with 160 ms ∗ 25 traces local subtraction window size. (c) Stacked section of the final estimated primaries after LPMO. The arrows in (a) and (b) denote more severe multiple leakage compared to (c). The rectangles in (a) and (b) denote more primary damage compared to (c).

the most advanced interpolation approaches still bring some reconstruction errors to the data, and then those errors might result in the relatively weaker amplitude of the predicted multiples. Therefore, combined with phase-shift errors and 2D/3D effects, there might be a chance that the estimated multiples are weaker than the multiple leakage. Weights larger than 1 can then be tested to see its performance. Based on our experiences, the robust range for the thresholding operator $\mathbf{T}$ is between 0 and 1. When there are still some obvious phase-shift multiple leakage left, the range can be revised to between -0.5 and 1. For the field data set, the upper limit of the thresholding operator should be smaller than 2 based on our experiences.

Smoothing is also an important part in shaping regularization. In this chapter, the triangle smoothing operator is utilized in the shaping regularization based inversion. The sampling in time for both lens-shaped model and field data is 4 ms while the sampling for complex salt model is 8 ms. The smoothing radii of triangle smoothing operator for all the examples is set as 2 time samples for higher resolution. The range for smoothing radii based on our experiences can range from 2 to 10 time samples depending on the desired resolution.

The proposed framework is still based on the basic assumption that the primaries and multiples should not correlate. Thus, it is worth noting that some red areas in the local similarity maps are unchanged before and after LPMO. These high similarity areas indicate where the multiples and primaries are highly correlated and overlapped, which violates the initial assumption of most adaptive subtraction methods. Therefore, most meth-

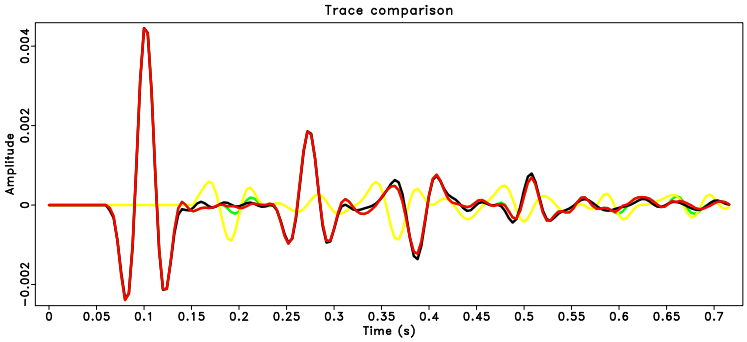

Figure 4.21: Single trace comparison before and after LPMO from the lens-shaped synthetic model. The black line denotes the true modeled primaries, the green line denotes the conservative SRME primaries, the red line denotes the proposed primaries after LPMO, and the yellow line indicates the estimated multiples from the conservative SRME.

ods in the literature fail to correctly extract the leakage if it exists in these areas. For our proposed approach, its multiple leakage extraction power is within the limitation of the orthogonal assumption. However, if the conservative primary estimation (e.g. the conservative SRME) is used and followed by LPMO in our proposed framework, the primary damage can be kept to a minimum compared to other standard methods.

As for the computational time consumption, it depends on the actual situations and is relatively difficult to compare. In general, most time consumption for the standard SRME comes from the parameter tuning of the adaptive subtraction. Practitioners have to test a set of different window sizes and filter lengths to find the desired optimal setting, which usually is a tedious process. Besides, some amount of time is required to compare different results and the trade-off between multiple leakage and primary damage has to be decided by the practitioners. Therefore, all the parameter tuning related time consumption is hard to estimate. As for the proposed framework, the LPMO definitely takes some extra time for inversion (e.g. around ten times more expensive for the field data example), but it saves practitioners time from fine-tuning parameters. Above all, you could also consider the LPMO as an extra QC step to evaluate whether the multiple energy is leaked or not.

From almost-perfect-world synthetic examples, the leaked surface-related multiples may not seem to have strong influences on primaries due to its relatively small amplitude. However, real-world field data with both 2D/3D effects and interpolation errors always tend to show much more obvious and severe surface-related multiple leakage. The proposed two-step framework, thus, can be a quite helpful toolbox to attack the multiple leakage without damaging primaries. Meanwhile, it can also be regarded as another tool in the toolbox of various multiple prediction and subtraction techniques.

For very complex field data, extracting leaked multiples in the shot domain might not be enough, therefore, multi-domain LPMO is suggested [28]. The common-offset domain is an appropriate choice, in which we might observe the leakage with less efforts. The whole framework is exactly the same as the shot-domain extraction based on LPMO. The

only difference is to sort the data to common-offset domain in advance.

Our proposed two-step framework based on LPMO aims to solve the surface-related multiple leakage problem for all the existing primary and multiple estimation approaches. That is to say, as long as there is multiple leakage in the estimated primary model, our proposed LPMO can be attached to any primary estimation approach. For example, more advanced inversion-based CL-SRME or EPSI is, to some extent, able to alleviate the multiple leakage problem, but may still suffer from such multiple leakage, especially for complex coarsely sampled field data with 2D/3D effects. Therefore, we can regard either CL-SRME or EPSI as our primary estimation engine for the initial step, and then the second step, LPMO, as a remedy can be applied to extract the leaked multiples. Moreover, model-driven multiple prediction approaches (e.g. model-based water-layer demultiple [29]) can also be attached by the proposed LPMO step as long as the adaptive subtraction is involved.

Currently, there is no requirement of broadband data for our proposed framework. In terms of the leakage as a function of frequency, a possible solution might be: the low-frequency components can be processed with large local windows in the adaptive subtraction, while the high-frequency components can be processed with smaller local windows. The proposed LPMO step could be further applied to both low and high-frequency components with different parameter settings. Future research is needed to investigate this issue in detail.

4.6. CONCLUSIONS

We have introduced a new two-step framework for surface-related multiple leakage extraction, and thus obtain a better estimated primary model. This two-step framework using local primary-and-multiple orthogonalization (LPMO) is highly efficient for leaked multiple extraction and can work for various multiple prediction methods. A conservative SRME is used as the initial estimation step followed by the LPMO as the remedy to correct the estimated primaries and multiples in this chapter. Applications to two synthetic data sets and one field data set demonstrate a good performance of the proposed framework for primary estimation compared with the standard SRME results.

REFERENCES

[1] J. V. Ryu, *Decomposition (DECOM) approach applied to wave field analysis with seismic reflection records,* Geophysics **47** (1982), pp. 869–883.

[2] D. Hampson, *Inverse velocity stacking for multiple elimination,* in *56th SEG Technical Program Expanded Abstracts* (Society of Exploration Geophysicists, 1986).

[3] D. J. Verschuur and A. J. Berkhout, *Estimation of multiple scattering by iterative inversion, Part II: Practical aspects and examples,* Geophysics **62** (1997), pp. 1596–1611.

[4] A. B. Weglein, F. A. Gasparotto, P. M. Carvalho, and R. H. Stolt, *An inverse-scattering series method for attenuating multiples in seismic reflection data,* Geophysics **62** (1997), pp. 1975–1989.

[5] W. Chen, J. Xie, S. Zu, S. Gan, and Y. Chen, *Multiple-reflection noise attenuation using adaptive randomized-order empirical mode decomposition,* IEEE Geoscience and Remote Sensing Letters **14** (2017), pp. 18–22.

[6] D. J. Verschuur, *Seismic multiple removal techniques : past, present and future* (EAGE Publications, 2013).

[7] M. P. Brown and A. Guitton, *Least-squares joint imaging of multiples and primaries,* Geophysics **70** (2005), pp. S79–S89.

[8] D. Zhang and G. T. Schuster, *Least-squares reverse time migration of multiples,* Geophysics **79** (2014), pp. S11–S21.

[9] S. Lu, D. N. Whitmore, A. A. Valenciano, and N. Chemingui, *Separated-wavefield imaging using primary and multiple energy,* The Leading Edge **34** (2015), pp. 770–778.

[10] A. Nath and E. Verschuur, *Using surface-related multiples in imaging for data with large acquisition gaps,* in *87th SEG Technical Program Expanded Abstracts* (Society of Exploration Geophysicists, 2017).

[11] M. Davydenko and D. Verschuur, *Full-wavefield migration: using surface and internal multiples in imaging,* Geophysical Prospecting **65** (2016), pp. 7–21.

[12] M. Davydenko and D. J. Verschuur, *Including and using internal multiples in closed-loop imaging — Field data examples,* Geophysics **83** (2018), pp. R297–R305.

[13] N. Gülünay, *Signal leakage in f-x deconvolution algorithms,* Geophysics **82** (2017), pp. W31–W45.

[14] Y. Chen, W. Huang, Y. Zhou, W. Liu, and D. Zhang, *Plane-wave orthogonal polynomial transform for amplitude-preserving noise attenuation,* Geophysical Journal International **222** (2020), pp. 1789–1804.

[15] Y. Chen and S. Fomel, *Random noise attenuation using local signal-and-noise orthogonalization,* Geophysics **80** (2015), pp. WD1–WD9.

[16] Y. Chen, S. Jiao, J. Ma, H. Chen, Y. Zhou, and S. Gan, *Ground-roll noise attenuation using a simple and effective approach based on local band-limited orthogonalization,* IEEE Geoscience and Remote Sensing Letters **12** (2015), pp. 2316–2320.

[17] Y. Chen, *Iterative deblending with multiple constraints based on shaping regularization,* IEEE Geoscience and Remote Sensing Letters **12** (2015), pp. 2247–2251.

[18] D. Zhang, E. Verschuur, and Y. Chen, *Surface multiple leakage extraction using local primary-and-multiple orthogonalization,* in *81st EAGE Conference and Exhibition* (European Association of Geoscientists & Engineers, 2019).

[19] A. J. Berkhout, *Seismic migration: Imaging of acoustic energy by wave field extrapolation, A: Theoretical aspects* (Elsevier (second edition), 1982).

[20] A. J. Berkhout and D. J. Verschuur, *Estimation of multiple scattering by iterative inversion, Part I: Theoretical considerations,* Geophysics **62** (1997), pp. 1586–1595.

[21] S. Fomel, *Shaping regularization in geophysical-estimation problems,* Geophysics **72** (2007), pp. R29–R36.

[22] A. J. Berkhout, *Review paper: An outlook on the future of seismic imaging, Part I: forward and reverse modelling,* Geophysical Prospecting **62** (2014), pp. 911–930.

[23] S. Fomel, *Local seismic attributes,* Geophysics **72** (2007), pp. A29–A33.

[24] A. Guitton and D. J. Verschuur, *Adaptive subtraction of multiples using the L1-norm,* Geophysical Prospecting **52** (2004), pp. 27–38.

[25] G. Cambois, D. Carlson, C. Jones, M. Lesnes, W. Söllner, H. Tabti, and A. Day, *Dual-sensor streamer data – calibration, acquisition QC and attenuation of seismic interferences and other noises,* in *71st EAGE Conference and Exhibition* (European Association of Geoscientists & Engineers, 2009).

[26] M. M. N. Kabir and D. J. Verschuur, *Restoration of missing offsets by parabolic Radon transform,* Geophysical Prospecting **43** (1995), pp. 347–368.

[27] R. H. Baardman, D. J. Verschuur, R. G. van Borselen, M. O. Frijlink, and R. F. Hegge, *Estimation of primaries by sparse inversion using dual-sensor data,* in *80th SEG Technical Program Expanded Abstracts* (Society of Exploration Geophysicists, 2010).

[28] D. Zhang, E. Verschuur, S. Qu, and Y. Chen, *Multi-domain surface multiple leakage extraction using local primary-and-multiple orthogonalization,* in *89th SEG Technical Program Expanded Abstracts* (Society of Exploration Geophysicists, 2019).

[29] P. Wang, H. Jin, S. Xu, and Y. Zhang, *Model-based water-layer demultiple,* in *81st SEG Technical Program Expanded Abstracts* (Society of Exploration Geophysicists, 2011).

5

FAST LPMO

Usually adaptive subtraction cannot fully correct for surface-related multiple leakage without primary damage. Local primary-and-multiple orthogonalization (LPMO) is recently proposed to partially mitigate the surface multiple leakage, by multiplication of the estimated primaries with a weight function that scales down residual multiples while preserving primaries. The weight function is determined by shaping regularization followed by thresholding and median filtering. Although effective leakage extraction can be achieved, LPMO requires a large computational cost due to many conjugate-gradient iterations within the shaping regularization-based inversion framework. A spatially-constrained scaled point-by-point division can be used to avoid the iterative inversion within the LPMO method. Based on this, we propose a fast LPMO (FLPMO) for surface-related multiple leakage estimation and extraction. Applications on two different field data sets demonstrate the very similar surface multiple leakage extraction performances for both LPMO and FLPMO, while showing that the scaled point-by-point division in FLPMO is around 40 times faster on real data sets than the shaping regularization-based inversion in LPMO.

This chapter is an extended version of the published paper "D. Zhang, D. J. Verschuur, and Y. Chen, Fast local primary-and-multiple orthogonalization for surface-related multiple leakage estimation and extraction, Geophysics 86 (2021), pp. V353–V360".

5.1. INTRODUCTION

Due to its solid physical foundation and data-driven property, surface-related multiple elimination (SRME) has become one of the standard surface multiple removal methods [1–3]. Coarse data sampling or overlapping primaries and multiples still make the applications of SRME workflows challenging, especially for shallow water scenarios [4]. The resulting surface-related multiple leakage can easily cover the real geology and convey fake information to interpreters [5, 6]. To overcome the long-standing and commonly-seen surface multiple leakage problem, the exploration seismology community has made lots of efforts on attacking both the sampling issue and the adaptive subtraction dilemma [7–10].

In this chapter, we focus on an alternative solution for the adaptive subtraction given the multiple prediction results. Traditionally, a more aggressive adaptive subtraction (i.e., small processing windows) might solve the leakage issue to some extent, however, it tends to distort or dim the primaries. In contrast, a more conservative adaptive subtraction (i.e., large processing windows) is capable of preserving primaries, while it leaves more residual multiples. The classic trade-off between a more conservative SRME and a more aggressive SRME needs careful attention in practice. Recently, [11] proposed a new local primary-and-multiple orthogonalization (LPMO) framework based on local signal-and-noise orthogonalization [12] to partially mitigate the aforementioned adaptive subtraction dilemma, where initial surface multiples and primaries are estimated in a more conservative manner, followed by an extra surface multiple leakage extraction step without hurting primaries. Note that the conservative adaptive subtraction used for LMPO framework is based on matching filters designed in large overlapping windows with short filter length. The logic behind LPMO is that the troubling surface multiple leakage issue can be considered as a typical signal leakage problem if multiples are temporarily regarded as the signal and primaries as the noise. With the help of shaping regularization-based inversion framework, LMPO utilizes the initial estimated multiples to match the leaked multiples contained in the initial primaries. Therefore, LPMO is capable of extracting the leaked multiples without hurting primaries. Mathematically, the idea behind LPMO is that a local weight function to be applied to the multiples can be determined, based on a shaping regularization process that takes as a priori input a local coherency length in time and space at which primaries and multiples can be considered orthogonal. The weight-determining process is augmented by some non-linear steps. Note that primaries and multiples are not orthogonal on sample by sample basis but only when considering a certain window length, which is the local coherency length.

Instead of pursuing a more complex assumption for adaptive subtraction, we assume the simple local orthogonality assumption holds, and we also bring in some non-linear element (i.e., thresholding on the LPMO weights) in case the assumption fails to be met. LPMO has been demonstrated with both synthetic and field data to work well when its assumptions of orthogonality between primaries and multiples are met and that in areas where the assumptions are not met (overlap of primaries and multiples) the use of the non-linear element (i.e., thresholding and median filtering) prevents damage to primaries. Although effective, the computational cost of LPMO remains a challenge. Due to many conjugate-gradient iterations inside the shaping regularization-based inversion framework of LPMO and the large data size itself, LPMO could cost at least several times

more than the least-squares adaptive subtraction step. A similar cost issue occurs for the nonstationary prediction filters. [13] first introduced the concept of streaming prediction-error filters, and [14] further applied it to random noise attenuation. The so-called streaming version can easily avoid the iterative or recursive approaches for the nonstationary prediction filters. Inspired by [13] and [14], the shaping regularization-based iterative inversion in LPMO could also be avoided to improve the efficiency. Therefore, in this chapter, we propose a fast LPMO (FLPMO) for surface-related multiple estimation and leakage extraction. Assuming that the scalar LPMO weight is closely related to its neighboring time-and-space points, FLPMO can be achieved via a spatially-constrained scaled point-by-point division without any iterative inversions, where a key mean-averaging operator is proposed to make the system more stable and smooth. The mean-averaging operator is an unique component for FLPMO, which can improve the complete framework performance. Applications to two North Sea field data sets demonstrate that the surface multiple leakage extraction performances for LPMO and FLPMO are nearly the same, while the computational cost for FLPMO is much less than LPMO.

This chapter is organized as follows: first, a review of LPMO is introduced, and then we provide the detailed descriptions for the proposed FLPMO framework. In addition, two field data examples from the North Sea are presented. A conclusion is drawn in the end.

5.2. REVIEW OF LPMO

LPMO for surface-related multiple leakage extraction consists of two separate steps: an initial surface multiple and primary estimation step via conservative SRME and a surface multiple leakage extraction step via LPMO [11]. A brief review of LPMO is introduced here. Note that LPMO can also be considered as an external remedy for compensating and correcting any initial surface multiple and primary estimation approach. Based on a vector notation, we reformulate the classic surface multiple and primary relation in the time domain:

$$\mathbf{p} = \mathbf{m} + \mathbf{p}_0, \tag{5.1}$$

where $\mathbf{p}$, $\mathbf{m}$ and $\mathbf{p}_0$ indicate the upgoing full wavefield, initially estimated surface multiples and primaries from any surface multiple estimation approach, respectively. Note that both $\mathbf{m}$ and $\mathbf{p}_0$ are assumed imperfect. Assuming that the final estimated surface multiples $\tilde{\mathbf{m}}$ and primaries $\tilde{\mathbf{p}}_0$ should be locally orthogonal to each other, the orthogonalization can be achieved by:

$$\tilde{\mathbf{m}} = \mathbf{m} + \mathbf{w} \circ \mathbf{m}, \tag{5.2}$$

$$\tilde{\mathbf{p}}_0 = \mathbf{p}_0 - \mathbf{w} \circ \mathbf{m}, \tag{5.3}$$

where $\circ$ represents the Hadamard product (i.e., point-by-point multiplication) and $\mathbf{w}$ denotes the LPMO weight. Next, by solving the following unconstrained minimization problem the unknown LPMO weight can be estimated:

$$\min_{\mathbf{w}} \| \overbrace{\mathbf{p} - \mathbf{m}}^{\mathbf{p}_0} - \mathbf{w} \circ \mathbf{m} \|_2^2. \tag{5.4}$$

Essentially, this unconstrained minimization problem indicates that the surface multiple leakage in the initially estimated primaries can be matched by the LPMO weighted surface multiples in a least-squares sense. We further impose a local smoothness constraint, which can be solved by shaping regularization [15]:

$$\hat{\mathbf{w}} = [\lambda^2\mathbf{I} + \mathcal{T}(\mathcal{M}^T\mathcal{M} - \lambda^2\mathbf{I})]^{-1}\mathcal{T}\mathcal{M}^T\mathbf{p}_0, \tag{5.5}$$

where $\mathcal{M}$ represents $diag(\mathbf{m})$, $\mathcal{T}$ indicates a triangle smoothing operator, λ denotes a scaling parameter and $[\cdot]^T$ is the matrix transpose. The thresholding $\mathcal{H}$ and median filtering $\mathcal{F}$ operators are implemented on the estimated LPMO weight to achieve more stable and physical results:

$$\mathbf{w}_{\texttt{LPMO}} = \mathcal{F}\mathcal{H}(\hat{\mathbf{w}}). \tag{5.6}$$

At last, the final estimated LPMO weight $\mathbf{w}_{\texttt{LPMO}}$ can be substituted back into equations 5.2 and 5.3 to extract the surface multiple leakage. The achieved results by LPMO are promising, and it is able to partially mitigate the adaptive subtraction dilemma by removing most multiple leakage without seriously hurting primaries [11].

Besides, the assumption of local orthogonality versus the practical requirements needs to be addressed. First of all, the problem we are focusing on is the multiple leakage issue typically seen in shallow water data, which comes from the classic dilemma of standard adaptive subtraction. The trade-off, i.e., either damaging primaries (aggressive subtraction) or leaving multiple leakage (conservative subtraction), always exists. Secondly, the fundamental assumption for LPMO is local orthogonality between primaries and multiples/multiple leakage. Note that this is the same assumption as used with $L2$ subtraction. In fact, most subtraction methods assume local orthogonality, which is unfortunately rarely met in practice, especially for shallow water. The violation of local orthogonality actually leads to the aforementioned dilemma. However, unlike other methods, LMPO is able to achieve the most given this dilemma, meaning fully extracting the leaked multiples for the area where local orthogonality is met and preventing serious primary damages where local orthogonality fails. This is the fundamental difference and advantage of LPMO compared to other methods, and it is achieved by introducing non-linear elements (i.e., thresholding on the estimated LPMO weights) into the LPMO framework. Note that it is not claimed that LPMO can fully solve the non-orthogonal (or overlapping) events. However, LPMO can at least simultaneously extract the multiple leakage for non-overlapping events, where local orthogonality is met, and protect the overlapping events, where local orthogonality fails, without hurting the primaries by introducing a non-linear element (i.e., thresholding on the estimated LPMO weights) into the LPMO framework.

To better understand the original concept of LPMO, we provide a very straightforward demonstration in Figure 5.1. This example can also be regarded as an experimental proof of local primary-and-multiple orthogonalization. The model is a simple two layer model, which consists of a shallow water depth and a deep target layer. Figure 5.1(b) shows the ground truth primaries, and we can clearly notice those two primary events. Figure 5.1(a) demonstrates the modeled full wavefield after deghosting. Surface-related multiples are visible throughout the whole shot record. Note that perfect orthogonality occurs in this example, as indicted by frame boxes A and C. In other words, primaries and multiples do not correlate in area A and C, which fulfills the assumption of local orthogonality. As for area B, our target deep primary partially overlaps with the second-order water bottom multiple,

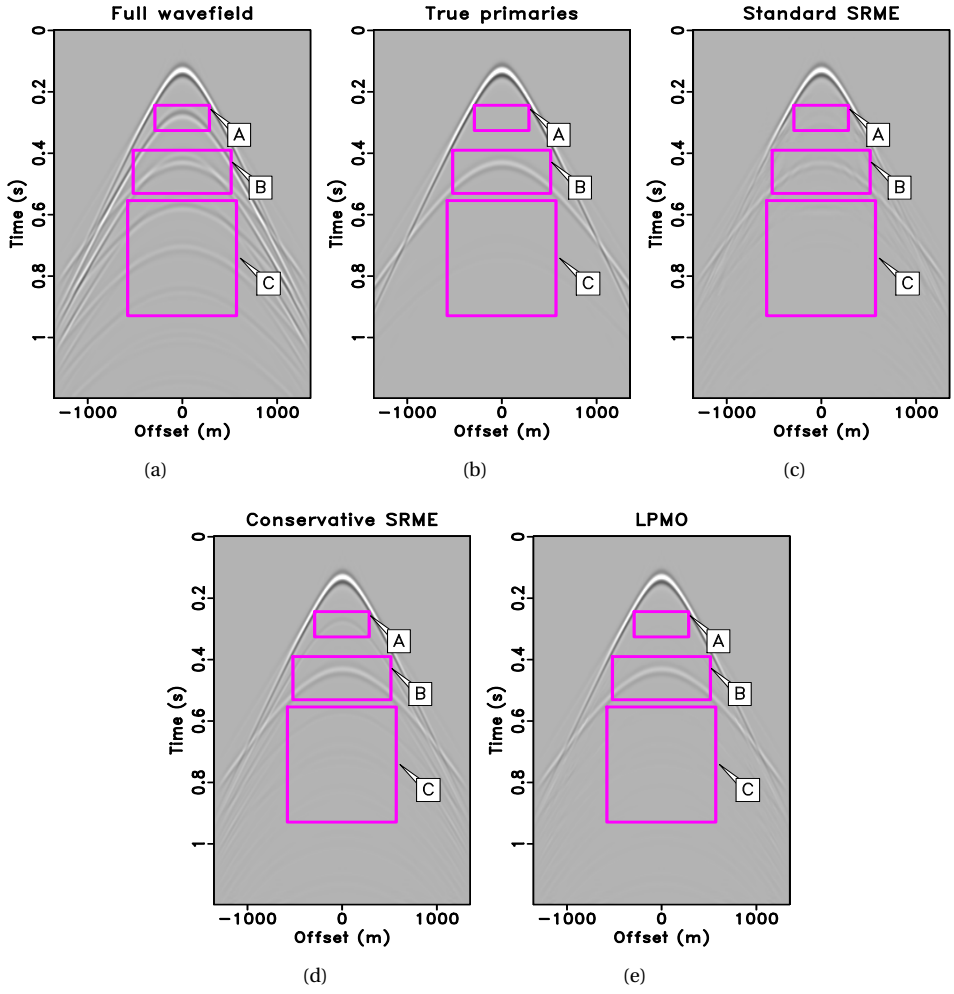

Figure 5.1: Illustrative example from a two layer model for better understanding of the original LPMO theory. (a) Modeled full wavefield with surface-related multiples after deghosting. (b) Modeled true primaries. (c) Standard SRME estimated primaries using local processing windows. (d) Conservative SRME estimated primaries using global window. (e) Estimated primaries after LPMO.

which fails to meet the local orthogonal assumption. First, we apply the standard SRME on this simple but illustrative data set. “Standard" here means the *L2* adaptive subtraction within local processing windows, which tends to be aggressive in terms of multiple suppression. The corresponding standard SRME result is displayed in Figure 5.1(c). Apparently, we have achieved a decent primary estimation result with most surface multiples being removed in areas A and C, and only slight residual multiples are left, thanks to an

aggressive *L2* subtraction. However, due to the overlaps between primary and multiple in area B, it is obvious that the aggressive *L2* subtraction has damaged the primary event. Note that primaries at far offsets are also damaged. In contrast, we also apply a conservative SRME on the same data set, and the result is shown in Figure 5.1(d). Conservative SRME uses a global subtraction, and tends to be more preservative on primaries. However, it can lead to more residual surface multiples as indicated by area A and C. Primaries in area B are untouched compared to Figure 5.1(c). Finally, the proposed local primary-and-multiple orthogonalization is based on the conservative SRME result. After LPMO as shown in Figure 5.1(e), the residual multiples are removed and the primaries are still preserved. Therefore, from this example, it is clear that LPMO can effectively extract the residual multiples for an area that meets the local orthogonal assumption, e.g., area A and C. At the same time, LPMO with the help of its non-linear element (thresholding operator) can preserve primaries for an area that fails to meet the local orthogonal assumption, e.g., area B.

Differences need to be addressed between LPMO and the nonstationary matching filter [16], as one can regard LPMO as the extreme version of nonstationary matching filter, i.e., one-point matching filter. Moreover, the hyper parameters within the shaping regularization-based inversion framework and the related thresholding and median filtering operators for LPMO have already been extensively discussed in [11]. Other application cases of the local orthogonalization include ground-roll removal [17], blended signal separation [18], elastic wavefield decomposition [19], weak microseismic signal detection [20], and elastic full waveform inversion [21]. As long as the noise model can be obtained, local orthogonality is capable of achieving the signal leakage extraction.

5.3. FAST LPMO

Although LPMO is effective for extracting multiple leakage without hurting primaries, a limitation lies in its computational cost. Due to many conjugate-gradient iterations embedded in the shaping regularization-based inversion framework and the large data itself, the computation cost for LPMO is quite large (e.g., the cost for LPMO is at least several times more than the standard least-squares adaptive subtraction). We, therefore, propose a fast LPMO (FLPMO) for surface multiple leakage extraction to mitigate the cost issue. In fact, the simplest and fastest method to solve the unconstrained minimization problem 5.4 is the direct point-by-point division:

$$w(t,x) = \frac{p_0(t,x)}{m(t,x)}, \tag{5.7}$$

where $w(t,x)$, $m(t,x)$ and $p_0(t,x)$ indicate the scalar value at a specific discrete temporal and spatial location (t,x) of the weight, initially estimated surface multiples and primaries, respectively. This direct division might be very unstable and produce nonphysical values, which can be solved by a costly shaping regularization, as done in LPMO. Alternatively, using information on the typical local coherency length of primaries and multiples, we could assume that the scalar weight $w(t,x)$ is closely related to both the neighboring time point $w(t-dt,x)$ and space point $w(t,x-dx)$ [13]. Note that dt and dx represent the time and space interval, respectively. Then, we have the following relations regarding

the scalar weight:

$$\begin{bmatrix} m(t,x) \\ \sqrt{\alpha_1} \\ \sqrt{\alpha_2} \end{bmatrix} w(t,x) \approx \begin{bmatrix} p_0(t,x) \\ \sqrt{\alpha_1}\, w(t-dt,x) \\ \sqrt{\alpha_2}\, w(t,x-dx) \end{bmatrix}, \tag{5.8}$$

where α_1 and α_2 are the regularization parameters that can control time and space resolutions for the estimated weight, respectively. The solution to the above equations in a least-squares sense is as follows:

$$w(t,x) = \frac{m(t,x)\, p_0(t,x) + \alpha_1\, w(t-dt,x) + \alpha_2\, w(t,x-dx)}{m(t,x)^2 + \alpha_1 + \alpha_2 + \beta}, \tag{5.9}$$

where β is introduced for better scaling the final estimated weight to match the standard LPMO weight $\mathbf{w}_{\texttt{LPMO}}$ in terms of the energy distribution. The above recursive scheme is started by putting the edge to zero. Equation 5.9 can be considered as a scaled version of point-by-point division 5.7, which is able to avoid unstable and nonphysical values. Next, we reformulate all the estimated scalar weights $w(t,x)$ to the vector notation $\bar{\mathbf{w}}$. Still, we need to apply the necessary thresholding and median filtering operators. Note that an extra mean-averaging operator $\mathscr{A}$ is implemented first to better smooth and preserve more physically stable results. The complete filtering process is as follows:

$$\mathbf{w}_{\texttt{FLPMO}} = \mathscr{F}\mathscr{H}\mathscr{A}(\bar{\mathbf{w}}). \tag{5.10}$$

Because of the absence of many conjugate-gradient iterations within the inversion scheme, the proposed method will be significantly faster than the original LPMO process. Hence, equations 5.9 and 5.10 together are referred to the fast LPMO framework. Similarly, we can substitute the final estimated FLPMO weight $\mathbf{w}_{\texttt{FLPMO}}$ back into equations 5.2 and 5.3 to extract the surface multiple leakage.

5.4. FIELD DATA RESULTS

In this chapter, we apply both LPMO and FLPMO to two different field data sets from the North Sea to compare their computational costs and performances in detail. The general data information and the computational costs can be directly checked in Tables 5.1 and 5.2. More specifically, Table 5.1 indicates the local computational cost comparison between the shaping regularization-based inversion in LPMO and the scaled point-by-point division with mean-averaging filtering in FLPMO for two field shots with different data size. Table 5.2 displays the overall computational cost comparison between the proposed complete framework (conservative $L2$ method + LPMO/FLPMO) and the standard $L2$ method for two field examples. Note that all the tests are conducted on a Linux system using C codes without any parallelization, and the shaping regularization-based inversion here is already the most optimized in the literature [15].

5.4.1. NELSON DATA SET FROM THE NORTH SEA - SHALLOW WATER DEPTH

The first example is based on the Nelson field from the North Sea and the water depth is relatively shallow (around 95 m in depth). The original field data with surface-related multiples, which is extracted from a 2D line, and the initial conservative SRME results with

Test	Nelson	Haltenbanken
Size (time samples × receivers)	350×201	1024×161
Shaping regularization (ms)	40.45	147.28
Scaled point-by-point division (ms)	1.02	3.07
Local speedup	39.66	47.97

Table 5.1: Local computational cost comparison between the shaping regularization-based inversion in LPMO and the scaled point-by-point division in FLPMO for two field shots with different data size. Note that the scaled point-by-point division includes the cost of mean-averaging filtering. Both examples have a time interval of 4 ms with 12.5 m spatial (both source and receiver) interval for Nelson and 25 m for Haltenbanken.

Test	Nelson	Haltenbanken
Size (time samples × receivers × shots)	350×201×201	1024×161×161
Standard $L2$ (s)	2.80	6.14
Conservative $L2$ + LPMO (s)	10.76	31.25
Conservative $L2$ + FLPMO (s)	2.98	7.99
Overall speedup	3.61	3.91

Table 5.2: Overall computational cost comparison between the proposed complete framework (conservative L2 method + LPMO/FLPMO) and the standard L2 method for two field examples with different data size.

large processing windows can be found in Chapter 4. Due to the large processing windows for conservative SRME, surface multiple leakage can be observed. Although this leakage is not very strong, it might still provide false information for interpreters. Therefore, surface multiple leakage extraction is required.

Figure 5.2 demonstrates the shot-domain surface multiple leakage removal comparison in detail. The LPMO and the FLPMO estimated weights, shown in Figures 5.2(a) and 5.2(d), respectively, are very similar, and all the surface multiple leakage can be well detected for both approaches. More specifically, the estimated surface multiples for both methods in Figures 5.2(b) and 5.2(e) extract their leaked energy back compared to Figure while at the same time primaries for both methods in Figures 5.2(c) and 5.2(f) end up successfully removing the surface multiple leakage compared to Figure. In terms of the overall performance, surface multiple leakage removal indicated by the arrows is visually the same for both LPMO and FLPMO as shown in Figure 5.2, thus, we use local similarity map [12, 22] for a more detailed comparison between LPMO and FLPMO. The local similarity map takes the estimated surface multiples and primaries as the input to demonstrate their similarities. Figure 5.3(a) presents the local similarity map before LPMO/FLPMO, which clearly indicates the surface multiple leakage due to a conservative SRME. Note that the most obvious leakage, coming from the first order multiples of the primaries around 0.55 s, is indicated by the white arrow. After the surface multiple leakage extraction step, local similarity maps from LPMO and FLPMO, as shown in Figures 5.3(b) and 5.3(c), both demonstrate substantial leakage improvement. Although the FLPMO residual leakage

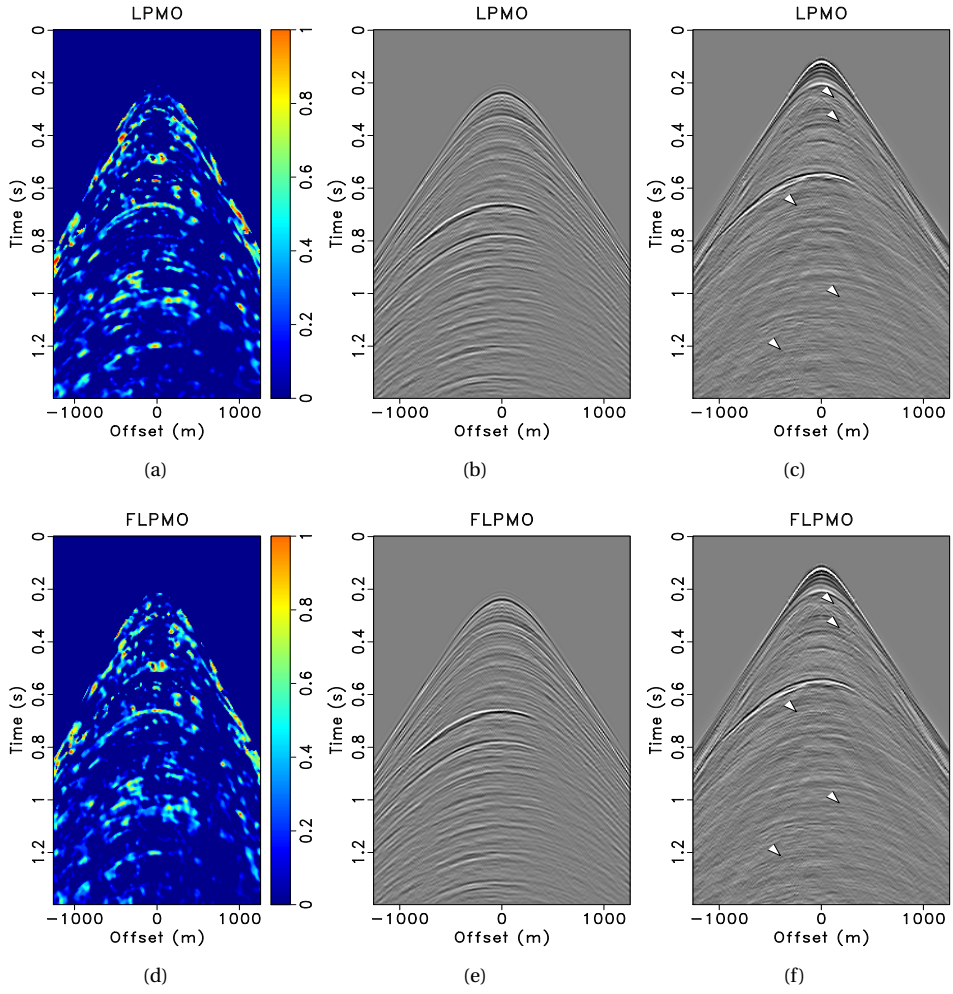

Figure 5.2: Nelson data middle shot gather comparison for LPMO and FLPMO. (a) & (d) Estimated weight using LPMO and FLPMO, respectively. (b) & (e) Leakage compensated surface multiples using LPMO and FLPMO, respectively. (c) & (f) Leakage extracted primaries using LPMO and FLPMO, respectively. Note that all white arrows in this chapter indicate the surface multiple leakage positions.

from the most obvious position indicated by the white arrow is slightly worse than LPMO, the computational costs are quite different as shown in Table 5.1, where the local speedup for scaled point-by-point division in the proposed FLPMO is 39.66 compared to the shaping regularization-based inversion in LPMO. Generally, the overall speedup for the proposed FLPMO framework (i.e., conservative $L2$ + FLPMO) is 3.61 compared to the LPMO framework (i.e., conservative $L2$ + LPMO) according to Table 5.2. From the same table, it

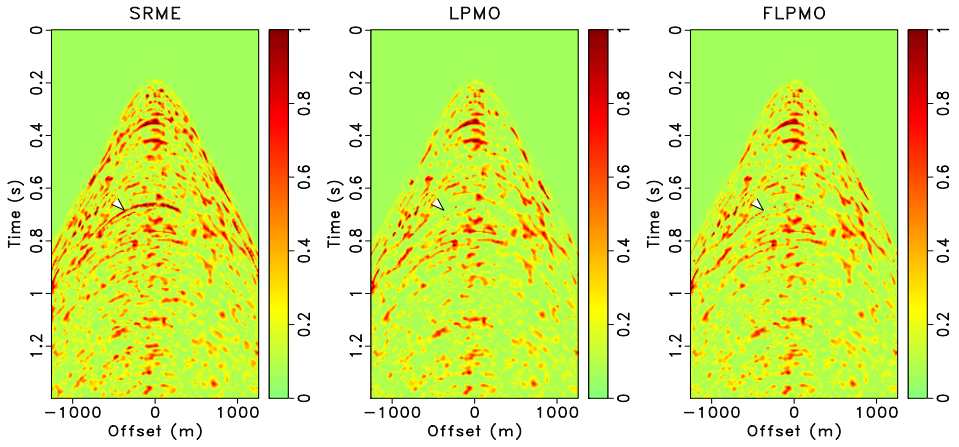

Figure 5.3: Local similarity map comparison for the middle shot from the Nelson data set. (a) Local similarity map before LPMO or FLPMO. (b) & (c) Local similarity maps after LPMO and FLPMO, respectively. The arrow indicates the most obvious surface multiple leakage. Note that the local similarity map takes the estimated surface multiples and primaries as the input to demonstrate their similarities.

is clear that the cost of the proposed FLPMO framework is almost equivalent to the cost of the standard *L2* method, while the LPMO framework is around 4 times more costly than the standard *L2* method.

To better observe the leakage extraction performances before and after both LPMO and FLPMO methods, we provide another comparison in stacked profiles. From the perspective of stacked profiles in Figures 5.4(a), 5.4(b), and 5.4(c), similar effects can be seen in a much easier and clearer way due to the power of stacking. The original stacked profile of the data with surface-related multiples and the post-SRME primaries stacked profile are presented in Figures and 5.4(a), respectively. Although conservative, SRME works properly here for removing most surface multiples. Still, some surface multiple leakage is visible from the initial estimated post-SRME primaries. LPMO and FLPMO are applied to further extract this leaked energy. Figures 5.4(b) and 5.4(c) demonstrate the final results after LPMO and FLPMO surface multiple leakage extraction, respectively. According to the leaked positions pointed by the arrows, LPMO and FLPMO have shown an equally powerful leakage extraction capability and visually the same results.

5.4.2. HALTENBANKEN DATA SET FROM THE NORTH SEA - MEDIUM WATER DEPTH

The second example is from the Haltenbanken field, the North Sea, with a medium water depth (approximately 300 m). Figure 5.5(a) displays the original recorded data with surface-related multiples. The data is also extracted from a 2D line. A fixed-spread data set is obtained with 161 shots and 161 receivers after data regularization. The spacing for

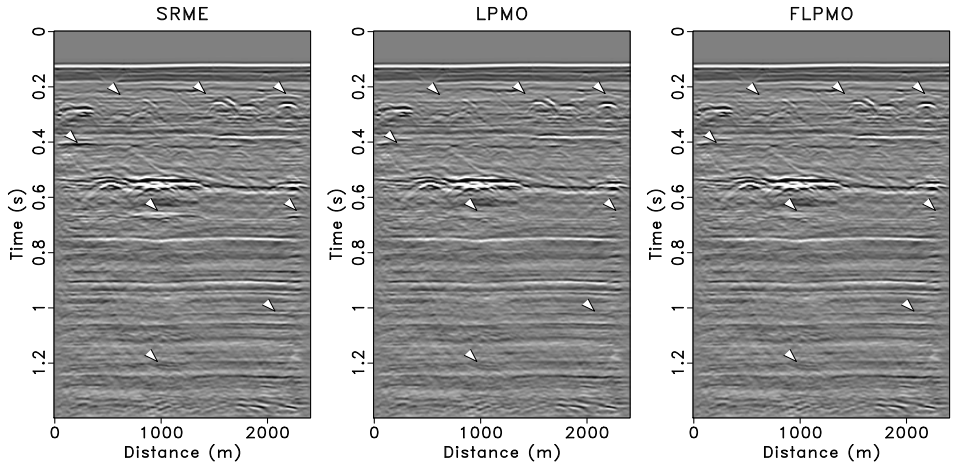

Figure 5.4: Stacked profile comparison for the Nelson data set. (a) & (b) Stacked profiles of the original data and the conservative SRME estimated primaries, respectively. (c) & (d) Stacked profiles of the leakage extracted primaries using LPMO and FLPMO, respectively.

both shots and receivers is 25 m. There are 1024 samples for each trace with a time interval of 4 ms. Note that compared to the Nelson data set the data size of Haltenbanken is around two times larger in terms of the total number of time samples. Strong interference between surface multiples and primaries can be observed in Figure 5.5(a). Figures 5.5(c) and 5.5(b) show the initially estimated primaries and surface multiples after the conservative SRME, respectively. Although SRME attenuates large amounts of surface multiple energy, visible surface multiple leakage can still be observed around the arrows due to large processing windows (1000 ms * 60 traces).

Next we apply both LPMO and the proposed FLPMO to this data, and both methods can extract the surface multiple leakage effectively as shown in Figure 5.6. In terms of the estimated weights in Figures 5.6(a) and 5.6(d), LPMO and FLPMO are nearly the same with only small differences. As for the leakage compensated surface multiples and leakage extracted primaries, both approaches display visually identical results, especially for those arrow-indicated areas in Figure 5.6. Therefore, we take advantage of local similarity map to amplify their little differences. Figure 5.7 shows the local similarity maps before and after surface multiple leakage extraction. The white arrows denote the most obvious leakages, where FLPMO still has slightly more residual leakage left compared to LPMO. However, as shown in Table 5.1, the computational costs are far from each other, where the local speedup for scaled point-by-point division in the proposed FLPMO reaches 47.97 compared to the shaping regularization-based inversion in LPMO. Besides, according to Table 5.2, the overall speedup for the proposed FLPMO framework (including the conservative $L2$ subtraction) is 3.91 compared to the LPMO framework with hardly any loss in performance. Most importantly, the current cost of the proposed FLPMO framework is

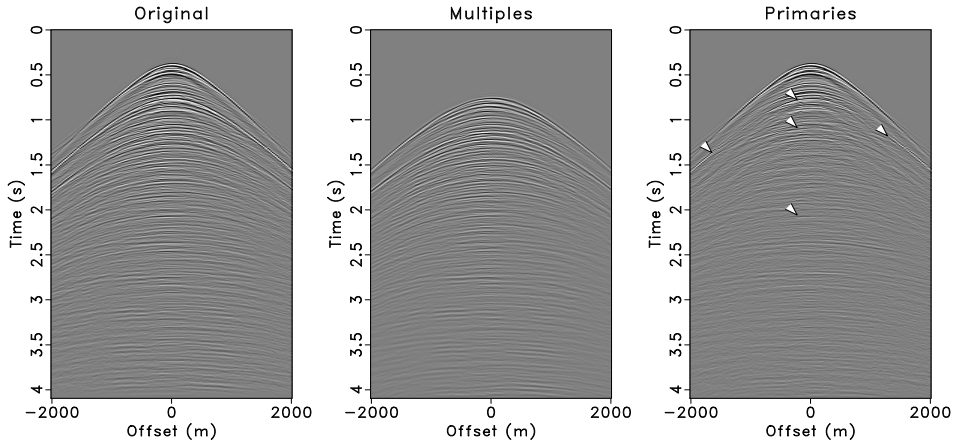

Figure 5.5: Middle shot record from the Haltenbanken data set with medium water depth. (a) Original input data with surface-related multiples. Initially estimated surface multiples (b) and primaries (c) using conservative SRME. The arrows indicate the surface-related multiple leakage.

nearly equivalent to the cost of the standard *L*2 method, while the LPMO framework is around 5 times more costly than the standard *L*2 method.

Figure 5.8 demonstrates a similar behavior as the shot gather comparison from the perspective of stacked profiles. Conservative SRME gets rid of most surface multiples while some leakage is still visible around the areas indicated by the arrows. Both LPMO and FLPMO can again achieve visually the same surface multiple leakage extraction performance.

5.5. DISCUSSION

The clear advantage of both LPMO and the proposed FLPMO frameworks versus the adaptive subtraction is their simultaneous surface-related multiple leakage extraction and primary preservation properties. In contrast, surface multiple leakage can also be attenuated to some extent via a more aggressive SRME strategy, however, it risks a dimming or even damaging of primaries due to small processing windows. Here, a more aggressive SRME refers to the standard SRME because such setting is not uncommon. For better awareness of the potential hazards, we also provide the stacked profile for standard SRME result with local processing windows (160 ms * 25 traces) in Figure 5.9. Note that we only show this for the Haltenbanken field, but the same comparison for the Nelson field can be found in [11]. From the standard SRME stacked profile, we can still see some surface multiple leakage, although they have been attenuated compared to the conservative SRME result in Figure 5.8(b). However, more leakage can be observed compared to both LPMO and FLPMO stacked profiles in Figures 5.8(c) and 5.8(d). On the other hand, the primaries in Figure be-

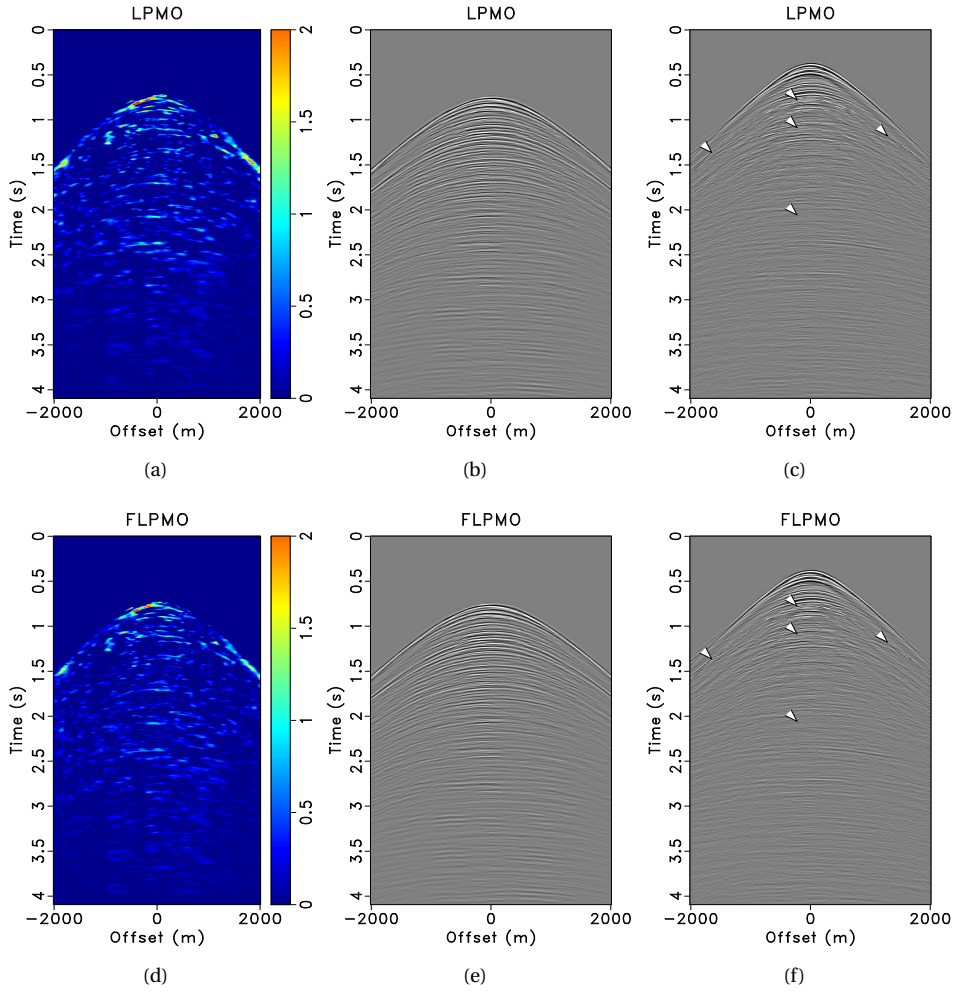

Figure 5.6: Haltenbanken middle shot gather comparison for LPMO and FLPMO. (a) & (d) Estimated weight using LPMO and FLPMO, respectively. (b) & (e) Leakage compensated surface multiples using LPMO and FLPMO, respectively. (c) & (f) Leakage extracted primaries using LPMO and FLPMO, respectively.

tween 2 and 3 s display clear dimming effects compared to the LPMO and FLPMO results, which proves the strong risk of hurting primaries via local window processing.

The hyper parameters within shaping regularization-based inversion framework and related thresholding and median filtering operators for LPMO have already been extensively discussed in [11]. For the new proposed FLPMO, parameter fine-tuning is a bit more complex, involving two regularization parameters α_1 and α_2 and one scaling parameter β. Specifically, α_1 controls the resolution of the estimated FLPMO weights along the time

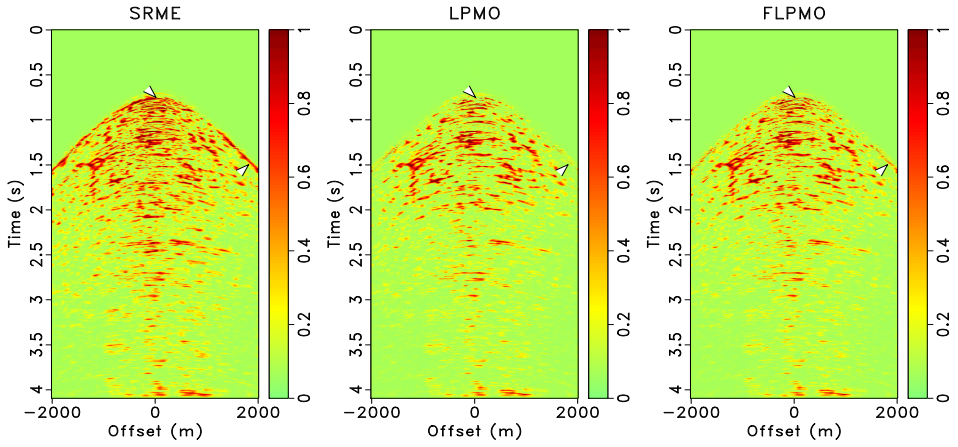

Figure 5.7: Local similarity map comparison for the middle shot from the Haltenbanken data set. (a) Local similarity map before LPMO or FLPMO. (b) & (c) Local similarity maps after LPMO and FLPMO, respectively. The arrows indicate the most obvious surface multiple leakage.

direction, while α_2 controls this along the spatial direction. β scales the estimated FLPMO weight as a final adjustment. Our strategy for parameter tuning is first obtaining the LPMO weight from only one shot (e.g., the middle shot record) as the template, where the computational cost of LPMO is trivial for one shot record. Our goal is to fine-tune a similar FLPMO weight by adjusting α_1, α_2 and β, and then fix these parameters for all the shots. Note that both LPMO and FLPMO are implemented shot by shot. Based on our experience, α_1 is slightly more important and sensitive than α_2. β should be adjusted in the end to match the energy distribution as close as possible to the LPMO weight. Another important factor for FLPMO is the mean-averaging operator $\mathscr{A}$, which can significantly smooth and stabilize the estimated FLPMO weight. To better demonstrate its effect, we show the FLPMO weights without the help of mean-averaging operator for both Nelson and Haltenbanken shot gathers in Figure 5.10. It is very straightforward and clear that both FLPMO weights show much less stable and continuous features compared to Figures 5.2(d) and 5.6(d). For both field data sets, the averaging radius for both time and space directions is set as 3 sample points. Besides, hyper parameter α_1, α_2 and β vary from data set to data set, as they depend on the scale of the data itself.

Regarding the computational cost, the shaping regularization-based inversion framework inside LPMO requires many conjugate-gradient iterations, and its cost increases when the data size becomes larger (e.g., the Haltenbanken data set). Currently, we use 20 conjugate-gradient iterations for shaping regularization, and the current local speedup for the Haltenbanken data set is already 47.97. As more conjugate-gradient iterations and larger data set applied to LPMO, both the local and overall speedup could reach even higher. As the original LPMO consumes considerable resources, its wide application in

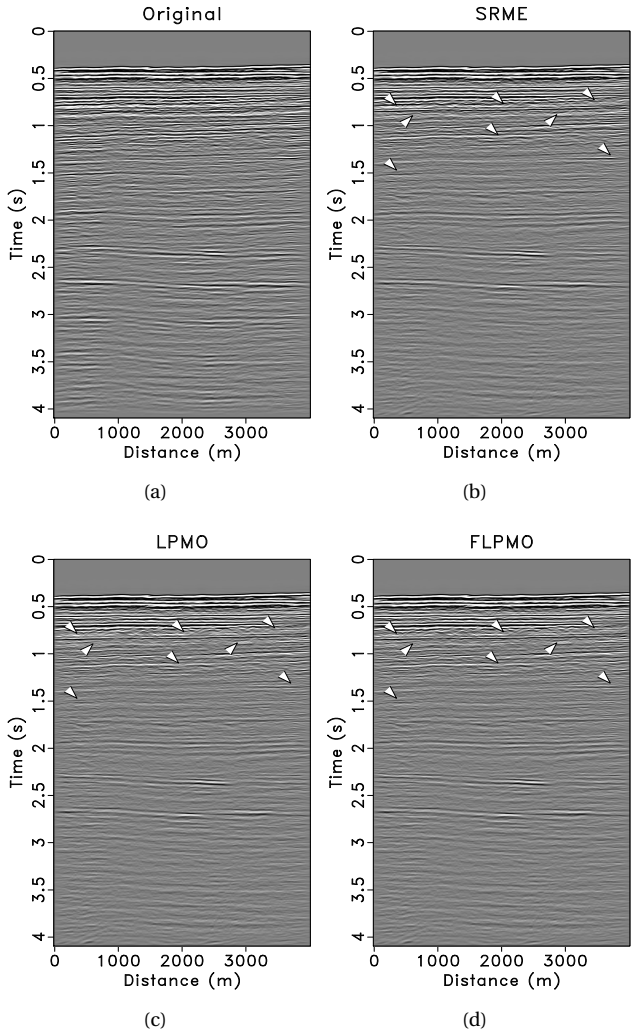

Figure 5.8: Stacked profile comparison for the Haltenbanken data set. (a) & (b) Stacked profiles of the original data and the conservative SRME estimated primaries, respectively. (c) & (d) Stacked profiles of the leakage extracted primaries using LPMO and FLPMO, respectively.

industry will be limited. However, FLPMO, whose cost is now equivalent to the industry standard *L2* adaptive subtraction, smartly replaces the shaping regularization-based inversion framework with a scaled point-by-point division and, thus, makes fast implementation feasible with only slight performance degrade. For example, the inversion-based SRME (i.e., closed-loop SRME [23]) usually needs many iterations. Thanks to the fast implementation, closed-loop SRME constrained by LPMO becomes more practical and is

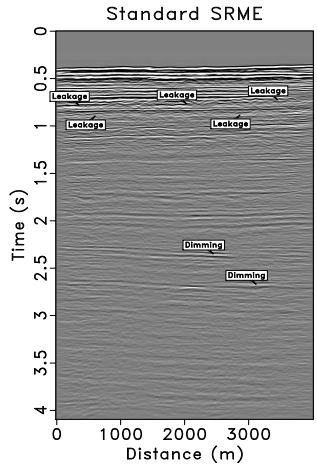

Figure 5.9: Haltenbanken stacked profile from a standard SRME result using small local processing windows (160 ms × 25 traces) during adaptive subtraction. Note that some surface multiple leakage is still visible and some primaries are dimmed due to these adaptive subtraction settings.

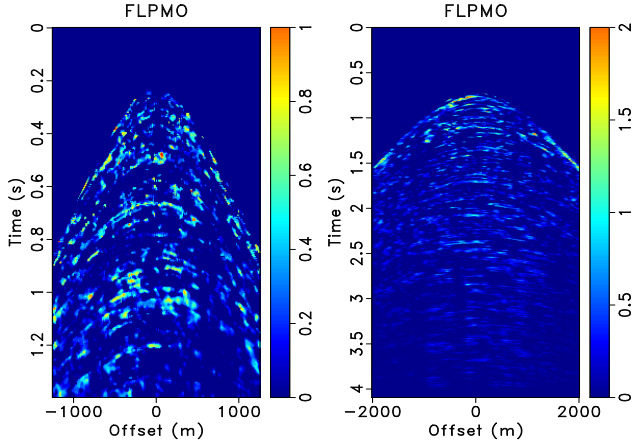

(a) (b)

Figure 5.10: Effects of the mean-averaging operator on the proposed FLPMO weight. (a) Estimated FLPMO weight without the mean-averaging operator on the Nelson data set (compare to Figure 5.2(d)). (b) Estimated FLPMO weight without the mean-averaging operator on the Haltenbanken data set (compare to Figure 5.6(d)).

currently under research. Besides, FLPMO can also be attached to any surface multiple estimation approach (e.g., model-based multiple prediction [24] or estimation of primaries

by sparse inversion (EPSI) [25]) as an external processing step to help extract the surface multiple leakage. Meanwhile, a fast quality control (QC) using FLPMO to check the multiple leakage is possible for any multiple estimation approaches. Applications of the proposed FLPMO method to more complicated and time-consuming multiple subtraction methods are worth investigating, but are considered beyond the scope of this research.

5.6. CONCLUSIONS

We have introduced a new FLPMO framework for faster surface multiple leakage estimation and extraction. By using a scaled point-by-point division in FLPMO, the shaping regularization-based iterative inversion in LPMO is avoided, and thus a local speedup factor of around 40 is achieved. Application to two different field data sets demonstrates an equally good performance of the proposed FLPMO and LPMO framework for surface multiple estimation and leakage extraction, and the overall cost of the complete FLPMO framework is around 4 times faster than the LPMO framework, which is now equivalent to the costs of the industry standard *L2* adaptive subtraction.

5.7. ACKNOWLEDGMENTS

The authors would like to thank PGS and Equinor for providing the Nelson and Haltenbanken field data sets, respectively.

REFERENCES

[1] D. J. Verschuur, A. J. Berkhout, and C. P. A. Wapenaar, *Adaptive surface-related multiple elimination,* Geophysics **57** (1992), pp. 1166–1177.

[2] A. J. Berkhout and D. J. Verschuur, *Estimation of multiple scattering by iterative inversion, Part I: Theoretical considerations,* Geophysics **62** (1997), pp. 1586–1595.

[3] B. Dragoset, E. Verschuur, I. Moore, and R. Bisley, *A perspective on 3D surface-related multiple elimination,* Geophysics **75** (2010), pp. 75A245–75A261.

[4] C. Kostov, F. Xavier de Melo, A. Raj, A. Zarkhidze, A. Cooke, G. Miers, and J. Bacon, *Multiple attenuation for shallow-water surveys: Notes on old challenges and new opportunities,* The Leading Edge **34** (2015), pp. 760–768.

[5] R. Abma, N. Kabir, K. H. Matson, S. Michell, S. A. Shaw, and B. McLain, *Comparisons of adaptive subtraction methods for multiple attenuation,* The Leading Edge **24** (2005), pp. 277–280.

[6] D. J. Verschuur, *Seismic multiple removal techniques : past, present and future* (EAGE Publications, Houten, Netherlands, 2013).

[7] M. M. N. Kabir and D. J. Verschuur, *Restoration of missing offsets by parabolic Radon transform,* Geophysical Prospecting **43** (1995), pp. 347–368.

[8] A. Guitton and D. J. Verschuur, *Adaptive subtraction of multiples using the L1-norm,* Geophysical Prospecting **52** (2004), pp. 27–38.

[9] F. J. Herrmann, D. Wang, and D. J. Verschuur, *Adaptive curvelet-domain primary-multiple separation,* Geophysics **73** (2008), pp. A17–A21.

[10] D. Zhang and E. Verschuur, *Integration of closed-loop surface-related multiple estimation and full wavefield migration for shallow water,* in *81st EAGE Conference and Exhibition* (European Association of Geoscientists & Engineers, 2019).

[11] D. Zhang, D. J. Verschuur, S. Qu, and Y. Chen, *Surface-related multiple leakage extraction using local primary-and-multiple orthogonalization,* Geophysics **85** (2020), pp. V81–V97.

[12] Y. Chen and S. Fomel, *Random noise attenuation using local signal-and-noise orthogonalization,* Geophysics **80** (2015), pp. WD1–WD9.

[13] S. Fomel and J. Claerbout, *Streaming prediction-error filters,* in *86th SEG Technical Program Expanded Abstracts* (Society of Exploration Geophysicists, 2016).

[14] Y. Liu and B. Li, *Streaming orthogonal prediction filter in the t-x domain for random noise attenuation,* Geophysics **83** (2018), pp. F41–F48.

[15] S. Fomel, *Shaping regularization in geophysical-estimation problems,* Geophysics **72** (2007), pp. R29–R36.

[16] S. Fomel, *Adaptive multiple subtraction using regularized nonstationary regression,* Geophysics **74** (2009), pp. V25–V33.

[17] Y. Chen, S. Jiao, J. Ma, H. Chen, Y. Zhou, and S. Gan, *Ground-roll noise attenuation using a simple and effective approach based on local band-limited orthogonalization,* IEEE Geoscience and Remote Sensing Letters **12** (2015), pp. 2316–2320.

[18] Y. Chen, *Iterative deblending with multiple constraints based on shaping regularization,* IEEE Geoscience and Remote Sensing Letters **12** (2015), pp. 2247–2251.

[19] Y. Sripanich, S. Fomel, J. Sun, and J. Cheng, *Elastic wave-vector decomposition in heterogeneous anisotropic media,* Geophysical Prospecting **65** (2016), pp. 1231–1245.

[20] W. Huang, R. Wang, and Y. Chen, *Regularized non-stationary morphological reconstruction algorithm for weak signal detection in microseismic monitoring: methodology,* Geophysical Journal International **213** (2018), pp. 1189–1211.

[21] W. Jeong, C. Tsingas, and Y. S. Kim, *Enhanced elastic wavefield separation using local orthogonalization filtering with applications in elastic modelling and inversion,* Journal of Applied Geophysics **160** (2019), pp. 131–143.

[22] S. Fomel, *Local seismic attributes,* Geophysics **72** (2007), pp. A29–A33.

[23] G. A. Lopez and D. J. Verschuur, *Closed-loop surface-related multiple elimination and its application to simultaneous data reconstruction,* Geophysics **80** (2015), pp. V189–V199.

[24] H. Jin and P. Wang, *Model-based water-layer demultiple (MWD) for shallow water: from streamer to OBS,* in *82nd SEG Technical Program Expanded Abstracts* (Society of Exploration Geophysicists, 2012).

[25] G. J. van Groenestijn and D. J. Verschuur, *Estimating primaries by sparse inversion and application to near-offset data reconstruction,* Geophysics **74** (2009), pp. A23–A28.

6

DL-BASED MULTIPLE ADAPTIVE SUBTRACTION

Surface-related multiple elimination remains one of the most robust primary estimation approaches for decades, in which the adaptive subtraction step is a non-trivial task. Due to imperfections in the made assumptions during prediction, the perfect adaptive subtraction is a highly non-linear and non-stationary process, which is suitable for the popular deep learning (DL)-based image processing. Different from the most straightforward DL-based adaptive subtraction (i.e., the full wavefield and the advanced estimated primary training pair), we propose to include both the original full wavefield and the initial globally estimated multiples as the two-channel input, and train a DL neural network (U-Net) on the synthetic modeled primaries. In this way, the robust physics (i.e., the globally estimated multiples) is utilized, and the ground truth primary labels can be beneficial to the framework. Both synthetic and field examples are provided to demonstrate the performance of our proposed framework.

This chapter is a slightly modified version of the proceeding "D. Zhang, M. de Leeuw, and E. Verschuur, Deep learning-based seismic surface-related multiple adaptive subtraction with synthetic primary labels, in First International Meeting for Applied Geoscience & Energy Expanded abstracts (Society of Exploration Geophysicists, 2021) pp. 2844–2848".

6.1. INTRODUCTION

Surface-related multiple elimination (SRME) remains one of the most robust primary estimation approaches for decades [1–3]. The multiple model with correct kinematic properties are obtained via a multi-dimensional convolution process. With the estimated multiple model, most adaptive subtraction methods aim to match and remove the multiple events from the original full wavefield under some type of assumption, e.g., the minimum residual primary energy ($L2$ norm) [4, 5]. However, every assumption is imperfect with its own flaws, and most will fail when there are some overlapping events between primaries and multiples. In theory, the perfect adaptive subtraction is a highly non-linear and non-stationary process, which is suitable for the popular deep learning (DL)-based image processing [6].

The most common DL-based adaptive subtraction is very straightforward, in which the input is the original full wavefield and the primaries are the target labels. The DL neural network (NN) is able to learn to directly map the full wavefield to the multiple-free data. Although it works, two concerns emerge: (1) The real challenge comes from the training data set [7]. It is impossible to provide the true primaries for the field data set, so one usually utilizes the most advanced demultiple approach to obtain the best estimated primaries [8]. Thus, the DL performance can never outperform current demultiple methods, which is not our goal; (2) Only providing the original full wavefield and the target primaries to the DLNN lacks physics (i.e., primary and multiple relation), which will lower the chance to have the physically correct primaries. [8] introduce the Generative adversarial network (GAN) to map from full wavefield to the best possible primaries (i.e., EPSI estimated primaries [9]) without using synthetic training pairs, which leads to efficient results rather than the desired better primaries we are pursuing. Although they also mention that providing the NN with a relative cheap prediction of multiples can improve the performance, the related details are missing in [8]. Therefore, we propose to include both the original full wavefield and the initial estimated multiples as the two-channel input, and train DLNN (i.e., U-Net) on the synthetic modeled primaries. In this way, the robust physics (i.e., the globally estimated multiples) is utilized, and the ground truth primary labels can be beneficial to the framework. Both synthetic and field examples are provided to demonstrate the performance of our proposed NN framework.

6.2. DL-BASED ADAPTIVE SUBTRACTION WITH SYNTHETIC PRIMARY LABELS

The conventional adaptive subtraction step for SRME is implemented in the time domain using a minimum-energy constraint [4]:

$$\mathbf{E} = \sum_{t,x_r,x_s} [p(t,x_r,x_s) - a^{(k+1)}(t) * \hat{m}^{(k+1)}(t,x_r,x_s)]^2, \tag{6.1}$$

where $p(t,x_r,x_s)$, $\hat{m}^{(k+1)}(t,x_r,x_s)$ and $a^{(k+1)}(t)$ represent the estimated primaries, the unadapted multiples (i.e. $-\mathbf{P}_0\mathbf{P}$) and the surface operator in the time domain, respectively. The length of the surface operator is also known as the filter length, which is capable of controlling the trade-off between under-fitting and over-fitting. x_r and x_s are the source and receiver locations of seismic data. For the standard SRME, it is first matched and sub-

tracted in a global window during the first 1 or 2 iterations. Small local windows and a long filter length are then utilized for adaptive subtraction in the last iteration to better remove the multiples [4, 10]. It is worth noting that small local windows and a long filter length for standard SRME can damage the primaries though more multiples are removed due to its over-fitting nature. On the other hand, when the last iteration of adaptive subtraction is still implemented in a global window or large local windows with a short filter length, the conservative SRME result with much less primary damage and relatively more multiple leakage is expected due to its under-fitting nature. This dilemma requires more non-linear and non-stationary elements to be solved, and DLNN is able to provide this.

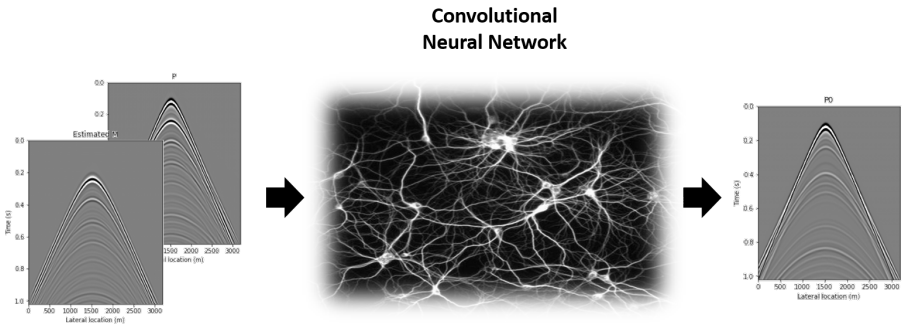

Figure 6.1: The proposed DL-based adaptive subtraction workflow. Note that the original full wavefield and the globally estimated surface multiples (i.e., belonging to the real physics) are fed in the two channels of the input, and the true primaries are used as the target labels.

The biggest problem for DL-based adaptive subtraction is defining a proper training data set. To correctly remove the interfering surface multiples, we would always prefer the ground truth primaries as our target labels. Nevertheless, we can never know the ground truth primaries in the real world. Ideally, the synthetically modeled primaries can be obtained without too much efforts. Therefore, we propose to utilize the synthetic primary labels to learn the most accurate features involved in the adaptive subtraction. On the other hand, direct mapping from the original full wavefield to primaries might be too aggressive for the learning process. The initial estimated multiples are obtained from a global adaptive subtraction, which have the correct kinematic properties. We can regard these multiples as the physics because they are estimated in a physically robust manner (i.e., multi-dimensional convolution). In this way, there is much higher chance to arrive at a physically correct estimated primaries. By combining the mentioned suggestions, the physics-informed adaptive subtraction with synthetic primary labels can be achieved, and the proposed convolutional NN (CNN) workflow can be seen in Figure 6.1. The original full wavefield and the globally estimated multiples are combined together as the input for CNN, and then the CNN output is compared with the ground truth primary label to minimize their differences.

6.3. U-NET FOR ADAPTIVE SUBTRACTION

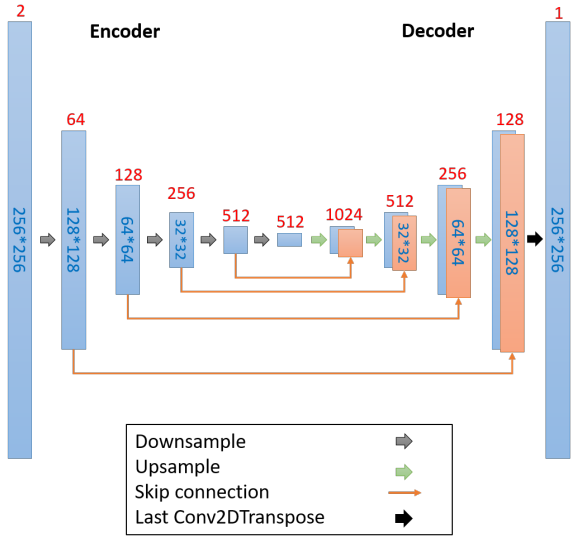

Figure 6.2: U-Net architecture used in this study.

Essentially, the seismic adaptive subtraction task can be treated as one of image-to-image mapping. The famous U-Net might be the most suitable mapping tool (or data fitting) among all different kinds of DLNNs. Originally designed for medical image segmentation [11], the CNN architecture-based U-Net is very powerful in terms of image processing. The convolutional autoencoder is its ancestor, and it consists of two parts: the encoder and the decoder [6]. The encoder downsamples the image and searches for a sparse representation. The decoder does the opposite and includes both upsampling and back-projection. Most importantly, there exist some extra skip connections between the mirrored layers, which can reduce the loss of useful information and result in a more accurate reconstruction. Both encoder and decoder in this chapter are fully convolutional. Figure 7.1 demonstrates the designed architecture of our U-Net. More specifically, each encoder block consist of a 2D convolution with 4×4 filters and stride 2, a batch normalization and a leaky ReLU. Correspondingly, each decoder includes a similar setup except for a 2D deconvolution. More detailed descriptions of the U-Net can be found in [6]. The channel information (or filter) is indicated by the red number on top of each block, which increases along downsampling direction and decreases along upsampling. The core objective function is as follows:

$$\begin{aligned} J &= \frac{1}{N}\sum_{N} \| p_0(t,x_r,x_s) - \hat{p}_0(t,x_r,x_s) \|_1 \\ &= \frac{1}{N}\sum_{N} \| p_0(t,x_r,x_s) - \mathbf{D}(\mathbf{E}(p(t,x_r,x_s), \hat{m}_g(t,x_r,x_s))) \|_1, \end{aligned} \tag{6.2}$$

where $p_0(t,x_r,x_s)$, $\hat{p}_0(t,x_r,x_s)$ and $\hat{m}_g(t,x_r,x_s)$ represent the ground-truth primaries, the

U-Net estimated primaries, and the globally adapted multiples, respectively. N indicates the total number of training data pairs, and $\|.\|_1$ is the $L1$ norm. $\mathbf{E}$ and $\mathbf{D}$ describe the encoding and decoding operators. The aforementioned objective function directly explains the data fitting nature of the U-Net, i.e., minimize the difference between the U-Net estimated primaries and the true primaries. More specifically, the U-Net estimated primaries can be obtained via first encoding the original full wavefield and the globally estimated multiples into their sparse representations, and then decoding back-projects the sparse signals to the final estimated primaries.

The unique feature of our U-Net is its special two-channel input, i.e., the original full wavefield as the first channel and the globally estimated multiples as the second channel. Thus, it can provide the physics (multiples) into the U-Net, which leads to a more accurate estimation than the direct mapping from the original full wavefield to primaries.

6.4. RESULTS

We have applied our proposed NN framework on three different cases: (1) train on synthetic data and test on different synthetic data; (2) train on field data and test on different subsets from the same field data; (3) train on synthetic data and test on field data. Figure 6.3 display two different models used for generating all the synthetic data. Both models contain a shallow water layer with several subsurface layers. Model 1 from Figure 6.3(a) generates all the synthetic training data pair used in this chapter as shown in Figure 6.4, which consist of 256 shots. Each shot has 256 receivers with 256 time samples for each trace. Both source and receiver sampling are 12.5 m, and time sampling is 4 ms. So the input seismic data size is 256×256. Note that the acquisition parameters are the same for all synthetic and field data sets.

6.4.1. CASE 1: TRAINED ON SYNTHETIC AND APPLIED ON SYNTHETIC

We first only trained on synthetic data from one model, and applied the learned NN on the data generated from another model. Figure 6.4 shows the results during the training phase. The original full wavefield and the globally estimated multiples (Figure 6.4(a) and 6.4(b)) are regarded as the two input channels of the U-Net. The ground truth primaries (Figure 6.4(c)) is considered as the U-Net target. 10% (random picking) of the training shots (i.e., 26 shots) are designed as the development data to fine-tune the hyperparameters (e.g., NN channels, layers, epoch, etc) for avoiding over/under-fitting. Figure 6.4(d) and 6.4(e) indicate the ground truth primaries and the U-Net estimated primaries on the development data, and they are visually the same. Thus, the proposed NN framework has learned well from the training synthetic data. However, the general performance of the learned NN needs to be confirmed on the test data set.

Figure 6.5 demonstrates the performance of the proposed NN framework on the synthetic test data generated from Model 2. The original full wavefield (Figure 6.5(a)), the ground truth primaries (Figure 6.5(b)) and the globally estimated primaries (Figure 6.5(c)) are provided for better comparison. From the globally estimated primaries, it can be seen that there are large primary and multiple overlapping area as indicated by the arrow, which leads to either primary damage or multiple leakage for the traditional adaptive subtraction methods. The U-Net estimated primaries are shown in Figure 6.5(d), which partly

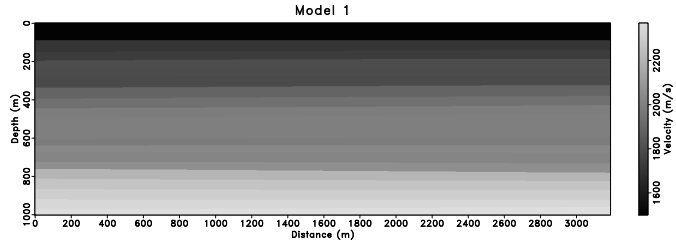

(a)

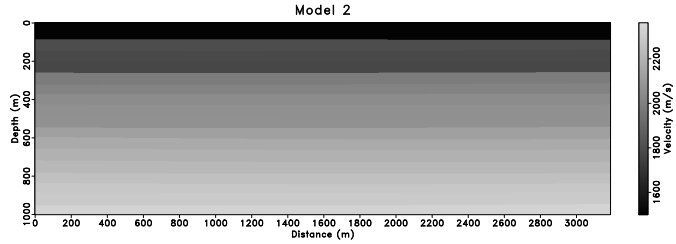

(b)

Figure 6.3: Two subsurface models used for generating data. (a) Model used for generating training data. (b) Model used for generating test data.

6

improves the globally estimated primary result with clearer primary events and less residual multiple events. Although it is not perfect because of the different data distribution of the two synthetic examples, it is surprising how close these primaries resemble to true ones.

6.4.2. CASE 2: TRAINED ON FIELD AND APPLIED ON FIELD

Next, to pursue a similar data distribution, we select two close subsets of the 2D field data set, and train our NN on one and test on the other. Note that in this case, we do not know the ground truth primaries, so we need to provide the target primaries in advance. Local primary-and-multiple orthogonalization (LPMO) [12] is used to obtain a good estimated of primaries. In theory, the upper limit that NN can learn is LPMO. Figure 6.6 displays the training data pair. After training, we applied the learned NN on the nearby test field data, which is shown in Figure 6.7. It can be noticed from the globally estimated primaries that there exist some multiple leakage as shown by the arrow. LPMO, from which NN is learned, is good at extracting those leaked multiple. The proposed U-Net estimated primaries are shown in Figure 6.7(c), which can reduce the multiple leakage at the arrow-indicated area. Therefore, our proposed NN framework can successfully learn the LPMO feature under the same data distribution. Note again that the training data are selected from a different part in the field data compared to the test data, to avoid the NN just acts as a data interpolator.

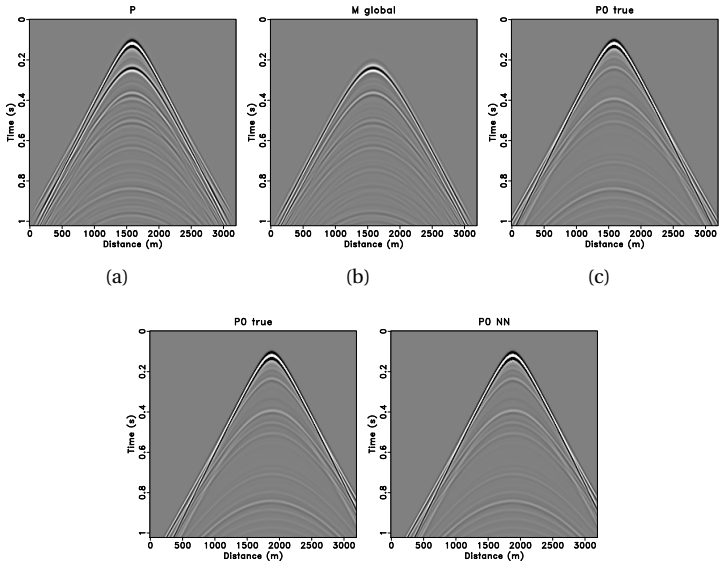

Figure 6.4: U-Net training data pair, and its performance on the development data. (a) & (b) The original full wavefield and the globally estimated multiples as two input channels of U-Net, respectively. (c) The ground truth primaries as the target label channel. (d) & (e) The ground truth primaries and the U-Net estimated primaries on the development data. Note that the data are modeled from Figure 6.3(a).

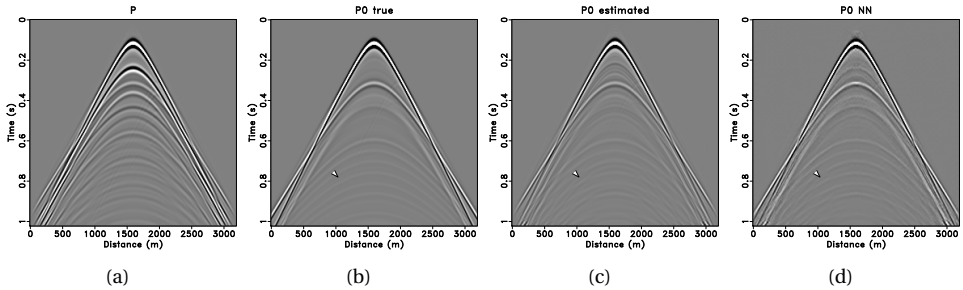

Figure 6.5: DL-based adaptive subtraction performance on the test data. (a) & (b) The original full wavefield and the ground truth primaries, respectively. (c) Globally estimated primaries. (d) The U-Net estimated primaries. Note that the data are modeled from Figure 6.3(b).

6.4.3. CASE 3: TRAINED ON SYNTHETIC AND APPLIED ON FIELD

The last case is we train on synthetic data and applied on the field data, which is the ideal scenario and also the most challenging situation due to very different data distribution.

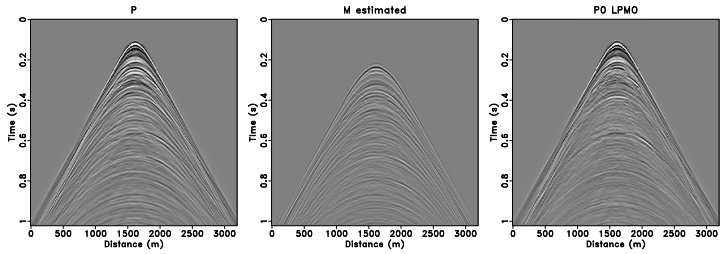

(a) (b) (c)

Figure 6.6: Training field data set. (a) & (b) The original full wavefield and the globally estimated multiples as two input channels of U-Net, respectively. (c) The estimated primaries from LPMO as the target.

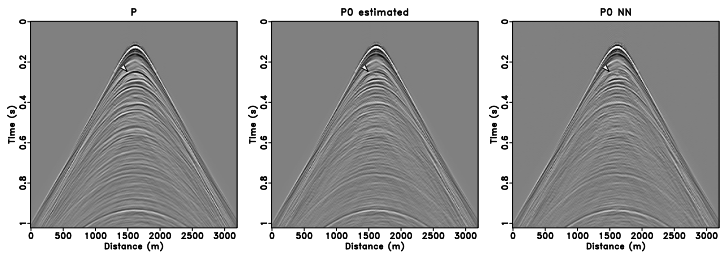

(a) (b) (c)

Figure 6.7: Test field data set (trained on the field data). (a) & (b) The original full wavefield and the global estimated primaries, respectively. (c) The U-Net estimated primaries.

Note that in this case we have to cut the data into small patches first and then apply the proposed NN on those patches due to strong non-stationary feature of seismic field data. The patch size is 64 by 64. Note that the corresponding U-Net size and layers will also decrease. Figure 6.8 demonstrates the current results in this most difficult scenario. The original full wavefield and the global estimated primaries are shown in Figure 6.8(a) and 6.8(c), respectively. The U-Net estimated primaries trained only on synthetic data are displayed in Figure 6.8(c). We notice that the originally weak primary events are enhanced after the proposed NN framework, especially for events marked by the arrows. The NN might learn to compensate the amplitude loss caused by the deghosting process from the synthetic data. Still, the overall energy distribution is different from the original data. Thus, we propose to include 1% of field data training pair (primaries from LPMO), and the result is shown in Figure 6.8(d), which is closer to the original distribution.

6.5. CONCLUSIONS

We have proposed the DLNN framework for primary estimation via a U-Net with both total data and predicted multiples as input channels. The data distribution between train-

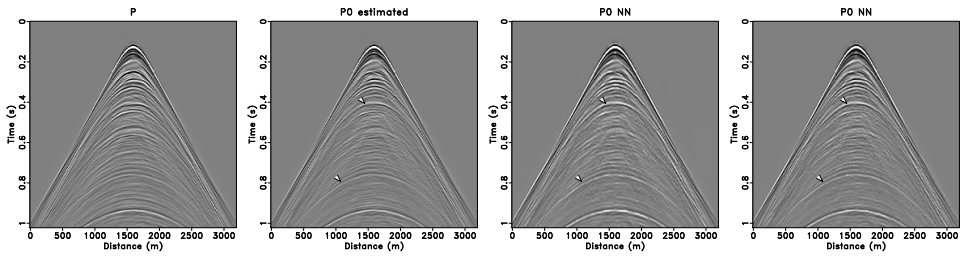

(a) (b) (c) (d)

Figure 6.8: Test field data set (trained on the synthetic data). (a) & (b) The original full wavefield and the global estimated primaries, respectively. (c) The U-Net estimated primaries. (d) The U-Net estimated primaries with 1% field data as the training data.

ing and test data plays an important role on the U-Net primary estimation performance. Training on field data and test on nearby field data gives the best performance due to the similar data distribution. The globally estimated multiples as the second channel of the input provide robust physics for the proposed framework, and using synthetic primaries as target labels can enhance the weak primary energy. Applications on three different cases demonstrate the promising performance of the proposed framework, where the most promising is the scenario of training on synthetic data and applying it to field data. Please note that the initial results in this chapter are currently optimal, which might not be the best due to limited training data set and various U-Net settings.

6.6. ACKNOWLEDGEMENTS

The authors would like to thank PGS for providing the Nelson field data.

REFERENCES

[1] D. J. Verschuur, A. J. Berkhout, and C. P. A. Wapenaar, *Adaptive surface-related multiple elimination,* Geophysics **57** (1992), pp. 1166–1177.

[2] A. J. Berkhout and D. J. Verschuur, *Estimation of multiple scattering by iterative inversion, Part I: Theoretical considerations,* Geophysics **62** (1997), pp. 1586–1595.

[3] B. Dragoset, E. Verschuur, I. Moore, and R. Bisley, *A perspective on 3D surface-related multiple elimination,* Geophysics **75** (2010), pp. 75A245–75A261.

[4] D. J. Verschuur and A. J. Berkhout, *Estimation of multiple scattering by iterative inversion, Part II: Practical aspects and examples,* Geophysics **62** (1997), pp. 1596–1611.

[5] R. Abma, N. Kabir, K. H. Matson, S. Michell, S. A. Shaw, and B. McLain, *Comparisons of adaptive subtraction methods for multiple attenuation,* The Leading Edge **24** (2005), pp. 277–280.

[6] I. Goodfellow, Y. Bengio, and A. Courville, *Deep learning* (The MIT Press, 2016).

[7] S. Qu, E. Verschuur, D. Zhang, and Y. Chen, *Training deep networks with only synthetic data: Deep-learning-based near-offset reconstruction for (closed-loop) surface-related multiple estimation on shallow-water field data,* Geophysics **86** (2021), pp. A39–A43.

[8] A. Siahkoohi, D. J. Verschuur, and F. J. Herrmann, *Surface-related multiple elimination with deep learning,* in *89th SEG Technical Program Expanded Abstracts* (Society of Exploration Geophysicists, 2019).

[9] G. J. van Groenestijn and D. J. Verschuur, *Estimating primaries by sparse inversion and application to near-offset data reconstruction,* Geophysics **74** (2009), pp. A23–A28.

[10] D. J. Verschuur, *Seismic multiple removal techniques : past, present and future* (EAGE Publications, Houten, Netherlands, 2013).

[11] O. Ronneberger, P. Fischer, and T. Brox, *U-net: Convolutional networks for biomedical image segmentation,* in *Lecture Notes in Computer Science* (Springer International Publishing, 2015) pp. 234–241.

[12] D. Zhang, D. J. Verschuur, S. Qu, and Y. Chen, *Surface-related multiple leakage extraction using local primary-and-multiple orthogonalization,* Geophysics **85** (2020), pp. V81–V97.

7

DL-BASED MULTIPLE DE-ALIASING

The main prediction engine in surface-related multiple elimination (SRME) is the multi-dimensional convolution process, where data sampling plays an essential role for accurate surface multiple prediction. Therefore, fully sampled sources and receivers are preferred. If especially the source sampling is far from ideal, the estimated multiples will suffer from the severe aliasing effect. Consequently, this can lead to poorly estimated primaries. Interpolation of coarsely sampled sources is not a trivial task. Dealiasing on the estimated multiples from limited sources might provide a potential solution. In theory, this dealiasing problem is highly non-linear, which suits well for deep learning (DL)-based methods. Therefore, we propose a U-Net-based approach to dealiase the estimated surface multiples from limited sources. Applications on two subsets of the field data demonstrate the effective performance of the proposed method.

This chapter is a slightly modified version of the proceeding "D. Zhang and E. Verschuur, Deep learning-based dealiasing for estimated surface-related multiples from limited sources, 82nd EAGE Conference and Exhibition Expanded abstracts (European Association of Geoscientists & Engineers, 2021)".

7.1. INTRODUCTION

Surface-related multiple elimination (SRME) requires two necessary steps: the multidimensional convolution and adaptive subtraction [1, 2]. During the first step, data sampling plays an essential role for accurate surface multiple prediction. At the receiver side sampling is usually such that interpolation can be carried out. However, also fully sampled sources are preferred. If the source sampling is far from ideal, the estimated multiples will suffer from the severe aliasing effect [3, 4]. Consequently, this can lead to poorly estimated primaries. Source interpolation is usually applied to overcome the sampling issue for better unaliased multiples [5]. However, source-side interpolation is extremely challenging in real 3D case due to the limited recorded data (around 2% of the desired data) and the huge data storage. Regarding the aforementioned issues, dealiasing on the estimated multiples from limited sources might provide a potential solution to the real 3D problem. In theory, this dealiasing problem is highly non-linear, which suits well for deep learning (DL)-based methods. Therefore, we propose a convolutional neural network (CNN)-based approach (i.e., U-Net) to dealiase the estimated surface multiples from limited sources. Note that we currently demonstrate the proposed method on a 2D field data example, and the 3D application will be studied in the future.

7.2. MULTIDIMENSIONAL CONVOLUTION-BASED MULTIPLE ESTIMATION

The multidimensional convolution for kinematic multiple estimation can be described as follows:

$$\hat{\mathbf{M}} = -\mathbf{P}_0\mathbf{P}, \tag{7.1}$$

where $\hat{\mathbf{M}}$, $\mathbf{P}_0$ and $\mathbf{P}$ denote the estimated multiples, the estimated primaries and the original full wavefield, respectively. We use $\mathbf{P}$ to replace $\mathbf{P}_0$ for initial multiple estimation. Note that depending on source type an obliquity factor may be included [6]. This multidimensional convolution is the most robust step in SRME under the condition that the recorded full wavefield data are fully sampled in both source and receiver side. Otherwise, the estimated multiples will suffer from the aliasing effects. Note that in this chapter we focus on the source side sampling. Source side interpolation is usually only feasible in the 2D case, and is very challenging in 3D. When applying multiple prediction with sparsely sampled source creates a distinct aliasing pattern on the predicted multiples. Therefore, dealiasing on the estimated multiples from limited sources might provide a potential solution, which requires a highly non-linear mapping operator.

7.3. U-NET FOR MULTIPLE DE-ALIASING

Essentially, the seismic dealiasing task can be treated as one of the image-to-image mapping, which is highly non-linear. The famous U-Net might be the most suitable mapping tool (or data fitting) among all different kinds of DL neural networks. Originally designed for medical image segmentation [7], a CNN architecture-based U-Net is very powerful in terms of image processing. The convolutional autoencoder is its ancestor, and it consists of two parts: the encoder and the decoder [8]. The encoder downsamples the image and searches for a sparse representation. The decoder does the opposite, which includes both

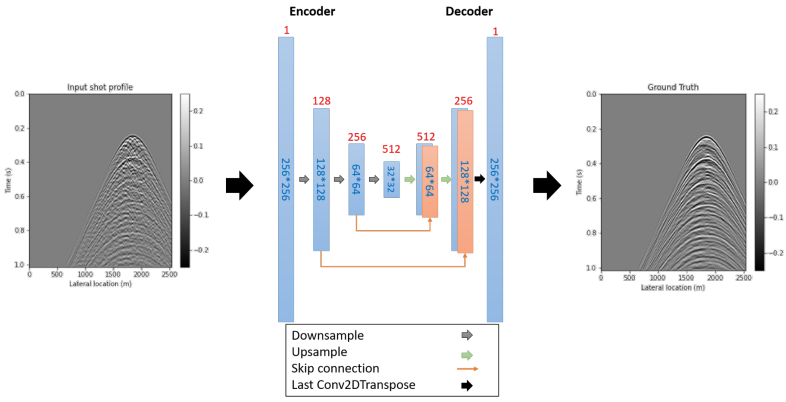

Figure 7.1: U-Net architecture used in this study.

upsampling and back-projection. Most importantly, there exist some extra skip connections between the mirrored layers, which can reduce the loss of useful information and result in a more accurate reconstruction. Both encoder and decoder in this chapter is fully convolutional. Figure 7.1 demonstrates the designed architecture of our U-Net, in which the input is the aliased multiples and the output is the dealiased multiples. More specifically, each encoder block consist of a 2D convolution with 4×4 filters and stride 2, a batch normalization and a leaky ReLU. Correspondingly, each decoder includes a similar setup except for a 2D deconvolution. More detailed description of the U-Net can be found in [8]. The channel information (or filter) is indicated by the red number on top of each block, which increases along the downsampling direction and decreases during upsampling. The core objective function is as follows:

$$J = \frac{1}{N} \sum_{N} \|\mathbf{M} - \mathbf{D}(\mathbf{E}(\hat{\mathbf{M}}))\|_1, \tag{7.2}$$

where $\mathbf{M}$ represent the target multiples with fully sampled sources and $\hat{\mathbf{M}}$ the input multiple prediction with aliasing imprint. N indicates the total number of training data pairs, and $\|.\|_1$ is the $L1$ norm. $\mathbf{D}$ and $\mathbf{E}$ describe the encoding and decoding operators. The aforementioned objective function directly explains the data fitting nature of the U-Net, i.e., minimizing the difference between the U-Net estimated multiples and the target multiples. More specifically, the U-Net estimated multiples can be obtained via first encoding the aliased multiples into a sparse representation, and then decoding back-projects the sparse signals to the final estimated multiples.

7.4. RESULTS

We extract two fixed-spread fully sampled data subsets from the same 2D Nelson North Sea data. Two subsets come from adjacent areas, which have similar geological structures. For each subset, there are 256 shots, and each shot contains 256 receivers. The time sampling is 4 ms. Figure 7.2 shows the stacked sections of the aforementioned two subsets. The idea behind is that one subset (7.2(a)) is regarded as the training data with fully

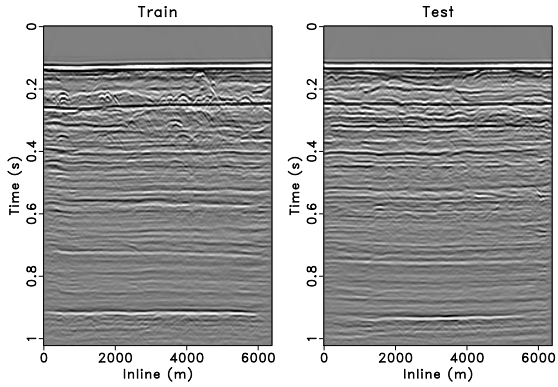

(a) (b)

Figure 7.2: Two fixed-spread fully sampled subsets from the same 2D Nelson line. (a) Subset used for training. (b) Subset used for testing.

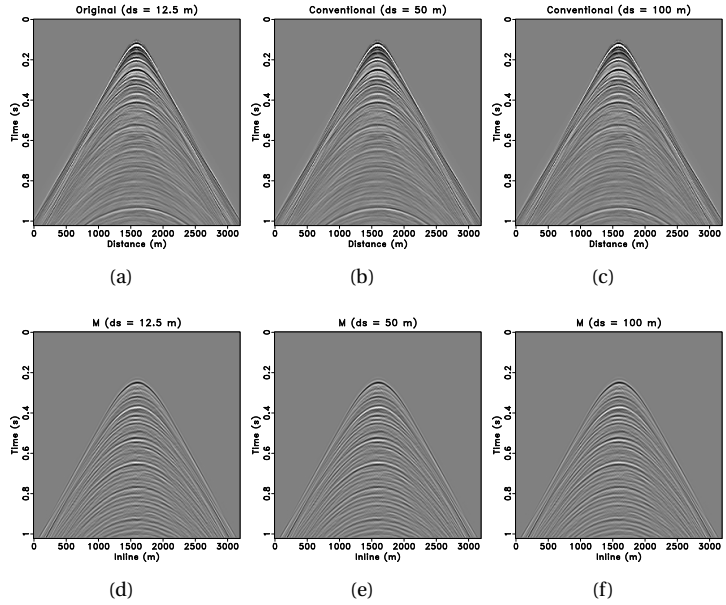

(a) (b) (c)

(d) (e) (f)

Figure 7.3: Conventional source interpolation results and their corresponding estimated multiples. (a) & (d) Original shot and its multiples with 12.5 m source spacing. (b) & (e) Interpolated shot with 50 m source spacing and the estimated corresponding multiples after interpolation. (c) & (f) Interpolated shot with 100 m source spacing and the estimated corresponding multiples after interpolation.

sampled sources, while the other subset (7.2(b)) is considered as the test data with limited sources. In reality, it represents that we can intensively record fully sampled sources in one area for training the NN, and for the adjacent areas we only need to record sparse sources to reduce the cost. The resulting aliasing effects can be resolved by the proposed DL-based approach. Note that we test two different source spacing in this chapter, i.e., 50 me and 100 m, to demonstrate the DL power on source side dealiasing.

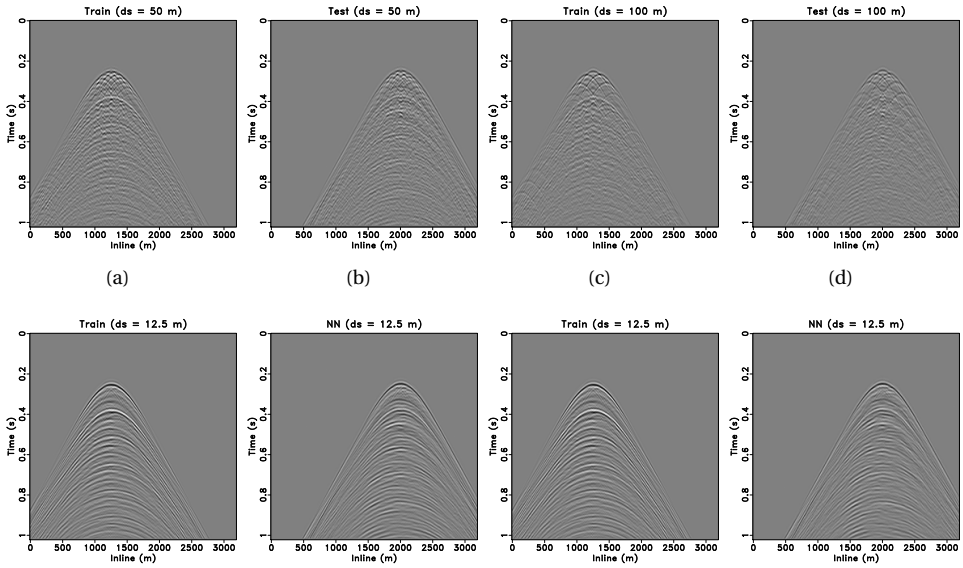

Figure 7.4: U-Net training data pair, and its performance on the test data. (a) & (e) The aliased multiples (50 m source spacing) and its unaliased target multiples from the training data, respectively. (b) & (f) The aliased multiples (50 m source spacing) and the DL estimated dealiased multiples from the test data, respectively. (c) & (g) The aliased multiples (100 m source spacing) and its unaliased target multiples from the training data, respectively. (d) & (h) The aliased multiples (100 m source spacing) and the DL estimated dealiased multiples from the test data, respectively.

First, we display some conventional interpolation results as a comparison in Figure 7.3. Conventional method interpolates the missing sources based on the low-frequency components of the data in the common offset domain. The multiples are thus estimated after the interpolation to reach the desired performance. From both interpolation results and the corresponding multiples, it is clear that the conventional method can provide a good interpolation performance for further multiple estimation for both 50 m and 100 m source spacing. However, some tiny details are lost along the seismic events, which cannot be easily noticed from the shot gather displays. In contrast, all specular reflections are well interpolated.

Next, Figure 7.4 demonstrate the performance of the proposed DL dealiasing method.

The training pair of the aliased multiples with 50 m source spacing and the unaliased target multiples are shown in Figure 7.4(a) and 7.4(e). After the training phase, we apply the learned NN on the similar aliased test shot gather (Figure 7.4(b)) from the adjacent area. The dealiased result via the DL-based approach is displayed in Figure 7.4(f). We can notice that most events are well recovered and all aliased energy has been successfully removed. Then, we apply the same method to the training pair with 100 m source spacing as shown in Figure 7.4(c) and 7.4(g). The learned NN is applied to the aliased test data with 100 m source spacing in Figure 7.4(d). Figure 7.4(h) indicates the final DL-based dealising result, which removes most aliased energy. However, some of the weak seismic events are not well recovered.

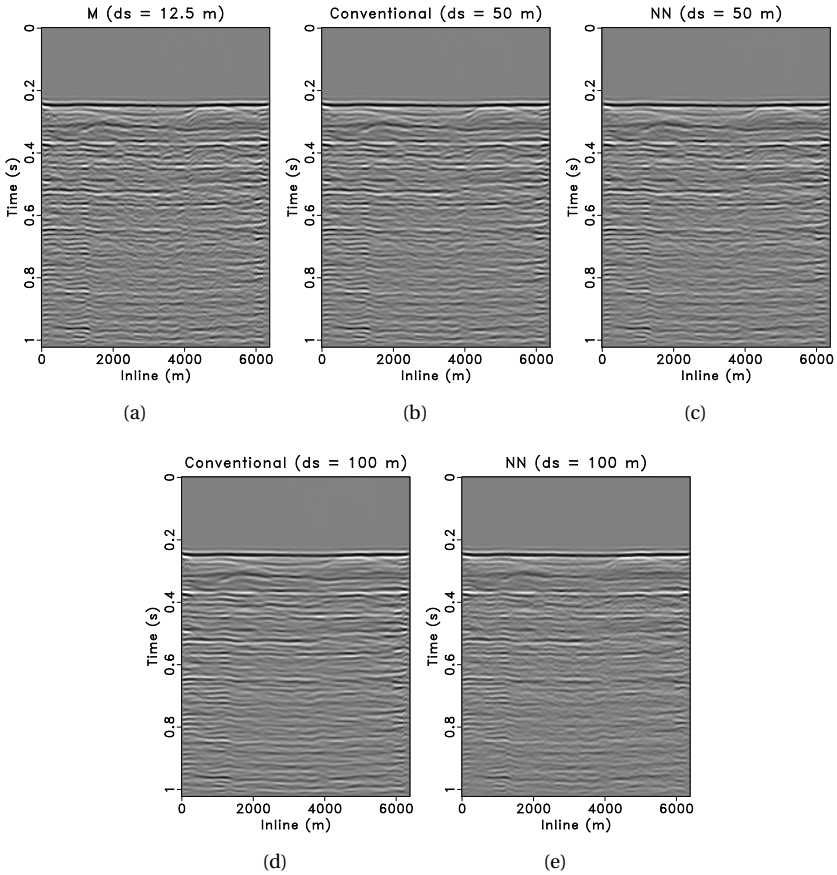

Figure 7.5: Stacked section comparison for estimated multiples from (a) the original fully sampled sources (12.5 m source spacing), (b) & (c) the conventional interpolated data and the NN dealised data (50 m source spacing), and (d) & (e) the conventional interpolated data and the NN dealised data (100 m source spacing).

For better and clearer comparison, we provide the stacked sections for the estimated

multiples in Figure 7.5. Figure 7.5(a) is considered as the benchmark multiple stacked section, which comes from the original fully sampled sources. Figure 7.5(b) and 7.5(d) demonstrate the stacked multiple sections from the conventional interpolated data. It can be seen that most specular reflections are well preserved. However, those events become smoother than the benchmark section, in which we can observe more small scale discontinuities. Also note that the 100 m source spacing result is much smoother than the 50 m source spacing. In contrast, both stacked multiple sections from the DL-based dealiasing method in Figure 7.5(c) and 7.5(e) contain more small-scale information and shows a better resemblance with the benchmark results (Figure 7.5(a)).

7.5. CONCLUSIONS

We have proposed a DL-based dealising method for multiple estimation. The non-linear mapping power of DL can successfully project the aliased multiples to its corresponding unaliased target multiples. Applications on two subsets of the field data demonstrate the effective performance of the proposed method. Note that we also need to compare a DL-based dealiasing with a DL-based source interpolation method, in order to find out which approach is most suitable. However, the real potential value lies in 3D cases, where most data are not recorded. Conventional interpolation method works well for the relative flat geology in 2D, while it will fail under complex structures in 3D. The proposed DL-based dealiasing framework can be potentially extended to 3D environment, which will be our future research. Also note that such approach will have an impact on acquisition design: to benefit from this approach it can be decided to shoot certain areas with dense sampling for training purpose.

7.6. ACKNOWLEDGEMENTS

The authors would like to thank PGS for providing the field data.

REFERENCES

[1] A. J. Berkhout and D. J. Verschuur, *Estimation of multiple scattering by iterative inversion, Part I: Theoretical considerations,* Geophysics **62** (1997), pp. 1586–1595.

[2] D. J. Verschuur and A. J. Berkhout, *Estimation of multiple scattering by iterative inversion, Part II: Practical aspects and examples,* Geophysics **62** (1997), pp. 1596–1611.

[3] D. J. Verschuur, *Seismic multiple removal techniques : past, present and future* (EAGE Publications, Houten, Netherlands, 2013).

[4] B. Dragoset, E. Verschuur, I. Moore, and R. Bisley, *A perspective on 3D surface-related multiple elimination,* Geophysics **75** (2010), pp. 75A245–75A261.

[5] J. Cai, M. Guo, S. Dong, R. Camp, G. Abarr, and B. Wang, *True azimuth surface multiple elimination,* in *80th SEG Technical Program Expanded Abstracts* (Society of Exploration Geophysicists, 2010).

[6] A. B. Weglein, F. A. Gasparotto, P. M. Carvalho, and R. H. Stolt, *An inverse-scattering series method for attenuating multiples in seismic reflection data,* Geophysics **62** (1997), pp. 1975–1989.

[7] O. Ronneberger, P. Fischer, and T. Brox, *U-net: Convolutional networks for biomedical image segmentation,* in *Lecture Notes in Computer Science* (Springer International Publishing, 2015) pp. 234–241.

[8] I. Goodfellow, Y. Bengio, and A. Courville, *Deep learning* (The MIT Press, Cambridge, Massachusetts, 2016).

8

CONCLUSION AND RECOMMENDATIONS

8.1. CONCLUSION

The traditional seismic surface-related multiple estimation and removal methods are limited by the unrecorded data reconstruction (e.g., the missing near offsets and the data gap between the crosslines) and the subsequent multiple adaptive subtraction performance. These issues become even more severe for the shallow water environment, which is defined as having typically around 50-200 m water depth when regarding the exploration seismic frequency range (i.e., 2-120 Hz) in this thesis. Shallow water creates highly curved seismic reflection events with strong lateral amplitude variations, and tends to generate complex seismic event overlap between primaries and surface-related multiples. Conventional data reconstruction methods fail to tackle the missing data in shallow water, and are even more problematic in 3D. Meanwhile, the dilemma between primary damage and surface multiple leakage during the adaptive subtraction usually becomes more severe for shallow water data. Therefore, a reconstruction approach to handle both the missing near offsets and large crossline data gaps and a robust tool to mitigate the adaptive subtraction dilemma is desired.

In this thesis, a new integrated closed-loop surface-related multiple estimation (CL-SRME) and full-wavefield migration (FWM) framework for better primary and surface-related multiple estimation is proposed to attack the unrecorded data reconstruction issue. This framework is able to support CL-SRME with good-quality near-offset data in order to avoid primary estimation failure that typically occurs in shallow-water environments. Near-offset data reconstruction in shallow-water environments is challenging where the seismic events are highly curved with strong lateral amplitude variations. Conventional data-driven reconstruction methods (e.g., using the parabolic Radon transform) fail to fill the missing gaps with correct phase and amplitudes. We, therefore, suggest to use multiples to provide information on the missing near-offset data by using FWM, where primaries and surface multiples together create an image of the shallow subsurface. Tak-

ing advantage of FWM - with its closed-loop simultaneous primaries and multiples imaging approach - as the data reconstruction method and feeding the reconstructed near-offsets to CL-SRME are the most important components to success. Good performance of the proposed integrated framework for shallow-water environments has been demonstrated based on a 2D synthetic and a 2D North Sea field data. This new integrated framework will have its main impact on a full 3D implementation with coarse sampling. Therefore, a similar cascaded framework for 3D surface-related multiple estimation in shallow-water scenarios, which consists of a data reconstruction step via 3D FWM and a surface multiple estimation step via 3D SRME or general surface multiple prediction (GSMP), is also introduced in the thesis. 3D FWM has demonstrated its strong data reconstruction power through two different shallow-water 3D synthetic data sets. More specifically, FWM-aided 3D SRME is indeed capable of delivering the best surface multiple estimation result because of fully taking advantage of the 3D FWM reconstruction power and perfectly fulfilling the data sampling requirement of 3D SRME. However, FWM-aided 3D SRME is currently not affordable due to the huge data storage issue and the intensive computational cost. Therefore, only partial reconstruction power of 3D FWM on recovering the near offsets is used by FWM-aided GSMP, in which an acceptable result with less data storage and computational resources is achieved.

In order to mitigate the surface-related multiple adaptive subtraction dilemma, we have also introduced an innovative two-step framework for surface multiple leakage extraction in this thesis, and thus extended our seismic multiple processing toolbox. The aforementioned two-step framework based on local primary-and-multiple orthogonalization (LPMO) is both versatile and efficient for leaked multiple extraction, therefore, primaries can be better preserved without leaving much multiple energy. The initial estimation step usually prefers a conservation SRME, and LPMO is followed to compensate the initial estimated primaries and multiples. Applications to two synthetic data sets and one North Sea field data set show a good performance of the proposed framework for alleviating the adaptive subtraction dilemma. Although effective, LPMO is relatively computational intensive. Therefore, a fast LPMO (FLPMO) is further introduced to accelerate this process. More specifically, the time-consuming shaping regularization-based iterative inversion in LPMO can be replaced by a scaled point-by-point division in FLPMO. In this way, we can achieve a local speedup factor of around 40. Two different North Sea field data sets are tested to display the equally good performance of FLPMO compared to LPMO for surface multiple leakage extraction. However, the overall cost of the complete FLPMO framework is around 4 times faster than the LPMO framework, which is now equivalent to the costs of the industry standard $L2$ adaptive subtraction.

With the advance of deep learning (DL) technology, two DL neural network (NN) frameworks are investigated for better surface-related multiple estimation in shallow water. Both NN are based on the U-Net setting. DL-based dealising NN is introduced for the initial multiple estimation, where the strong data fitting power of DL can directly project the aliased multiples due to coarse sampling to its corresponding unaliased target multiples. Such approach might have an impact on the acquisition design, in which certain areas can be shot densely for DL training purpose. At the same time, DL-based adaptive subtraction NN is proposed with both total full wavefield and the predicted multiples as two input channels. The globally estimated multiples, as the second input channel, are

regarded as the robust and helpful physics. In general, it is preferable to train and test on data sets with the same characteristics. Training on field data and test on nearby field data gives the best performance due to the similar data distribution. In this case, only limited training data are required because all the data have the same characteristics. Transferring from synthetic data to field data, however, requires much more efforts in order to find the same data distribution. The corresponding benefit is training with the ground truth data. Applications on the North Sea field data show promising performances of both DLNN for surface-related multiple estimation.

Shallow water is very challenging for surface-related multiple estimation. Physics-based deterministic approaches, e.g., FWM-based data reconstruction and LPMO, can help geophysicists better understand and partially solve the essentials of the problem. For poorly described deterministic problems, e.g., adaptive subtraction and multiple de-aliasing, DL can find the underlying relationships that are not easily achievable by the deterministic methods. Combination of deterministic methods and DL will result in an optimal performance. This is where further research should concentrate on.

8.2. RECOMMENDATIONS FOR FURTHER RESEARCH

8.2.1. SOURCE SIDE SAMPLING WITH 3D EXTENSION

Current work of data reconstruction for the missing near offsets and coarse sampling via FWM is still restricted to the receiver side. It is necessary to include source side data reconstruction as well to achieve the best surface-related multiple estimation. However, the data storage tends to explode with full sampling on the source side [1]. Balance between the data storage issue and optimal performance needs more attention for further research.

8.2.2. ATTACKING/MITIGATING AVO EFFECTS

Because of the over-parametrization danger from angle-dependent FWM [2], the current version of FWM-based data reconstruction cannot easily handle the angle-versus-offset (AVO) effects in the large offsets. Some simplified AVO approximation (e.g., Shuey approximation [3] or DL-based approximation [4]) might help FWM to better fit the data at large offsets without over-parametrization. Oppositely, one can think of removing or mitigating the AVO effects in the data rather than explaining them [5]. Thus, FWM-based data reconstruction is expected to perform even better in the future.

8.2.3. SHALLOW SUBSURFACE MODEL

The shallow subsurface model proves to be extremely important for model-based FWM-type data reconstruction approach. An accurate near-surface model is usually very challenging to obtain [6], therefore, an integrated study with high-resolution seismic imaging/inversion is desired to achieve such a good shallow subsurface model.

8.2.4. LPMO CONSTRAINED CL-SRME OR SRME

LPMO, attached behind any conservative multiple estimation method, has been demonstrated to be effective on extracting the leaked multiples in this thesis. In theory, more advanced inversion-based CL-SRME can achieve an optimal separation without the help from LPMO [7]. However, data can never be perfect, due to 2D/3D effects, coarse sam-

pling, source/receiver directivity, etc. This can lead to undesired multiple estimation even for CL-SRME. LPMO acting as an internal constraint might help condition the inversion framework, thus, reach a better primary and multiple model. Similarly, LPMO might also constrain the iterative SRME, meaning LPMO can be applied after every iteration of SRME to improve both the efficiency and performance.

8.2.5. EFFECTS OF OVERLAPPING MULTIPLES FROM DIFFERENT ORDERS ON LPMO

As water depth decreases, the issue of interfering multiples from different orders becomes more severe. The case of a first-order SRME prediction can be more interesting since this is often the prediction in industrial practice. For such a prediction, overlapping multiples from different orders may require different corrections during the adaptive subtraction. Thus, the corresponding effects on the proposed LPMO framework are worth further investigating in detail. LPMO results might even indicate issues related the overlapping order of multiples. It should be informative to compare closely and quantitatively the results from this iterative approach with results from CL-SRME or EPSI that have the capability to solve this issue of interfering multiples from different orders.

8.2.6. SEPARATION-RELATED TOOLBOX

In order to become a standard seismic separation-related processing toolbox, LPMO requires much more further studies with different initial separation methods and scenarios. We only tested on $L2$-based adaptive subtraction, and methods such as curvelet [8] and non-stationary regression [9] approaches need more validation.

8.2.7. BEYOND LIMITED TRAINING DATA SET

DL-based results in this thesis only utilize limited number of training data sets, and we are actually already surprised by the current performances. Nevertheless, more training data will keep improving the power of our NN especially for more challenging scenarios, i.e., training on the synthetic data and applied on the field data. Searching for the optimal training size by itself is worth further investigation. Note that it is always preferable to train and test on the data with similar distribution.

8.2.8. DL-BASED DE-ALIASING VS DL-BASED INTERPOLATION

Conventionally for seismic surface-related multiple estimation, one usually interpolates the missing data first and then applies the multidimensional convolution to obtain the multiple model. Alternatively, one can directly apply the convolution on the coarse data set, and implement de-aliasing on the aliased multiples. Note that the interpolation task can also be achieved via DLNN [10, 11]. Therefore, it is imperative to compare the performances of these two different routes, and study the role and effectiveness of DLNN on each route.

8.2.9. DL-BASED OPTIMAL METRIC FOR ADAPTIVE SUBTRACTION

Choosing the optimal metric for adaptive subtraction is usually very challenging and troublesome in practice [12]. DL might come in handy if we train the NN to evaluate different

metric, e.g., $L1$, $L2$, Lp, etc. In this way, we can apply adaptive metric for different part of the data to reach the optimal subtraction performance. It would be extremely helpful for the future practitioners in the industry.

8.2.10. IMAGING OR REMOVING MULTIPLES

The choice of multiple imaging or multiple removal relies on the original data sampling pattern [13]. Note that multiple removal methods require dense sampling on both source and receiver side. If either source or receiver side is poorly sampled, e.g., in the situation of ocean bottom node (OBN), multiple imaging is the preferred route. Also, the relation between seismic acquisition and FWM needs to be further investigated.

8.2.11. APPLICATION TO A LARGER AND MORE REPRESENTATIVE DATA SET

In this thesis, several methods were only demonstrated on the 2D Nelson field data, that may not represent all typical issues. Therefore, application on a 2D marine line of some 50 km or longer, with representative variations in geology, towing conditions, sources operations, weather, and noise, would be more beneficial for the industry. Also, sufficient advanced processing including imaging/inversion such that one could assess the sensitivity of advanced processing results to the proposed enhancements.

REFERENCES

[1] B. Dragoset, E. Verschuur, I. Moore, and R. Bisley, *A perspective on 3D surface-related multiple elimination,* Geophysics **75** (2010), pp. 75A245–75A261.

[2] M. Davydenko and D. Verschuur, *Full-wavefield migration: using surface and internal multiples in imaging,* Geophysical Prospecting **65** (2016), pp. 7–21.

[3] R. T. Shuey, *A simplification of the Zoeppritz equations,* Geophysics **50** (1985), pp. 609–614.

[4] S. Qu, E. Verschuur, D. Zhang, and Y. Chen, *Training deep networks with only synthetic data: Deep-learning-based near-offset reconstruction for (closed-loop) surface-related multiple estimation on shallow-water field data,* Geophysics **86** (2021), pp. A39–A43.

[5] S. Qu, D. Verschuur, and Y. Chen, *Robust AVO-preserving joint migration inversion of seismic reflections using a data mismatch based on local orthogonalization,* in *82nd EAGE Conference and Exhibition Expanded Abstracts* (European Association of Geoscientists & Engineers, 2020).

[6] D. Boiero, E. Wiarda, and P. Vermeer, *Surface- and guided-wave inversion for near-surface modeling in land and shallow marine seismic data,* The Leading Edge **32** (2013), pp. 638–646.

[7] D. Zhang, D. J. Verschuur, S. Qu, and Y. Chen, *Surface-related multiple leakage extraction using local primary-and-multiple orthogonalization,* Geophysics **85** (2020), pp. V81–V97.

[8] F. J. Herrmann, D. Wang, and D. J. Verschuur, *Adaptive curvelet-domain primary-multiple separation,* Geophysics **73** (2008), pp. A17–A21.

[9] S. Fomel, *Adaptive multiple subtraction using regularized nonstationary regression,* Geophysics **74** (2009), pp. V25–V33.

[10] D. A. B. Oliveira, R. S. Ferreira, R. Silva, and E. V. Brazil, *Interpolating seismic data with conditional generative adversarial networks,* IEEE Geoscience and Remote Sensing Letters **15** (2018), pp. 1952–1956.

[11] H. Kaur, N. Pham, and S. Fomel, *Seismic data interpolation using deep learning with generative adversarial networks,* Geophysical Prospecting **69** (2020), pp. 307–326.

[12] D. J. Verschuur, *Seismic multiple removal techniques : past, present and future* (EAGE Publications, Houten, Netherlands, 2013).

[13] D. J. Verschuur and A. J. Berkhout, *From removing to using multiples in closed-loop imaging,* The Leading Edge **34** (2015), pp. 744–759.

A

APPENDIX A: LPMO FOR LEAKED INTERNAL MULTIPLE ATTENUATION ON FWM IMAGES

An important imaging challenge is creating reliable seismic images without internal multiple crosstalk, especially in cases with strong overburden reflectivity. Several data-driven methods have been proposed to attenuate the internal multiple crosstalk, for which fully sampled data in both source and receiver side are usually required. To overcome this acquisition constraint, model-driven full-wavefield migration (FWM) can automatically include internal multiples and only needs dense sampling in either source or receiver side. In addition, FWM can correct for the transmission effects at the reflecting interfaces. Although FWM has been shown to work effectively in compensating for transmission effects and suppressing the internal multiple crosstalk compared to the conventional least-squares primary wavefield migration (PWM), it tends to generate relatively weaker internal multiples during modeling. Therefore, some leaked internal multiple crosstalk can still be observed in the FWM image, which tends to blend in the background and can be misinterpreted as real geology. Thus, we propose a novel framework using local primary-and-multiple orthogonalization (LPMO) on the FWM image as a post-processing step for leaked internal multiple crosstalk estimation and attenuation. Due to their opposite correlation with the FWM image, a positive-only LPMO weight can be used to estimate the leaked internal multiple crosstalk, while a negative-only LPMO weight indicates the transmission effects that need to be retained. Application to North Sea field data validates the performance of the proposed framework for removing the weak but misleading leaked internal multiple crosstalk in the FWM image. Therefore, with this new framework, FWM can provide a reliable solution to the longstanding issue of imaging primaries and internal multiples automatically, with proper primary restoration.

This chapter is a slightly updated version of the published paper "D. Zhang, D. J. Verschuur, M. Davydenko, Y. Chen, A.M. Alfaraj, and S. Qu, Local primary-and-multiple orthogonalization for leaked internal multiple crosstalk estimation and attenuation on full-wavefield migrated images, Geophysics 86 (2021), pp. A7–A13".

A

A.1. INTRODUCTION

Internal multiples have drawn abundant interest for several decades due to the severe challenges in sub-salt imaging and land data processing, where strong reflectors generate rich internal multiples to prevent interpreters from seeing the real geology. Many solutions have already been brought forward for internal multiple elimination in a data-driven manner. Inverse-scattering series-based approaches can predict all possible internal multiples that will be subtracted from the original data [1]. Layer-related internal multiple elimination is capable of estimating important subsets of interbed multiples by direct multidimensional convolution and correlation of the surface data [2] or with the help of redatuming operators in which an approximated homogeneous velocity model is needed [3]. Marchenko multiple elimination utilizes the Marchenko scheme to retrieve artifact-free primaries and accurately estimate all orders internal multiples without any model knowledge and adaptive subtraction in theory [4, 5]. All these data-driven methods require dense sampling in both sources and receivers, which is difficult to meet especially in a full 3D sense. [6] introduce hybrid model- and data-based method for internal multiple prediction and attenuation. More recently, we have come to realize that full-wavefield migration (FWM) including internal multiples in a model-driven manner might show promising potentials to overcome the sampling issue in reality [7, 8]. Specifically, FWM only needs dense sampling in either source or receiver side, and the modeling strategy in FWM is redefined for imaging internal multiples. By allowing simulating transmission effects and multiple scattering in the subsurface through full-wavefield modeling (FWMod) [9], FWM reproduces the true physics and can better explain the internal multiples in the input data. Based on the estimated reflectivity model and given the migration velocity model, FWM handles all orders internal multiples in a data-consistent and closed-loop fashion, without strong sampling requirements.

[8] demonstrate good performance of FWM on North Sea field data set for attenuating internal multiple crosstalk that is overlying target reflections. Although FWM works effectively to compensate for transmission effects and suppress the internal multiple crosstalk compared to the conventional least-squares primary wavefield migration (PWM), it tends to underestimate the amplitudes of internal multiples during modeling. Therefore, some leaked internal multiple crosstalk is often observed in the FWM image, which might be interpreted as real geology and needs to be further attenuated. This can be regarded as a typical signal leakage problem. [10] propose local primary-and-multiple orthogonalization (LPMO) for successful surface-related multiple leakage extraction. Inspired by the aforementioned concept, we propose a novel framework using LPMO on the FWM image for leaked internal multiple crosstalk estimation and attenuation. Both PWM and FWM images are required to provide the difference image that consists of coupled transmission effects and initially estimated internal multiples. Application to the same Vøring field data as shown by [8] validates the promising performance of the proposed framework.

A.2. FWM AND ITS MODELING ENGINE FWMOD

To better understand the physics behind FWM and its advantages, a brief introduction of FWM and its modeling engine FWMod is given in this section. The objective function for

FWM can be written as follows:

$$J_{\mathrm{FWM}} = \frac{1}{2}\sum_{\omega}\sum_{shots} \|\mathbf{d}^{-}_{\mathrm{obs}}(z_0) - \mathbf{p}^{-}(z_0,\hat{\mathbf{r}})\|_2^2, \tag{A.1}$$

where $\mathbf{d}^{-}_{\mathrm{obs}}(z_0)$ and $\mathbf{p}^{-}(z_0,\hat{\mathbf{r}})$ represent the monochromatic observed and modeled upgoing wavefield at the surface z_0 for a single shot, respectively. $\hat{\mathbf{r}}$ denotes the reflectivity parameter as a function of subsurface coordinate that needs to be estimated during FWM. Equation A.1 can be augmented by an extra constraint term, e.g., a sparsity constraint. In terms of objective functions, FWM is similar to most least-squares type migrations and can be solved by gradient-based approaches [8]. However, the unique feature and power of FWM lies in its modeling engine FWMod, which takes multiple scattering and transmission effects into account, based on the estimated image. First, FWMod describes the two-way wavefield via one-way wavefields, i.e., the downgoing and upgoing wavefields. Migration velocity and reflectivity are decoupled to diminish non-linearity. Multiple-scattered reflections and transmission effects are handled at each depth level z_n in an elegant way [9]:

$$\begin{aligned}\mathbf{q}^{+}(z_n) &= \mathbf{s}^{+}(z_n) + \mathbf{T}^{+}(z_n)\mathbf{p}^{+}(z_n) + \mathbf{R}^{\cap}(z_n)\mathbf{p}^{-}(z_n),\\ \mathbf{q}^{-}(z_n) &= \mathbf{s}^{-}(z_n) + \mathbf{T}^{-}(z_n)\mathbf{p}^{-}(z_n) + \mathbf{R}^{\cup}(z_n)\mathbf{p}^{+}(z_n),\end{aligned} \tag{A.2}$$

where $\mathbf{p}^{\pm}(z_n)$, $\mathbf{q}^{\pm}(z_n)$ and $\mathbf{s}^{\pm}(z_n)$ denote the incoming, outgoing and source wavefields; superscripts + and − refer to downgoing and upgoing, respectively. $\mathbf{T}^{\pm}(z_n)$ represents transmission matrix. $\mathbf{R}^{\cup}(z_n)$ and $\mathbf{R}^{\cap}(z_n)$ represent upward and downward reflection matrix, respectively. Moreover, the wavefield propagation between two adjacent depth levels z_n and z_{n-1} is described by propagation matrices $\mathbf{W}(z_n, z_{n-1})$ and $\mathbf{W}(z_{n-1}, z_n)$:

$$\begin{aligned}\mathbf{p}^{+}(z_n) &= \mathbf{W}(z_n, z_{n-1})\mathbf{q}^{+}(z_{n-1}),\\ \mathbf{p}^{-}(z_{n-1}) &= \mathbf{W}(z_{n-1}, z_n)\mathbf{q}^{-}(z_n).\end{aligned} \tag{A.3}$$

Equations A.2 and A.3 introduce the basic ingredients of FWMod. We recursively repeat this process from the surface to bottom and vice versa, referred to as one round-trip. Only primary reflections are generated during the first round-trip. Multiple scattering will be successfully modeled as the number of round-trips increases. In this way, surface-related multiples, internal multiples and transmission effects can be taken into account during modeling, and via inversion, the recovered reflectivity is optimized [7].

A.3. LPMO FOR LEAKED INTERNAL MULTIPLE ESTIMATION

LPMO has shown promising results on surface-related multiple leakage estimation [10]. In this paper, we propose leaked internal multiple crosstalk estimation and attenuation using LPMO. Two clear differences from the surface-related multiple case are: first, instead of a data-domain (e.g., shot or offset domain) estimation for surface multiple leakages, the leaked internal multiple crosstalk is estimated in the image domain, i.e., the FWM image; second, initially estimated internal multiples are coupled with transmission effects, unlike estimated surface multiples. The main advantage for image domain LPMO is that the noise is already canceled by the summing process in FWM and a better grip on the internal

multiples can be obtained [11]. On the other hand, FWM also changes all primary contributions due to the restored transmission effects, so to minimize the coupled transmission effects on leaked internal multiple crosstalk estimation is the new challenge. Based on the PWM and FWM images, we rearrange the basic relations in vector notation:

$$\begin{aligned} \mathbf{r}_{\mathtt{PWM}} &= \mathbf{r}_{\mathtt{FWM}} + \mathbf{r}_{\mathtt{diff}}, \\ \mathbf{r}_{\mathtt{diff}} &= \mathbf{r}_{\mathtt{TE}} + \mathbf{r}_{\mathtt{IM}}, \end{aligned} \tag{A.4}$$

where $\mathbf{r}_{\mathtt{PWM}}$ and $\mathbf{r}_{\mathtt{FWM}}$ denote vectorized PWM and FWM images, respectively. The differences $\mathbf{r}_{\mathtt{diff}}$ between two images consist of two parts: the transmission effects $\mathbf{r}_{\mathtt{TE}}$ and the initially estimated internal multiples $\mathbf{r}_{\mathtt{IM}}$ by FWM. Due to its tendency to estimate relatively weaker internal multiples, the FWM image still contains some visible leaked internal multiple crosstalk. Our goal is to use the initially estimated internal multiples $\mathbf{r}_{\mathtt{IM}}$ to match and extract the leaked internal multiple crosstalk in the FWM image. However, the initially estimated internal multiples cannot be easily separated from the difference image. Therefore, we match the leaked internal multiple crosstalk with the differences between FWM and PWM in a least-squares sense:

$$\min_{\mathbf{w}} \|\mathbf{r}_{\mathtt{FWM}} - \mathbf{w} \circ \mathbf{r}_{\mathtt{diff}}\|_2^2, \tag{A.5}$$

where $\mathbf{w}$ denotes the LPMO weight and $\circ$ represents the Hadamard product (element-by-element multiplication). With the help of a smoothness constraint, the above unconstrained minimization problem can be solved by a shaping regularization-based inversion scheme [12]:

$$\mathbf{w}^+ = \mathscr{F}\mathscr{H}([\lambda^2\mathbf{I} + \mathscr{T}(\mathscr{D}^T\mathscr{D} - \lambda^2\mathbf{I})]^{-1}\mathscr{T}\mathscr{D}^T\mathbf{r}_{\mathtt{FWM}}), \tag{A.6}$$

where $\mathscr{D} = diag(\mathbf{r}_{\mathtt{diff}})$, λ is a scaling parameter and $[\cdot]^T$ denotes matrix transpose. $\mathscr{T}$, $\mathscr{H}$ and $\mathscr{F}$ represent triangular smoothing, thresholding and median filtering operators, respectively. Note that due to the non-separability between initially estimated internal multiples and transmission effects, the whole inversion framework not only matches the leaked internal multiple crosstalk with initially estimated internal multiples $\mathbf{r}_{\mathtt{IM}}$, but also the primaries in FWM image with transmission effects $\mathbf{r}_{\mathtt{TE}}$. However, FWM tends to estimate stronger events to compensate for the transmission effects, while typically underestimates the internal multiples, which leads to an opposite correlation in the difference image compared to FWM image, i.e., positive correlation for the leaked internal multiple crosstalk and negative correlation for the transmission effects. Therefore, we could take advantage of this prior knowledge by using positive-only LPMO weight through a thresholding operator. In this way, $\mathbf{w}^+$ indicates the estimated positive-only LPMO weight that is related to the leaked internal multiple crosstalk $\mathbf{r}_{\mathtt{LIM}}$ in the FWM image:

$$\mathbf{r}_{\mathtt{LIM}} = \mathbf{w}^+ \circ \mathbf{r}_{\mathtt{diff}}. \tag{A.7}$$

Thus, we obtain relations for the final estimated FWM and difference images:

$$\begin{aligned} \hat{\mathbf{r}}_{\mathtt{FWM}} &= \mathbf{r}_{\mathtt{FWM}} - \mathbf{w}^+ \circ \mathbf{r}_{\mathtt{diff}} = \mathbf{r}_{\mathtt{FWM}} - \mathbf{r}_{\mathtt{LIM}}, \\ \hat{\mathbf{r}}_{\mathtt{diff}} &= \mathbf{r}_{\mathtt{diff}} + \mathbf{w}^+ \circ \mathbf{r}_{\mathtt{diff}} = \mathbf{r}_{\mathtt{TE}} + \hat{\mathbf{r}}_{\mathtt{IM}}, \end{aligned} \tag{A.8}$$

where $\hat{\mathbf{r}}_{\mathtt{FWM}}$, $\hat{\mathbf{r}}_{\mathtt{diff}}$ and $\hat{\mathbf{r}}_{\mathtt{IM}}$ are the final estimated FWM image, difference image and internal multiples after LPMO, respectively.

A.4. RESULTS

The Vøring field data set from the Norwegian North Sea is used to test the proposed framework. [8] demonstrate the ability of FWM for handling internal multiples on the same data set, and detailed preprocessing steps and data information can be found therein. Note that these data are particularly suited for internal-multiple related research due to a large water depth and, therefore, the absence of surface-related multiples in the target area.

We start with the PWM, FWM and their difference images as shown in Figure A.1(a), A.1(b) and A.1(c), respectively. Generally, it is clear that there are mostly flat layers above 2.2 km depth and dipping layers below this level. Due to the conflicting dips below the anticline in Figure A.1(a) ranging from 2.3 km to 2.7 km, the crosstalk from internal multiples is obvious in the PWM image, as indicated by the arrows. Because of the modeling advantages for taking both internal multiples and transmission effects into consideration, FWM shows significant internal multiple crosstalk attenuation, as indicated by the arrows from the same area in Figure A.1(b). Even some crosstalk events above 2 km, indicated by the arrows, are slightly suppressed. However, the leaked internal multiple crosstalk in Figure A.1(b) still hinders geologic interpretation. Figure A.1(c) clearly demonstrates the differences between the PWM and FWM images, where initially estimated internal multiples and transmission effects are visible. Due to their opposite correlation in the difference image compared to FWM image, the LPMO weight related to leaked internal multiple crosstalk can be obtained via considering a positive-only weight (Figure A.1(d)). The locations of the leaked internal multiple crosstalk can be well detected in the estimated LPMO weight. Figure A.1(e) displays the final estimated FWM image after LPMO, where the leaked internal multiple crosstalk is further attenuated, especially for areas indicated by the arrows. The same image improves significantly when compared directly to the PWM image. Figure A.1(f) demonstrates the difference image after LPMO that extracts the leaked internal multiple crosstalk as shown by the arrows, while transmission effects are untouched. Note that because of the tendency of FWM to underestimate internal multiples, the LPMO weight for leaked internal multiple crosstalk estimation tends to be larger than the surface-related multiple case [10]. For this data, the LPMO weight ranges from 0 to 5. Special attention should be paid on the median filtering operator inside LPMO as there exists a trade-off for the window size of median filter. Edge effect starts to become severe with smaller window size while the multiple attenuation performance degrades with larger window size. We use 5×3 samples as our window size for this field data.

To better understand the power of FWM on compensating for transmission effects and attenuating internal multiple crosstalk and also to better demonstrate the LPMO performance on the FWM image, a zoom-in trace comparison is given in Figure A.2(a). It is obvious that the FWM trace (red line) has a stronger amplitude than the PWM trace (black line) especially above 2.2 km, which indicates that transmission effects are taken into account by FWM. As for the target area ranging from 2.2 km to 2.5 km, the FWM trace significantly attenuates the internal multiple crosstalk compared to the PWM trace. However, the leaked internal multiple crosstalk is still visible from the FWM trace, which means the FWM estimated internal multiples are weaker than the real ones. The FWM trace after LPMO (green line) from the zoom-in trace comparison shows further attenuation for the leaked internal multiple crosstalk, while retaining all transmission effects, which indicates

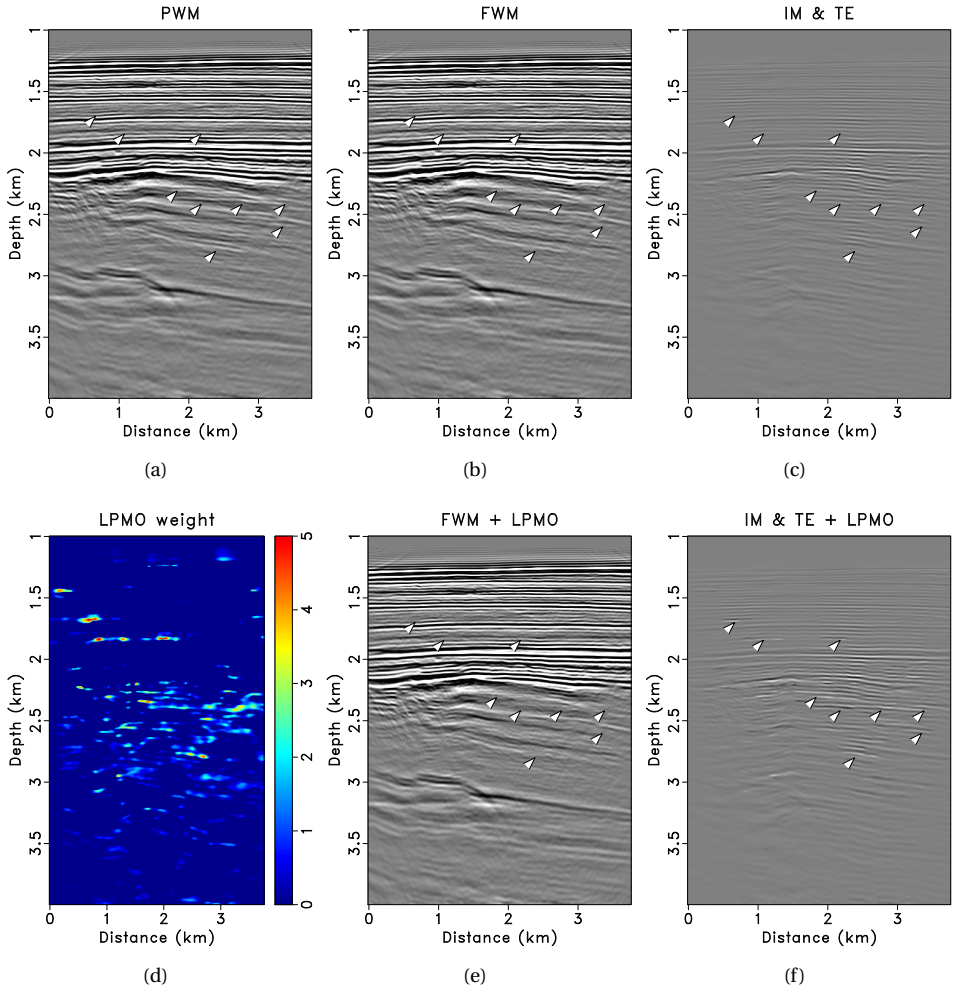

Figure A.1: LPMO on the FWM image of the Vøring field data set. (a) PWM image. (b) FWM image. (c) Difference image between PWM and FWM that includes the initially estimated internal multiples (IM) and transmission effects (TE). (d) Estimated positive-only LPMO weight related to the leaked internal multiple crosstalk in the FWM image. (e) Final estimated FWM image after LPMO. (f) Difference image that includes the final estimated internal multiples and transmission effects after LPMO.

the effectiveness of the proposed framework. We also provide the FWM and difference image similarity map [13, 14] comparison before and after using LPMO on the FWM image in Figure A.2(b) and A.2(c) for a more clear demonstration. It is also obvious from the similarity maps that the leaked internal multiple crosstalk on the FWM image has been effectively attenuated, as indicated by the arrows.

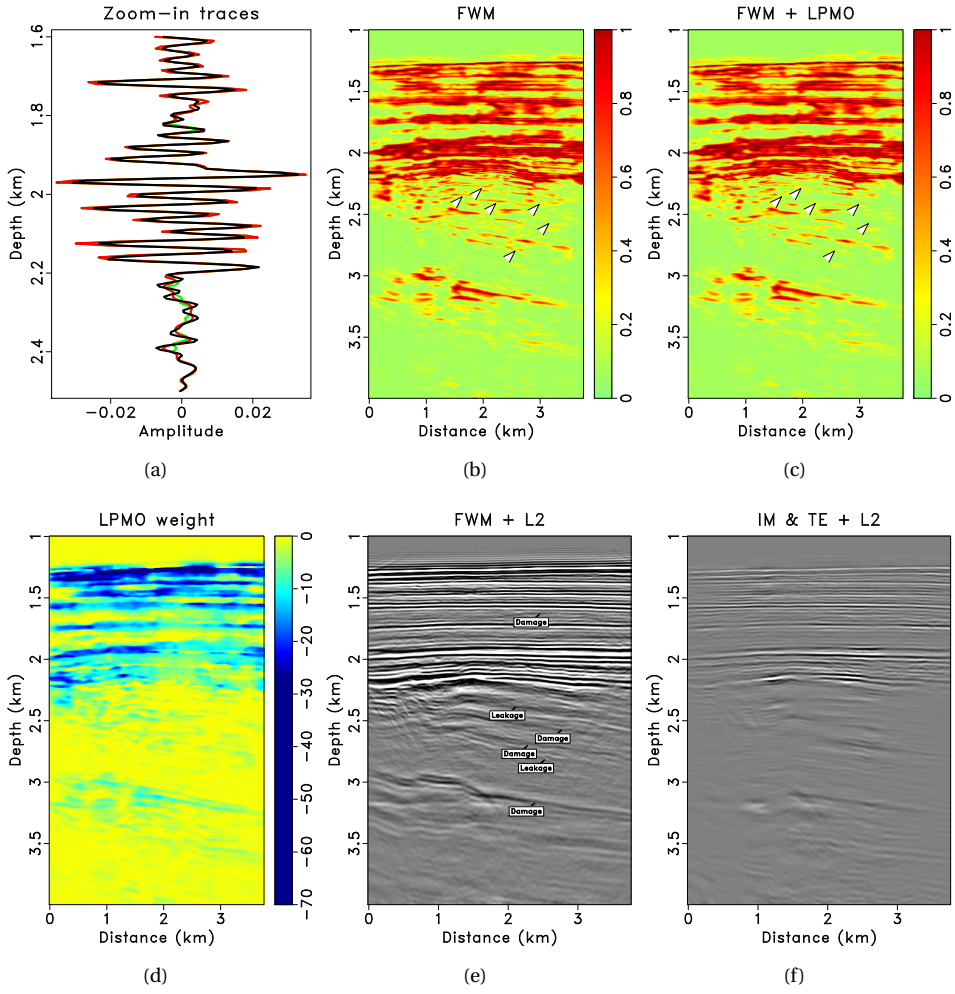

Figure A.2: (a) A zoom-in trace comparison at distance 2.2 km ranging from depth 1.6 km to 2.5 km where the black, red and green line denote the trace from the PWM image, the FWM image and the FWM image after LPMO, respectively. (b) & (c) Local similarity maps before and after using LPMO on the FWM image, respectively. (d) Estimated negative-only LPMO weight related to the transmission effects. (e) FWM image after conventional L2-norm adaptive subtraction of the difference image from Figure A.1(c). (f) Conventional L2-norm adaptive subtraction matched difference image.

To QC the retained transmission effects, we display the negative-only LPMO weights in Figure A.2(d). The negative LPMO weights (blue area) are in good agreement with most layer structures, where most transmission effects are generated. Thus, layer-structured primaries can be well preserved by simply rejecting the negative LPMO weight.

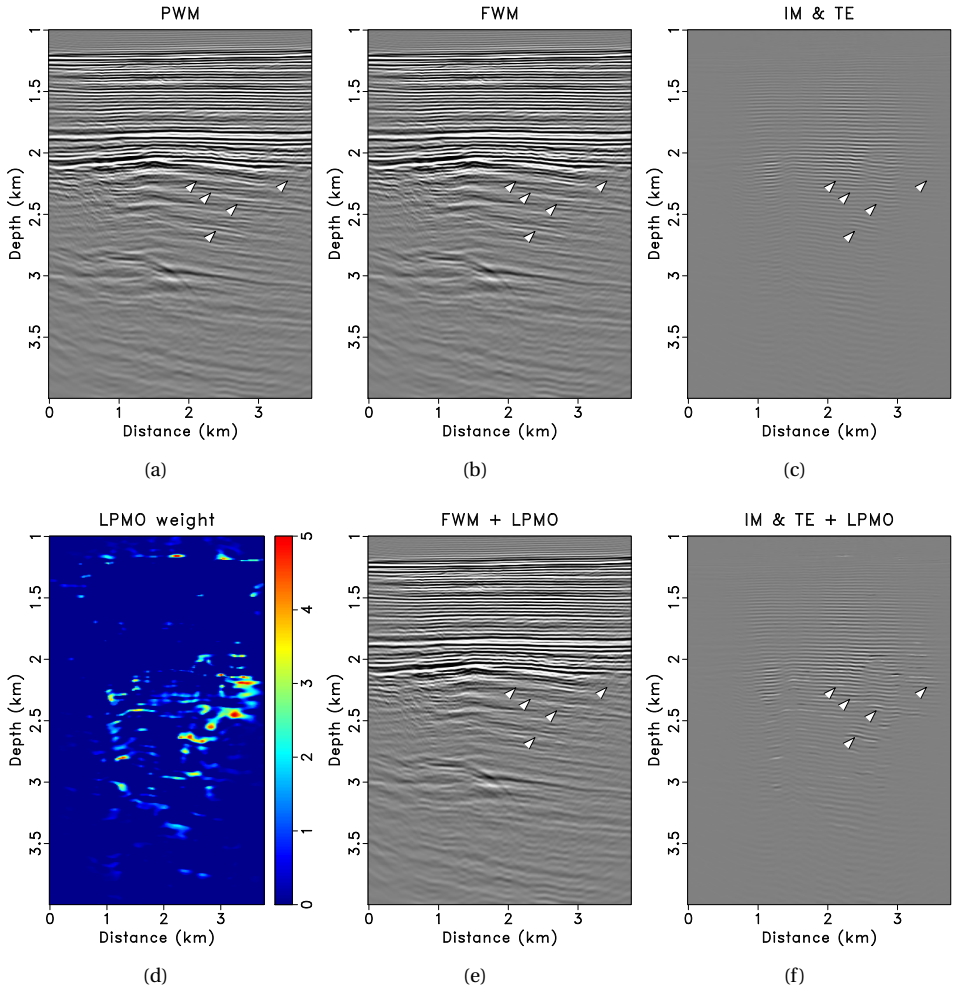

Figure A.3: LPMO on the FWM image of the Vøring field data set with 3% velocity errors. (a) PWM image. (b) FWM image. (c) Difference image between PWM and FWM that includes the initially estimated internal multiples and transmission effects. (d) Estimated positive-only LPMO weight related to the leaked internal multiple crosstalk in the FWM image. (e) Final estimated FWM image after LPMO. (f) Difference image that includes the final estimated internal multiples and transmission effects after LPMO.

However, using conventional *L*2-norm adaptive subtraction to match the leaked internal multiple crosstalk with the difference image will cause severe primary damage due to not accounting for transmission effects. This is shown in Figure A.2(e), where the primary damage occurs across the whole image. Moreover, some leaked internal multiple crosstalk is still visible after *L*2-norm adaptive subtraction of the difference image in Figure A.1(c).

In addition, the transmission effects in Figure A.2(f) mistakenly extract primary energy during $L2$-norm adaptive subtraction. The reason behind is because the $L2$-norm-based matching filter can be easily updated to match the negatively correlated transmission effects, which are usually happened to primaries.

To test the robustness of the proposed framework using LPMO on the FWM image, an extra experiment is applied on the same field data set, but with 3% velocity errors. From the PWM, FWM and their difference images in Figure A.3(a), A.3(b) and A.3(c), the internal multiple crosstalk indicated by the arrows can still be attenuated to some extent although the whole image is slightly shifted due to the velocity errors. Both transmission effects and internal multiples can again be observed from the difference image. By accepting positive-only LPMO weight, the leaked internal multiple crosstalk can be detected in Figure A.3(d). Figure A.3(e) and A.3(f) show the FWM and difference images after LPMO, respectively. We can observe that the leaked internal multiple crosstalk from the final estimated FWM image is further attenuated, while the estimated internal multiples extract their leaked energy in the final estimated difference image.

A.5. DISCUSSION

The FWM methodology is a very promising method which aims at solving a longstanding issue in imaging technology: including the internal multiples as part of the imaging scheme. In this way the traditional multiple removal and subsequent primary imaging method is being replaced by one inversion-type imaging process which handles all internal multiples on the fly. However, this technology sometimes struggles to find the exact balance between primaries and multiples, therefore an adaptive component from LPMO to improve its results will be playing a crucial role in its acceptance and success.

Regarding the general applicability of the proposed framework, on the one hand, a new imaging scheme has emerged, in which reverse time migration (RTM) is the main engine and multiples are explained on-the-fly as part of the traditional RTM-based imaging process [15]. From this perspective, the proposed methodology can be applied to the RTM-type methods. On the other hand, whether our proposed methodology is generally applicable to other traditional imaging methods depends on their own ability to handle internal multiples during imaging. For example, the conventional RTM cannot include internal multiples during the imaging process. Thus, we cannot directly apply our proposed framework on the conventional RTM. However, if the conventional RTM is combined with any conventional internal multiple removal technique, our proposed framework can definitely be applicable. Specifically, the internal multiples can be first attenuated in the data domain before RTM, and then RTM can produce an image with internal multiples attenuated. In this way, one can obtain two RTM images with and without internal multiples. Accordingly, a difference image with the estimated internal multiples can be achieved, and the internal multiple crosstalk in the RTM image can be further matched and attenuated using the difference image based on LPMO. Note that the transmission effects will not be taken into consideration by the conventional RTM. Still, LPMO will outperform the $L2$-norm adaptive subtraction in terms of internal multiple crosstalk attenuation due to its non-stationary property. Besides, our proposed framework is also useful for those model-based internal multiple removal methods as long as the estimated internal multiples are available.

A

Although all examples are shown for 2D data, this framework can be straightforwardly extended to the 3D case. 3D FWM has already been demonstrated and the details can be found in [16]. As for LPMO, it is also straightforward to be extended to the 3D case. In fact, the LPMO formulas in equations 4 - 6 do not have any limitations on the dimension. However, the computational cost might be an issue due to the smoothing process inside the shaping regularization-based inversion. Thus, we could still consider LPMO on 3D data in a 2D manner (i.e., data slice by slice) in terms of the efficiency. An extended image domain (e.g., by angle-dependent FWM [8]) might produce even better results than the original image domain. However, we still need to consider the issue of increased computational cost of LPMO from one image to hundreds of image gathers. Besides, although we ignore elastic effects, we do include multiple scattering and transmission effects that other methods usually ignore. Note that the anelastic Q-effect is another factor on top of the regular transmission effect, and this can be included in our FWM method by including it in the propagator [17], without influencing our proposed framework.

A.6. CONCLUSION

We have shown that the positive LPMO weight is able to estimate the leaked internal multiple crosstalk from an FWM image, whereas the negative LPMO weight indicates the transmission effects. From the Vøring field data set application, it has been demonstrated that the leaked internal multiple crosstalk in the FWM image can be further attenuated to a minimum by the LPMO process. The proposed framework, i.e., generating both PWM and FWM outputs and then using LPMO on the FWM image, should be considered as a routine procedure for internal multiple imaging, where LPMO could also be regarded as a QC step on the FWM image.

REFERENCES

[1] A. B. Weglein, F. A. Gasparotto, P. M. Carvalho, and R. H. Stolt, *An inverse-scattering series method for attenuating multiples in seismic reflection data,* Geophysics **62** (1997), pp. 1975–1989.

[2] H. Jakubowicz, *Wave equation prediction and removal of interbed multiples,* in *68th SEG Technical Program Expanded Abstracts* (Society of Exploration Geophysicists, 1998) pp. 1527–1530.

[3] D. J. Verschuur and A. J. Berkhout, *Removal of internal multiples with the common-focus-point (CFP) approach: Part 2 — Application strategies and data examples,* Geophysics **70** (2005), pp. V61–V72.

[4] J. van der Neut and K. Wapenaar, *Adaptive overburden elimination with the multidimensional Marchenko equation,* Geophysics **81** (2016), pp. T265–T284.

[5] L. Zhang and E. Slob, *Free-surface and internal multiple elimination in one step without adaptive subtraction,* Geophysics **84** (2019), pp. A7–A11.

[6] A. Pica and L. Delmas, *Wave equation based internal multiple modeling in 3D,* in

78th SEG Technical Program Expanded Abstracts (Society of Exploration Geophysicists, 2008) pp. 2476–2480.

[7] A. J. Berkhout, *Review paper: An outlook on the future of seismic imaging, Part II: Full-wavefield migration,* Geophysical Prospecting **62** (2014), pp. 931–949.

[8] M. Davydenko and D. J. Verschuur, *Including and using internal multiples in closed-loop imaging — Field data examples,* Geophysics **83** (2018), pp. R297–R305.

[9] A. J. Berkhout, *Review paper: An outlook on the future of seismic imaging, Part I: forward and reverse modelling,* Geophysical Prospecting **62** (2014), pp. 911–930.

[10] D. Zhang, D. J. Verschuur, S. Qu, and Y. Chen, *Surface-related multiple leakage extraction using local primary-and-multiple orthogonalization,* Geophysics **85** (2020), pp. V81–V97.

[11] B. Wang, J. Cai, M. Guo, C. Mason, S. Gajawada, and D. Epili, *Postmigration multiple prediction and removal in the depth domain,* Geophysics **76** (2011), pp. WB217–WB223.

[12] S. Fomel, *Shaping regularization in geophysical-estimation problems,* Geophysics **72** (2007), pp. R29–R36.

[13] S. Fomel, *Local seismic attributes,* Geophysics **72** (2007), pp. A29–A33.

[14] Y. Chen and S. Fomel, *Random noise attenuation using local signal-and-noise orthogonalization,* Geophysics **80** (2015), pp. WD1–WD9.

[15] M. Davydenko and E. Verschuur, *Full wavefield least-squares reverse time migration,* Geophysics **86** (2021), pp. WC67–WC74.

[16] M. Davydenko and D. Verschuur, *Full-wavefield migration: using surface and internal multiples in imaging,* Geophysical Prospecting **65** (2017), pp. 7–21.

[17] H. Alasmri and D. J. Verschuur, *Towards Q-compensation in full wavefield migration and joint migration inversion,* in *81st EAGE Conference and Exhibition* (European Association of Geoscientists & Engineers, 2019).

ACKNOWLEDGEMENT

Finally, I could start to write this very last part of my thesis, however, with a hard-to-describe feeling. I guess it is hard because of the mixed emotions of excitement, relief, regret, and gratefulness. After finalizing my thesis, a new chapter of my life will initiate which makes me excited. Relief steps in since there is only one more procedure left, the defense, to obtain my PhD and also prove I could do anything "in theory". Meanwhile, a tiny regretful voice reverberates in my heart and reminds me that during the last four and half years I could have achieved more if... Besides, I could have been better to those I cared about most. Suddenly, all those good old memories start popping up and keep flashing in my mind. Seeing those precious memories makes me realize, rather than being regretful, just how lucky I was to be here and to know every one of you in my life. So this is going to be a "tedious" list to thank all those people without whom I could not go this far.

First and foremost, I would like to thank my supervisor **Dr. Eric Verschuur** for his utmost patience and inspiration during my PhD journey. I am extremely honored and proud to be your student forever. As my role model, I have learned many things from you during the last four years, e.g., your enthusiasm for seismic problems, your patience in helping all the students, your brilliant ideas for the consortium, your outstanding and attractive presentation skills, and your accurate observations on figuring out what is the real problem from my initial bad results. To be honest, based on my original Chinese thinking, I never thought a supervisor could be that kind and nice to communicate with. It was almost like we were friends and we supported each other. From time to time, we also made little jokes and shared some anecdotes, which makes me feel relaxed. All my friends in China envy me so much because of you. I still remember when we first met at the China University of Petroleum in Beijing, I took your EAGE seismic multiple courses and gathered all my courage to invite you for a cup of coffee after the last day of the course. Beyond my expectation, you accepted my invitation immediately. Maybe I should also thank the China University of Petroleum for their "budget issue". Otherwise, you would be invited to dinner with those Chinese professors, and I wouldn't have the opportunity to know you better. Anyway, we had a nice talk and discussion about my experience and previous work in that coffee shop. We ended up in another Chinese restaurant and started to talk about other interesting things, such as culture, hobbies, your kids, etc. In the end, you told me I passed the interview if I was interested in pursuing a PhD with you in Delft. I was so happy that I couldn't fall asleep that night. Another story, maybe without your notice, also helps me a lot. That was the time when my first Delphi SEG abstract got rejected during my first year of PhD. I was very upset and you came to encourage me by defending my work. Because of your enormous support, I can regain my confidence and continue my work. Just like Shan mentioned before, your office is indeed a "magic room". Every time I anxiously entered the room full of questions, doubts, and unconfidence, I cheerfully left it with sufficient solutions, solid research plans, and faith. As time flies, gradually you seem to be a father-like model to me, and that's why sometimes I would like to share my private

stories with you. This also reminds me of the famous Chinese saying “a teacher for a day is a father for a lifetime”. You are always energetic, thus, I thought you might be a covered identity of “superman”. How come you are always full of brand new ideas? Anyway, I benefited a lot from this and that’s why my thesis is quite long already due to different kinds of ideas coming from you.

I would like to give many thanks to dear Delphi sponsors for their support. Because of the interesting discussions and helpful suggestions from sponsors, I can always update and improve my work in the right direction. I have also learned a lot from different project leaders in Delphi Consortium, therefore, I would like to acknowledge them for their inspiration. **Dr. Gerrit Blacquière**, thank you for your great presentations on seismic acquisition design and data processing, and I enjoyed all those small talks with you during the sponsor meetings. Now you could enjoy more after the retirement. **Dr. Koen van Dongen**, thank you for your inspiring talk on multi-physics inversion. Your expertise in medical imaging will help the group from a different perspective. **Prof. Evert Slob**, I have learned a lot from your nice introduction to both Marchenko methods and EM for geophysical applications. **Dr. Tristan van Leeuwen**, thank you for your host on the Dutch inverse problems meeting. I also thank **Dr. Femke Vossepoel** and **Dr. Deyan Dragonov** for their insightful work on different geophysical topics.

I am grateful to all the professors and project leaders in both Departments of Imaging Physics and Applied Geophysics. **Prof. Nico de Jong**, my other promoter, thank you for your help and suggestions on my PhD project. My mentor, **Dr. Kees Hagen**, thank you for your continuous care during the last four years. We had many great discussions on a wide range of topics. **Prof. Sjoerd Stallinga**, **Prof. Bernd Rieger**, and **Dr. Jeroen Kalkman**, thank you for enlightening me with all those nanoscale microscopy imaging technologies during the weekly CI group seminar. Although very different scale compared to earth science, we do share similar imaging and data reconstruction methods, and thus we could learn from each other. **Sjoerd**, I like your jokes, and thank you for pushing me to finish my thesis a bit earlier. **Dr. Qian Tao**, I would like to thank you for the discussions on AI-based medical image processing techniques. **Dr. Martin Verweij**, thank you for the insightful remarks on my PhD project and your great introduction to medical imaging. To **Prof. Kees Wapenaar**, I enjoyed your course, and thank you for deriving the wave equation in an extremely clear and accurate manner on the blackboard. **Dr. Guy Drijkoningen**, thank you for your great coding design on the seismic data processing course. **Dr. Jan Thorbecke**, thank you for sharing your coding experience on HPC-related applications and seismic modeling.

To all my PhD defense committee members, **Prof. Evert Slob**, **Prof. Yanghua Wang**, **Prof. Alle-Jan van der Veen**, **Dr. Jan van Gemert**, and **Dr. Clement Kostov**, thank you for your careful revision and helpful suggestions on my draft thesis. Especially, comments from the industry and non-geophysical communities are important to further improve this thesis from different perspectives.

Additionally, many thanks go to my unsung heroes behind the curtain, i.e., the group secretaries and IT experts. **Angela**, thanks for organizing many things for me. Actually, you started to help me out even before we met each other at Delft. I still remember all the tedious paperwork (contract and visa), DUWO account application, flight tickets from Beijing to Amsterdam, and taxi to pick me up at Schipol. It could never be that smooth

without your help and arrangement. Thanks for pushing me to speak Dutch although I am still very poor at it. Every time I enjoyed visiting your farmhouse very much. Tarzan, kitty, cows, sheep, rabbits, chicken, and grasslands always made me feel "gezellig". In my mind, it was just like yesterday that I helped you with some chores at the farmhouse during the summertime. For the first time in my life, I learned how to trim the branches of trees, paint the windows, and make hand-made pizza. You also taught me how to swing to the other side of the canal, and I was shocked by the size of the cow when I physically stood right in front of one. Thank you for always caring about me. I will never forget you asking your father to shelter me, you trying to find all possible renting information, and you worrying about me. Angela, I appreciate everything you did to help me. **Annelies**, you are always very kind, and also thank you for arranging everything for the students. Since we transferred to the CI group, I have always asked for your help regarding many paperwork. Thank you for all the help. One more thing, thank you and Angela for all the great ideas about the yearly day-out. **Henry**, thank you for fixing all my problems regarding the laptop and other experiment equipment. **Ronald**, thank you for taking care of the PC clusters, and I like to hear "Coffee" from you all the time. I would like to give my sincere thanks to **Gerrie**, my dear Delphi secretary. Thank you for your wonderful organization every time for Delphi meetings both in Houston and the Hague. As Shan used to call you "the Delphi mom", you took good care of us every time so that we could completely focus on the meeting without worrying about anything.

To all my Delphi consortium colleagues, thank you for being supportive and generous to share wonderful ideas. You were like a big family to me, since the previous one-child policy in China, I have never experienced such a big family before. During the last four years, we had a lot of cool discussions about each other's work, we learned from each other and we inspired each other. I still remember vividly one of my work was thanks to the whole group. It was after a group seminar and I was talking about the local orthogonality on surface multiple leakage extraction. In the office, Ali came up with the brilliant idea by simply suggesting "hey Dong, have you ever considered using the same method to extract the residue internal multiple?" Bang! A new idea was born. **Ali**, thanks for the inspiration. With the help of Mikhail's previous work on FWM and Eric's careful revision of the manuscript, we together push this work to Geophysics Letters. **Mikhail**, thanks a lot for helping me regarding 3D FWM. I am grateful to **Shan** for many helpful coding techniques and research discussions. Special thanks go to **Leo** for helping me translate my thesis summary to the corresponding Dutch version. To both my old office mates - **Apostolos**, **Aparajita**, and **Tiexing** - and current office mates - **Ali** and **Leo** - thank you for all those little talks literally about everything during the coffee breaks. **Aparajita**, thank you for the great Indian food you made for us. **Tiexing**, you were always considerate to everyone, and I should learn from you regarding this aspect. Thank you for all the drinks and the longest-running I have ever done (15+ km) around Delftse Hout. I still remember I was so tired but kept repeating those city names. **Runhai**, thank you for providing the unforgettable experience when we tried to visit Sweden. **Lele**, thank you for the great food and tutoring about the Marchenko methods. I would also like to thank **Jan** for organizing the Jupiter Notebook codes. **Halah**, it was a pity that you couldn't stay in Delphi. Thanks to you, I did enjoy the Persian food when we attended the training course in Houston. **Gabriel**, thanks a lot for helping me understand your codes and solving my confusion. We also had a great

time at the game shop in Utrecht. **Matteo**, thank you for sharing your working experience with me, and thank you for walking me to the train at Utrecht. **Camille**, your car is awesome and thank you for introducing the Michelin recommendation restaurant in Madrid. **Azin**, thank you for the delicious Persian food. **Leo**, **Billy**, **Ali**, **Siamak**, **Camille**, and **Andrea**, thanks to you, we could revive the weekly Delphi student lunch. **Dieter**, thank you for the nice Git introduction. I would also like to thank **Bouchaib**, **Shogo**, **Hussain**, **Siddarth**, **Sixue**, **Jan-Willem**, **Aayush**, **Junhai**, **Nick**, and **Shotaro** for your great presentations during the Delphi meeting. I wish you all the best in the future and we could meet each other again during the conferences or business trips. Besides, I could never forget all those lovely dinner nights with you guys in both Houston and the Hague.

I appreciate all the happy hours in the kitchen and table tennis room with my department colleagues. We had lots of fun playing table soccer and tennis against each other during the coffee break. **Boling**, "the spicy chicken", thank you for teaching me all your skills on table soccer so that I could beat you easily. **Gyllion**, your Chinese "mmp" always surprised me. **Jin**, thank you for defeating me in table tennis by using the cellphone as your racket, which "broke" my table tennis dream. **Tian**, I am grateful to your help in finding a great room at X-ray for me. **Yan**, I am still amazed by how early you were every day in the office, and thanks a lot for introducing job opportunities to me. **Yifeng**, your enthusiasm on basketball is impressive, and I enjoyed playing basketball with you, **Boling**, and **Tiexing** at X. **Jos**, your Chinese is impressive. **Joost**, thank you for the inspiration by firmly perusing your goal. **Fabian**, thank you for all the small talks during either lunch or coffee breaks. **Xin** from QuTech, you are a great pal for awesome Chinese food, and thank you for listening to my stories. **Jingming**, thank you for stopping by at my office and all the interesting discussions. **Johno**, thank you for hosting a great team-building activity for EAGE LC in the Netherlands. **Rene**, thank you for your invitation on the helicopter trip. Besides, to **Shan**, **Boling**, **Tiexing**, and **Kefei**, I do miss the good old days when we had lunch together and messed up with each other at Aula.

Many thanks also go to my colleagues outside of TU Delft. **Diego**, **Hannes**, and **Joeri**, thank you for welcoming me to join the family of the EAGE Local Chapter Netherlands. **Haorui**, thank you for your patience to my complaints during the international conferences. **David**, thank you for inviting me to the IICU seminar at Utrecht University. I had a great experience and discussions with people at the seminar. **Dr. Ivan Vasconcelos**, thank you for your encouragement and suggestions on my work. **Myrna**, thank you for helping me get a better understanding of Fugro during the virtual coffee break. **Yimin**, thank you for the discussions and suggestions on my project.

Although not many, I would like to thank all my foreign (non-Chinese) friends in the Netherlands. Without you guys, I would not notice how biased I was, and I would not have had the chance to understand this world better from different perspectives. Luckily, I found you were not that different from my Chinese friends. In fact, we have a lot in common and also share similar emotions. To **Christian**, **Elly**, **Yuki** and **Lotte**, thank you very much for all the nice food and board game nights. We might just meet each other every one or two months, but we kept doing this for the last five years. Starting from Catan, we have played many different board games, and I enjoyed playing every one of them. Thank you for guiding me into the world of board games. **Christian**, I was happy to see our photo hanging on the wall at your place, which reminded me of the Japanese Ramen

and we looking for a good place along the canal for that photo. I wish you and Elly success in Australia soon, and I hope I could manage to visit you in Sydney. **Elly**, as my first Dutch female friend, thank you for always being so kind to me. I really enjoyed watching you and Christian play board games, haha. **Prof. Yuki**, the most charming guy at TU Delft I guess, thank you for everything that we did together, tennis, ping pong, running, Nintendo and PS games, swimming, and beer pong. Still remember me breaking my knee? Anyway, my PhD life would be a lot more boring if you did not live in Zusterlaan from the beginning. **Lotte**, your Chinese is excellent, so just be more confident. To **Leo**, thank you very much for your support during my most difficult times. I actually don't know how to describe my feeling right now. I guess, to some extent, you saved me at that time. I was helpless and extremely desperate. If you didn't show up that night, I would have slept in the office for months, which could worsen my already bad mental health. Thanks to you, I could gradually get out of the shadow. Walking around the campus, going to Chinese restaurants, watching me kill zombies, playing Seven Wonders, and bouldering together all cheered me up. Thanks, Leo. Wait, we also had a great time in New York although four out of six pieces of New York big pizza that you ate amazed me. Legend about Leo's appetite continues!

To all my Chinese friends in the Netherlands, thank you. All of you have made my life, though ten thousand miles apart from home, much easier and more joyful than I could expect. **Dongbin** and **Hong**, thank you for inviting me to join the skateboarding practice and opening up a brand new bouldering world for me. Maybe without your notice, these exercises slowly helped me get through my depressed feelings. It was also great fun to play with Candy, and hopefully, she could always remember me. Surprisingly and magically, I have never expected to meet a group of lovely people from my hometown in the Netherlands. **Yuxuan**, **Yue**, **Sisi**, **Zichen**, **Jiali**, **Kaho**, **Yupeng**, **Shuaidong** and **Ruitao**, thank you so much for all the fun we had and all the delicious food we enjoyed. The knife-cut noodles at the big wok in Utrecht made me cry and enjoy at the same time; The werewolf made me realize how good you were as "actors"; Cart-driving forced everyone to conclude that Jiali was a "badass"; Pool and billiards reminded me of the similar atmosphere in Taiyuan. **Yuxuan** and **Yue**, thanks for all the beer, wine, Twenty-One, and the talk. You made me feel like I was at home back in Taiyuan. **Sisi**, what are the chances to meet someone here from the same high school back in China? **Zichen**, that was a great time playing basketball together with you. **Chunsheng**, many thanks for your fantastic cooking and barbecue in Rotterdam, and thank you also for listening to my complaints. **Yixuan**, my dear landlord and also known as the big chef at Ypenburg, thank you for all the delicious hand-made food and for introducing squash and snowboarding to me. **Qiwei**, the best roommate ever, I enjoyed all those hotpot nights and political discussions with you. To all the basketball guys in the center of Ypenburg, thank you for all the great games we had every Sunday afternoon.

Shan, I have already started to worry that the "thank Shan" part might even be longer than the "thank Eric" part. It is even harder to decide where to start. It seems you were always there when I check my memories for the last four years. Time sequence "thank Shan" note might be the only feasible way. Thank you for encouraging me and providing helpful information during my PhD application period. This was even before we met in the real world. We communicated through QQ and WeChat. You were very patient to help

me with all my silly questions and kindly shared all your previous application experiences. Still remember our first meeting? By your typical accent and a bit of luck, I immediately recognized you at the subway station in Vienna. You were so friendly that you invited me to museums and restaurants together without any hesitation. I would also like to thank you for taking care of me when I first arrived in the Netherlands. It was unforgettable that you took me to Jumbo for a quick tour. You seriously taught me how to survive by suggesting "this one 5 minutes in the microwave oven, and that one only needs two". Without this valuable advice, I would have been starving to death as a cooking rookie. Due to the delay of my first-month salary, I was quite worried about my rent and living expenses for the next month. Thanks to you again, I could make it smoothly. Besides, thanks for worrying about me being alone. You would invite me for dinner at your place at least twice a month. Every spring festival, you took me to your friends' place so that I would not be left behind. It helped me a lot to overcome the feeling of loneliness. Of course, many trips are memorable, such as authentic Chinese food in Houston, the biggest Legoland in Denmark, the first and oldest Disneyland in Anaheim, the cocktail at the tallest building in London, the most interesting "knowledge" at the British Museum, and the best journey at Mont Blanc. After all these years, you are like a big sister to me, and whatever happens, I will always be there as long as you need any help. **Ulas**, I still remember our visit to the Maritime Museum at Rotterdam and thank you for helping me get familiar with everything in the office. **Xinmin** and **Qian**, thanks to Shan, I could have the opportunity to know such an awesome couple like you two. Because of you, my life during the pandemic was not boring at all. Also thank you for sheltering me at your place when I was desperately looking for help. **Qian**, I had great fun with you playing all kinds of games, e.g., AOV, computer games, basketball, washing the crayfish, etc. Thank you for the driver training program and all the talks we had, which at least helped me hang in there.

Before I started my PhD at Delft, I suffered a lot trying to figure out what research really was. Once I was extremely disappointed about conducting research during my master's study, however, everything changed when I met you, **Dr. Yangkang Chen** from the University of Texas at Austin. Thank you Yangkang for everything. If it weren't for you, I could never find out what research looks like during my miserable three years of master's study. If it weren't for you, I could not even be there to meet Eric. If it weren't for you, my life could be much less interesting. To me, you were my real supervisor during those three years of master's study back in China. Thank you again for dragging me out of the desperation. People don't know how much effort you have spent on solving all those difficult projects one by one. They have never seen how you switch between coding, writing, revising, teaching others, and sleeping repeatedly day by day. They have no idea how many students sincerely appreciate your help in enlightening them in the world of geophysical research. You certainly deserve those credits, honors, and academic achievements. I also respect your efforts in transferring research to an open-source style in the geophysical community, which would benefit a lot for most students. Besides, thank you for pushing me hard during my PhD study, otherwise, I could not bear all the peer pressure from publications.

Apparently, I could never make it this far without the help and guidance from my lovely teachers throughout my life in China. To **Yana Mao**, **Dan Gao**, **Lina Zhao**, **Zengrong Wang**, **Changqing Zhang**, and **Sheng Lei**, my middle and high school teachers, thank you for

"bearing" my naughty behaviors and consistently encouraging me. To my college professors, thank you for those insightful lectures and unforgettable field trips. **Prof. Zhaofa Zeng**, thank you for all the help on the innovative student project. **Prof. Deli Wang**, thank you for supervising my Bachelor thesis. **Prof. Jing Li** and **Dr. Zhuo Xu**, thank you for both life and academic suggestions.

My dear old Chinese friends, I would also like to thank you and I miss all of you very much. My dorm mates at CUP **Huan**, **Shubo**, and **Zhigao**, thank you for arranging a wonderful trip in Xi'an so we could hangout again. **Huan**, thank you for the great host in Lanzhou, and I did enjoy my stay there. The brave colleagues at CUPB **Huan**, **Hao**, **Peifu**, **Li** and **Hongyu**, thank you for the support to each other, and we did great to fight against the injustice. **Shaohuan** and **Shuwei**, thank you both for teaching me the coding tips on Madagascar. **Ling**, **Bin**, **Rui**, and **Minpeng**, thank you for being there at JLU, and my bachelor's life would be way less wonderful without you guys. **Ling** and **Bin**, I appreciate your host and everything during my visit back to JLU in March of 2019. **Ling**, thank you very much for sharing GPR and LPR knowledge with me, and most importantly, thank you for comforting me during my difficult time last year. **Minpeng**, I would like to thank you for supporting me through all those miserable three years at CUPB. Every time I felt extremely depressed, you always took me to have a great dinner and patiently listened to all my complaints. Without you, I might have quit my master already, thank you. **Jingxuan**, thanks for the great host in Texas. All my great memories and unique experiences are thanks to your help, my first and only NBA live game, awesome experience in NASA museums, sightseeing at TAMU and Austin, etc. **Kaikai**, thank you picking me up at the airport and arranging everything for me in Beijing. I always remember our good old days in the middle school when we made fun of each other, went to the Internet bar playing Warcraft 3 together, and covered up each other from our parents. My childhood friends **Bo**, **Xin**, **Xiang**, **Jie**, and **Xin "the Monkey"**, thank you for always being there for more than twenty years. I believe our friendship would last much longer no matter where we are. **Bo**, you are probably the one who knows me most. I guess we have shared all our previous experiences (good or bad), relationships, and miserable stories with each other. You are literally the only one that I could talk to without pressure and worrying anything. Buddy, just take care of yourself and I am looking forward to seeing your son. **Jinyu**, thank you for all your tips and suggestions for great restaurants in New York. **Xue**, thank you for your accompany during the first two years of my PhD. Anyway, I hope you could live a happy life forever.

Last but definitely not least, a big thank you to my family, without whom I couldn't make it at all. I would like to thank my dearest two aunts **Yongmei** and **Yongming**, uncle **Yongzhong**, and uncle-in-law **Yaxin** for taking great care of me during my childhood. Cousin **Laohu**, thank you for being my strongest backup at home so that I could finish my PhD without worrying too much. Cousin **Xiaoyu** and **Qinqin**, thank you for all those happy memories through the time we grew up together. **Yanan**, thank you for taking good care of me and your accompany to experience this beautiful world together, and hopefully you could be one of my family members in the near future. My mom **Yongping**, thank you very much for everything you did for me and for being supportive during my PhD journey. It was hard for me to get through all those years, but it was a lot harder and much more pressure for you. Mom, you have already borne many unbearable, and now I would like you to relax and enjoy all the happiness that you deserve. Never thought I couldn't see you

for more than three years, I miss you, mom. Dad, at least, I hope you could stay healthy.

Dong Zhang
Delft, the Netherlands
May, 2022

CURRICULUM VITÆ

Dong Zhang

30-July-1991 Born in Taiyuan, Shanxi, China.

EDUCATION

2017–2022 PhD candidate in Applied Physics
Delft University of Technology, Delft, The Netherlands

2014–2017 M.E. in Geological Resources and Geological Engineering (cum laude)
China University of Petroleum, Beijing, China

2010–2014 B.E. in Applied Geophysics (cum laude)
Jilin University, Changchun, China

RESEARCH EXPERIENCE

2022–present Post-doc researcher
Delft University of Technology, Delft, The Netherlands
Research on geophysics-related machine learning

2017–2022 PhD candidate
Delft University of Technology, Delft, The Netherlands
Research on surface-related multiple estimation for shallow water

2014–2017 Research assistant
China University of Petroleum, Beijing, China
Research on seismic data reconstruction, denoising, and imaging

2012–2014 Research assistant
Jilin University, Changchun, China
Research on ground penetrating radar for archaeological investigation

List of Publications

Journal Papers

5. **D. Zhang** and D. J. Verschuur, *Closed-loop surface-related multiple estimation with full wavefield migration-reconstructed near-offsets for shallow water*, Geophysics **86** (2021), pp. WC21–WC30.

4. **D. Zhang**, D. J. Verschuur, and Y. Chen, *Fast local primary-and-multiple orthogonalization for surface-related multiple leakage estimation and extraction*, Geophysics **86** (2021), pp. V353–V360.

3. S. Qu, E. Verschuur, **D. Zhang**, and Y. Chen, *Training deep networks with only synthetic data: Deep-learning-based near-offset reconstruction for (closed-loop) surface-related multiple estimation on shallow-water field data*, Geophysics **86** (2021), pp. A39–A43.

2. **D. Zhang**, D. J. Verschuur, M. Davydenko, Y. Chen, A.M. Alfaraj, and S. Qu, *Local primary-and-multiple orthogonalization for leaked internal multiple crosstalk estimation and attenuation on full-wavefield migrated images*, Geophysics **86** (2021), pp. A7–A13.

1. **D. Zhang**, D. J. Verschuur, S. Qu, and Y. Chen, *Surface-related multiple leakage extraction using local primary-and-multiple orthogonalization*, Geophysics **85** (2020), pp. V81–V97.

Conference Papers

7. **D. Zhang**, M. de Leeuw, and E. Verschuur, *Deep learning-based seismic surface-related multiple adaptive subtraction with synthetic primary labels*, in International Meeting for Applied Geoscience & Energy Expanded abstracts (Society of Exploration Geophysicists, 2021) pp. 2844–2848.

6. **D. Zhang** and E. Verschuur, *Deep learning-based dealiasing for estimated surface-related multiples from limited sources*, in 82nd EAGE Conference and Exhibition Expanded abstracts (European Association of Geoscientists & Engineers, 2021).

5. **D. Zhang** and E. Verschuur, *3D Surface-related multiple estimation for shallow water aided by full wavefield migration*, in EAGE Conference and Exhibition Online Expanded abstracts (European Association of Geoscientists & Engineers, 2020).

4. **D. Zhang**, E. Verschuur, and Y. Chen, *Fast local primary-and-multiple orthogonalization for surface-related multiple estimation*, in 90th SEG Technical Program Expanded abstracts (Society of Exploration Geophysicists, 2020) pp. 3129–3133.

3. **D. Zhang**, E. Verschuur, S. Qu, and Y. Chen, *Multi-domain surface multiple leakage extraction using local primary-and-multiple orthogonalization*, in 89th SEG Technical Program Expanded abstracts (Society of Exploration Geophysicists, 2019) pp. 4585–4589.

2. **D. Zhang** and E. Verschuur, *Integration of closed-loop surface-related multiple estimation and full wavefield migration for shallow water*, in 81st EAGE Conference and Exhibition Expanded abstracts (European Association of Geoscientists & Engineers, 2019).

1. **D. Zhang** and E. Verschuur, *Surface multiple leakage extraction using local primary-and-multiple orthogonalization*, in 81st EAGE Conference and Exhibition Expanded abstracts (European Association of Geoscientists & Engineers, 2019).